FILM CONDENSATION OF LIQUID METALS - PRECISION OF MEASUREMENT

Stanley J. Wilcox
Warren M. Rohsenow

Report No. DSR 71475-62

Contract No. GK 1113

Department of Mechanical
Engineering
Engineering Projects Laboratory
Massachusetts Institute of Technology

April 1969

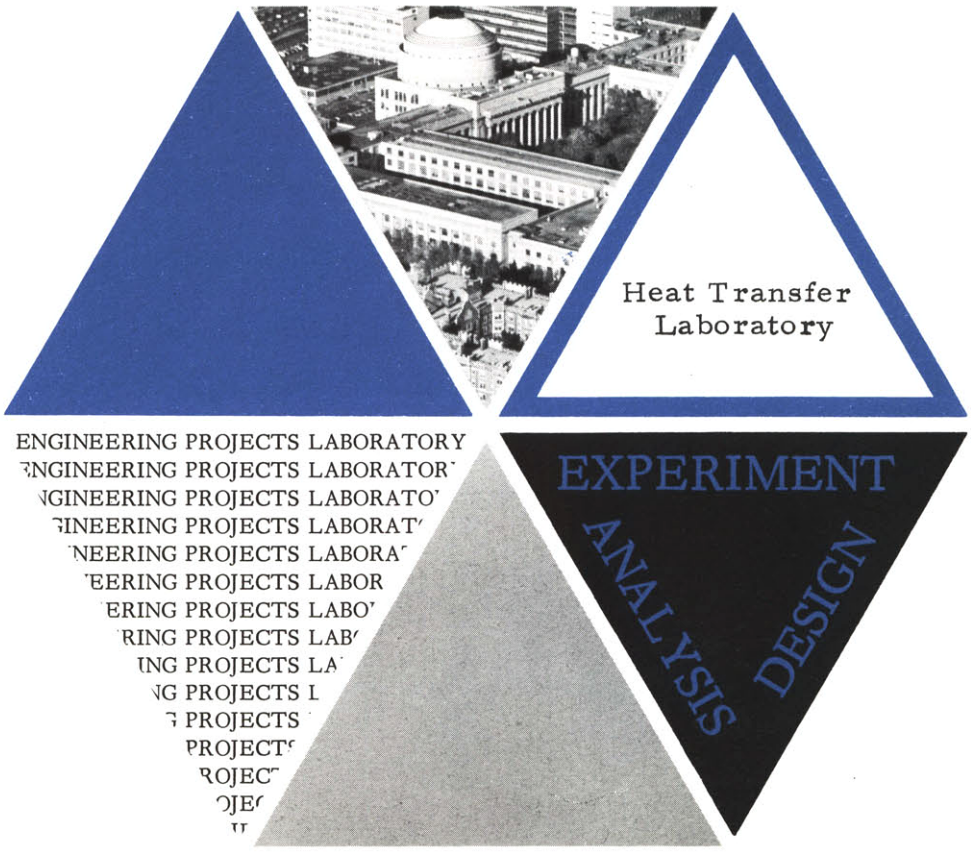

TECHNICAL REPORT NO. 71475-62

FILM CONDENSATION OF LIQUID METALS - PRECISION OF MEASUREMENT

by

Stanley J. Wilcox
Warren M. Rohsenow

Sponsored by

National Science Foundation
Contract No. GK 1113

APRIL 1969

Engineering Projects Laboratory
Department of Mechanical Engineering
Massachusetts Institute of Technology

FILM CONDENSATION OF LIQUID METALS - PRECISION OF MEASUREMENT

by

Stanley J. Wilcox
Warren M. Rohsenow

ABSTRACT

Major differences exist in results published by investigators of film condensation of liquid metal vapors. In particular, the reported dependence of the condensation coefficient on pressure has raised questions about both the precision of the reported data and the validity of the basic interphase mass transfer analysis.

An error analysis presented in this investigation indicates that the reported pressure dependence of the condensation coefficient at higher pressures is due to an inherent limitation in the precision of the condensing wall temperature measurement. The magnitude of this limitation in precision is different for the various test systems used. The analysis shows, however, that the primary variable affecting the precision of the wall temperature measurement is the thermal conductivity of the condensing block. To verify the analysis, potassium was condensed on a vertical surface of a copper condensing block. The copper block was protected from the potassium with nickel plating. Condensation coefficients near unity were obtained out to higher pressures than those previously reported for potassium condensed with stainless steel or nickel condensing blocks. These experimental results agree with the prediction of the error analysis.

In addition, a discussion of the precautions used to eliminate the undesirable effects of both non-condensable gas and improper thermocouple technique is included.

It is concluded from the experimental data and the error analysis that the condensation coefficient is equal to unity and that the pressure dependence reported by others is due to experimental error.

ACKNOWLEDGEMENTS

The authors are indebted to Professors P. Griffith, R.E. Stickney, J.W. Rose and B.B. Mikic for many fruitful discussions.

This work was sponsored in part by the National Science Foundation under Contract No. GK 1113 and sponsored by the Division of Sponsored Research at M.I.T.

TABLE OF CONTENTS

LIST OF TABLES AND FIGURES

NOMENCLATURE

A	area
c	heat capacity
E(z)	Expected Value of z
f(z)	density function for variable z
g	gravitational acceleration
h_{fg}	latent heat of vaporization
h'_{fg}	latent heat which includes change of enthalpy due to the subcooling of the liquid = $h_{fg} + 0.68\ c_{\ell}\ (T_s - T_w)$
k	thermal conductivity of condensing block
k_{ℓ}	thermal conductivity of liquid
L	condenser plate length
M	molecular weight
P_v	bulk saturation pressure of the vapor
P_s	saturation pressure which corresponds to liquid surface temperature T_s
q/A	measured heat flux for test condenser
r	radius of thermocouple hole in condensing block
R	universal gas constant
S	standard deviation
T	temperature (identified by subscripts)
W/A	mass flux
x	coordinate, normal to the wall
z	dummy variable
ρ	density
σ	condensation coefficient

μ average distance of thermocouple holes from wall

μ_ℓ dynamic viscosity

Subscripts

cu-ni copper-nickel boundary

i interface

s condensate surface

v vapor

w wall

ℓ liquid

1,2,..n thermocouple hole relative to condensing surface (1 is hole closest to surface)

I. INTRODUCTION

Condensation heat transfer has been studied since the original work of Nusselt in 1916 [1]. Recent measurements for condensation of liquid metals disagreed with the simple Nusselt theory. Although part of the discrepancy may be due to the presence of non-condensable gases, most of the experimenters seriously attempted to eliminate even traces of such gases. It has become clear for liquid metals that the resistance to heat transfer at the liquid-vapor interface is significant, particularly at low pressures. The analysis of this interphase resistance as given by Schrage [2] has been applied to many condensation experiments. The resulting condensation (or accomodation) coefficient is unity at very low pressures but is reported to decrease as pressure increases above some threshold value. This reported dependence of the condensation coefficient on pressure has raised questions about both the accuracy of the reported data and the validity of the basic interphase mass transfer analysis.

Measurements of condensation and evaporation coefficients suggest that as the system becomes successively cleaner, the magnitudes of the coefficients rise toward unity. In the condensation process, the liquid surface is continually being formed from clean condensing vapor. This clean interface, therefore, could also have a condensation coefficient of unity. The results of an error analysis presented here suggest that the condensation coefficient is indeed unity and independent of pressure. Data obtained in this investigation using a copper condensing block for increased precision of measurement substantiates this finding. The previously reported decrease of the condensation coefficient at higher pressure is explained on the basis of precision of measurement.

II. THEORY

Figure 1 shows schematically saturated vapor condensing on a surface. From experiment, the temperatures of the cold wall (T_w), the temperature of the saturated vapor far from the condensate (T_v), and the heat flux (q/A) are determined. From these measured quantities, the temperature at the free surface of the condensate (T_s), the temperature of the subcooled vapor (T_i), and the condensation coefficient (σ) can be calculated.

For vertical plates, T_s is obtained from a modified Nusselt analysis as presented in [3]:

$$q/A = 0.943 \sqrt[4]{\frac{\rho_\ell \, g(\rho_\ell - \rho_v)(k_\ell)^3 h'_{fg}}{L(\mu_\ell)}} \, (T_s - T_w)^{0.75} \qquad (1)$$

This analysis neglects momentum effects, shear stress on the liquid surface assuming a stagnant vapor, and the curvature in the actual temperature distribution through the film. Since consideration of these effects would change the calculated value of $(T_s - T_w)$ by less than 1%, equation (1) was used without correction.

In addition to the heat transfer resistance through the film, there is an interphase mass transfer resistance. The interphase mass transfer resistance is the predominant resistance in the experiments performed in this investigation. A kinetic theory analysis of this resistance is presented by Schrage [2] and leads to the following equation for the net mass flux toward the interface:

$$W/A = \frac{2\sigma}{2 - \sigma} \sqrt{\frac{M}{2\pi R}} \left[\frac{P_v}{\sqrt{T_i}} - \frac{P_s}{\sqrt{T_s}} \right] \qquad (2)$$

The derivation of this equation is based on a kinetic theory estimation of both the mass flow of vapor at pressure P_v and temperature T_i toward the interface and also the mass flow due to evaporation from the liquid surface at T_s. Under equilibrium conditions the evaporation rate from the surface is calculated using the saturation pressure P_s corresponding to T_s. It is assumed in the Schrage analysis that this same rate of evaporation does occur from the liquid at T_s even when the vapor is at P_v and T_i.

The theory allows for the possibility of some of the molecules being reflected; therefore, the mass of vapor which condenses is equal to the mass of molecules which strike the surface multiplied by the condensation (or accomodation) coefficient σ. The mass of liquid which evaporates is the amount estimated from kinetic theory multiplied by the evaporation coefficient σ_E. At equilibrium $\sigma = \sigma_E$. It is further assumed that at non-equilibrium, when net condensation occurs, σ is also equal to σ_E. These assumptions lead to Eq. (2).

A number of investigators [4], [5], [6], [7] have reviewed the interphase mass transfer process, and some have attempted to eliminate the simplifying assumptions embodied in the Schrage equation. The results of these studies produce only small corrections and lead to the conclusion that Eq. (2) adequately describes the process for condensation problems. The results of the present investigation suggest that σ, calculated from Eq. (2), equals unity at all pressures during condensation.

By defining $\Delta P = P_v - P_s$ and $\Delta T = T_i - T_s$, the "driving force" term in Eq. (2) may be rewritten as follows:

$$\left[\frac{P_v}{\sqrt{T_i}} - \frac{P_s}{\sqrt{T_s}}\right] = \frac{P_s}{\sqrt{T_i}}\left[1 + \frac{\Delta P}{P_s} - \left(1 + \frac{\Delta T}{T_s}\right)^{1/2}\right]$$

By expanding $(1 + \frac{\Delta T}{T_s})^{1/2}$ in a binomial series and setting higher order terms equal to zero, the following expression results:

$$\left[\frac{P_v}{\sqrt{T_i}} - \frac{P_s}{\sqrt{T_s}}\right] = \frac{P_s}{\sqrt{T_i}}\left[\frac{\Delta P}{P_s} - \frac{\Delta T}{2T_s}\right]$$

For most fluids and for liquid metals in particular, $\Delta T/2T_s$ is small compared with $\Delta P/P_s$ and hence may be neglected.

	$\left[\frac{\Delta T/2T_s}{\Delta P/P_s}\right]$	P_v(ATM.)
Potassium	0.03 - 0.05	0.001 - 1.0
Sodium	0.03 - 0.05	0.001 - 1.0
Mercury	0.03 - 0.04	0.001 - 1.0
Water	0.03 - 0.04	0.006 - 1.0

In the above calculation, ΔT was taken as $(T_v - T_s)$ which is greater than $(T_i - T_s)$; hence, the significance of $\Delta T/2T_s$ is even less than shown above. Realizing that $T_i \simeq T_s \simeq T_v$, $\sqrt{T_i}$ in Eq. (2) may be replaced with either $\sqrt{T_s}$ or $\sqrt{T_v}$ as an excellent approximation.

The above simplification permits Eq. (2) to be written as:

$$W/A = \frac{2\sigma}{2 - \sigma}\sqrt{\frac{M}{2\pi R T_v}}\,(P_v - P_s) \qquad (3)$$

A simple heat balance yields the relation between (W/A) and (q/A):

$$q/A = (W/A)(h'_{fg}) \qquad (4)$$

Since the saturation pressures P_v and P_s are functions of T_v and T_s respectively, Eq. (3) can be handled as a heat transfer resistance

by eliminating (W/A) using Eq. (4). The heat transfer resistance is then the sum of the two series resistances represented by Eq. (1) and Eqs. (3) and (4).

III. EXPERIMENTAL APPARATUS

The natural convection loop (Fig. 2), containing 2.5 lbs. of potassium, consists of a boiler, test condenser, second condenser, and return line. The basic loop was fabricated from seamless, type 304 stainless steel tubing.

3.1 Test Condenser

The test condenser is the most critical element in the system. The ability to measure with precision the temperature of the cold condenser wall is critical and is a function of the test condenser design. The test condenser consists of copper and stainless steel elements as shown in Fig. 3. After the elements were brazed together, the condensing surface was ground to a finish of 16AA and then plated with 0.0017 inches of nickel. This thickness of nickel plating was measured with a Magne-Gage to a tolerance of ±10%. The six thermocouple holes (Fig. 3) of 0.023 inch radius were drilled through the 2 inch wide, copper condenser. The positions of these holes were measured on a traversing microscope.

In operation, the test condenser was cooled by passing silicone oil through a 1/4 inch copper tube which was welded to the 0.5 inch copper block (Fig. 3). This copper block insured that the stainless steel resistance block would see a heat sink of uniform temperature.

3.2 Second Condenser

The apparatus also included a second condenser (Fig. 2) with which net velocities of various magnitudes could be generated over the test surface. This second condenser consisted of a stainless steel tube

welded to the far leg of the loop. By varying the velocity over the test surface as described in [8], one can determine whether non-condensable gas is accumulating at the test surface and affecting the experimental results. By measuring both the flow rate of silicone oil to the condenser as well as the inlet and outlet oil temperatures, the net heat extracted by the second condenser was determined. The mass of potassium vapor condensed was then determined by dividing the net heat extracted by the latent heat. Since the vapor which condensed at this condenser traveled through the test section region on its way from the boiler to the second condenser, a net velocity was generated over the test surface.

3.3 Thermocouples

All temperatures were measured with chromel-alumel thermocouples. All thermocouples were made from 28-gage wire from the same spool and heat treated at 750 °F for one hour to remove inhomogeneity due to cold working of the wire. (Cold working recovery temperature range for chromel-alumel is 500 °F to 1000 °F.) The thermocouple wire was continuous from the hot junction (chromel-alumel) to the cold junctions (chromel-copper and alumel-copper). From the cold junctions, which were in an ice bath, copper leads ran by means of a selector switch to a Leeds and Northrup K-2 Potentiometer which is capable of reading to ±2 microvolts.

Vapor temperature was obtained by inserting a thermocouple into a well which protruded into the vapor. The reported vapor temperature (T_v) was obtained by averaging the temperatures from the thermocouple wells near the test section. Three thermocouple wells were used during Series 1 and 2. Three additional wells were installed after Series 2; therefore, six wells were used to obtain T_v in Series 3. Temperature

readings from all wells generally were within ±0.30 deg. F.

The temperature of the vertical, condensing wall (T_w) was obtained indirectly by measuring the temperature at six locations in the condensing block. Tests showed that cooling of the chromel-alumel junction by conduction along the thermocouple leads was negligible as long as the junction was inserted at least 0.50 inches into the block. The six thermocouples were inserted 1.1 inches for all experiments. Using the position of the centerline of each hole and the temperature of the thermocouple junction in each hole, a straight line was fit to these data by the Method of Least Squares. From this line, the temperature of the copper-nickel boundary was obtained, and then by considering the thickness and conductivity of the nickel plating, the temperature of the condensing wall was calculated. The temperature of the condensate at the liquid-vapor interface was then calculated from Eq. (1).

From the slope of the line and the conductivity of copper, the heat flux (q/A) was obtained. Heat leakage into the copper block from the stainless steel mount was calculated using a conduction node method and found to be negligible.

IV. OPERATING PROCEDURE

While the boiler was being brought up to temperature, the argon atmosphere in the loop was evacuated by a mechanical vacuum pump. Boiling occurred at approximately 600 °F. Since the vacuum pump was connected via an external condenser to the loop, potassium vapor was initially permitted to exit from the loop. After approximately 20 minutes of boiling, the valve which isolated the loop from the vacuum system was closed. After the system reached equilibrium, data were taken. When two successive readings of the vapor and block temperatures agreed within 3 microvolts, the data qualified as an acceptable "Run". This is equivalent to less than 3 microvolts change in 2 minutes. Once a "Run" had been recorded, the boiler voltage was increased and another test condition approached. Each "Run" took an average of 1-1/2 hours.

V. SAMPLE-DATA AND CALCULATED RESULTS

Figure 4 and Fig. 5 are graphical presentations of both experimental data and calculated results for Run 3 and Run 18, respectively. The calculations were performed using the properties of [9] and the following saturation pressure-temperature relationship for potassium from [10]:

$$\log_{10} P(\text{atm}) = 4.185 - \frac{7797.6}{T(^{\circ}R)}$$

One can note that both the temperature drop across the nickel plating and the potassium film are small. Under the conditions shown, the main temperature drop is associated with the interphase mass transfer resistance. Since the overall temperature drop ($T_v - T_w$) is small, precision in the determination of T_w is essential. Although a quantitative error analysis will be presented toward the end of this paper, one should note qualitatively the improved accuracy in the determination of T_w due to the shallow slope of the line shown. If one used stainless steel instead of copper, the slope would be approximately twenty times steeper for the same heat flux. In addition, the number of thermocouples used in determining the line as well as both the position and size of hole into which these thermocouples are placed effect the precision of T_w.

VI. GENERAL-DATA AND CALCULATED RESULTS

Table I contains data and calculated results from this investigation. Figure 6 is a plot of Condensation Coefficient vs. Saturation Pressure for these data and the data of others [11-19]. All results were calculated using the properties found in [9]. One can note that at low pressure the data is distributed around a condensation coefficient of unity; whereas, at high pressure there is not only a great deal of scatter but also a general decrease in most data with increasing pressure. A closer analysis of Fig. 6 shows an effect of experimental accuracy. Specifically, the condensation coefficients obtained both by Subbotin [14] and in the present experiments maintain a value closer to unity out to a higher pressure than do the data of others. Subbotin used a copper block protected from his sodium by a thin layer of stainless steel; the present experiments were run with a copper block protected with nickel plating. Others used condensing blocks or condensing tubes made of nickel or stainless steel. The error analysis presented in Section VII predicts the pressure dependence shown in Fig. 6 and demonstrates, a posteriori, that the condensation coefficient is actually unity at all pressures.

When the interphase resistance is small compared to the Nusselt film resistance, inaccuracies in the analysis of the film resistance will have a very large effect on the calculated condensation coefficient. For example, if condensate from the area immediately above the test surface flows onto the test condenser, the film resistance will be larger than predicted by the Nusselt analysis, and therefore the calculated condensation coefficient will be smaller than the actual coefficient.

To avoid concern over the effect of inaccuracies in the analysis of the film resistance, experiments were curtailed in the present investigation when the interphase and Nusselt resistances were of approximately equal magnitude. However, the data of Subbotin [14] at $P_v \simeq 0.8$ atm. were obtained under conditions where the magnitude of the interphase resistance is only 1/4 of the size of the Nusselt film resistance. Although his calculated condensation coefficients at $P_v \simeq 0.8$ atm. are significantly higher than those obtained using nickel or stainless steel condensing blocks, a precise study of the interphase resistance under such conditions is not possible. Although this limitation applies to all the data at $P_v \simeq 0.8$ atm., precise determination of the condensation coefficient using nickel or stainless steel condensing blocks is limited to much lower pressures as will be discussed in Section VII. The relative size of the interphase and film resistances does, however, represent a limitation to the experimental determination of the condensation coefficient from film condensation experiments performed on apparatus designed for high precision.

VII. ERROR ANALYSIS

Although three quantities T_v, T_w, q/A are obtained from experiment and are subject to measurement error, this error analysis considers only errors in measurement of T_w. Unlike T_v which is measured directly, T_w is obtained indirectly and is, therefore, subject to cumulative inaccuracies. Error in q/A have comparatively little effect on the deduced magnitude of the condensation coefficient.

7.1 Sensitivity of σ to errors in $(T_v - T_s)$

Since the temperature at the surface of the condensate T_s is obtained from T_w via Eq. (1), any error in T_w is reflected as an error in T_s. The effect on the calculated condensation coefficient from an error in T_s can be realized using Fig. 7. The three curves shown in Fig. 7 represent three different pressure levels for potassium. As the pressure increases from 0.0055 atm. to 0.22 atm., the value of $(T_v - T_s)$ which gives a calculated value of $\sigma = 1.0$ decreases from 6.5 to 0.3 deg. F for the example shown. In addition, a comparison of the slopes of the three curves shows that the effect on the deduced condensation coefficient from a given temperature measurement error increases with increasing pressure. Associated with each experimental apparatus is a possible experimental error in the determination of $(T_v - T_s)$. Note, that a 1 deg. F error has little effect at low pressure. At high pressure, a 1 deg. F error not only has a tremendous effect on the value of the condensation coefficient but also injects the possibility of obtaining <u>negative</u> value of $(T_v - T_s)$. Although it is possible to obtain $T_s > T_v$, all would recognize that such a result is

due to experimental error. The following analysis is based on the assumption that any data which measures $T_s > T_v$ will remain unreported. Who could get such data published?

7.2 Constant Error for Each Assembly of a System

When a thermocouple is inserted into a condensing block, the exact location and, therefore, the exact temperature of the junction is unknown. It is reasonable to assume that the location of the junction will not change once the thermocouple has been inserted. If a junction of a homogeneous thermocouple is located such that its temperature is greater than the undisturbed temperature at the centerline of the hole, it will always read high. When a new set of thermocouples is inserted, a different set of errors in readings results.

As shown in Table I, the experiments were divided into three Series. Between each Series, all thermocouples were replaced. For any Series, the positions of the thermocouple readings relative to the line obtained using the Least Square Method remained virtually unchanged. For example in Series 1 (Fig. 4), thermocouples 2, 3, and 5 always read below the line and thermocouple 4 always read above the line at all heat fluxes and pressures. When all of the thermocouples were removed and new ones assembled for the data in Fig. 5, a different system characteristic is observed. Here thermocouples 1 and 4 are below and thermocouple 2 is above the Least Square Line.

Since at high temperatures the effect of thermocouple inhomogeneity is always present to a small degree even if the thermocouples have been heat treated, both position and inhomogeneity effects are present in Fig. 4 and Fig. 5. For the copper block, both effects are estimated at

being of the same order of magnitude; however, the effect of position for nickel and stainless steel blocks will be one to two orders of magnitude larger than the effect of inhomogeneity. Since in general inhomogeneity represents a small effect, all thermocouples are assumed to be homogeneous in the following analysis. To analyze both the magnitude of the possible experimental error in the wall temperature and the effect of this error on the condensation coefficient, the following steps will be performed:

(1) Estimate the distribution of possible thermocouple temperature readings in a hole.

(2) Obtain the distribution of possible values of wall temperatures obtained from these readings.

(3) Exclude data which indicate $T_s > T_v$ and then obtain the Expected Value of T_w and Expected Value of σ.

7.3 Distribution of Measured Temperatures in Thermocouple Hole

A typical hole of radius "r" is shown in Fig. 8a with an assumed linear temperature gradient (Fig. 8b) impressed across the hole. The actual position of the hole centerline is $\bar{x}_1$ and the undisturbed temperature at the centerline is $\bar{T}_1$. The bar over any symbol indicates the actual value instead of a measured value. Using the linear temperature gradient (Fig. 8b), the temperature may be related, for purpose of discussion, to position in the hole by the Fourier conduction equation:

$$\bar{x} - \bar{x}_1 = \frac{\bar{T} - \bar{T}_1}{\frac{q/A}{k}} \tag{5}$$

Although the thermocouple reading must lie between the temperatures at +r and -r, its exact magnitude is not known. Each experimenter

assumes, however, that the thermocouple junction lies on the centerline $\bar{x}_1$ and is, therefore, at the temperature $\bar{T}_1$. The error resulting from this assumption is determined by noting that the measured temperature T_1 may assume any of the values shown as $\bar{T}$ in Fig. 8b. The quantity $(T_1 - \bar{T}_1)$ is experimental error in the temperature reading at hole 1. It follows that x_1 is the position corresponding to the measured temperature T_1. After inserting T_1, x_1, and after making Eq. (5) dimensionless by dividing both sides by r, one obtains:

$$\frac{x_1 - \bar{x}_1}{r} = \frac{T_1 - \bar{T}_1}{\frac{q/A}{k} r} \tag{6}$$

It follows that the limits on $\frac{x_1 - \bar{x}_1}{r}$ are:

$$-1 \leq \frac{x_1 - \bar{x}_1}{r} \leq 1$$

In order to specify a distribution of measured temperatures at any hole, a density function representing possible thermocouple locations within the hole is first chosen. By definition, the integral of a density function f(z) between any two limits (a,b) yields the probability that the variable z lies in the interval (a,b). For example,

$$P(a \leq (\frac{x_1 - \bar{x}_1}{r}) \leq b) = \int_a^b f(\frac{x_1 - \bar{x}_1}{r})\, d(\frac{x_1 - \bar{x}_1}{r})$$

may be interpreted as the probility that the thermocouple lies between dimensionless positions a and b within thermocouple hole 1. With Eq. (6), $P(a \leq \frac{x_1 - \bar{x}_1}{r} \leq b)$ may also be interpreted as the probability that the temperature reading lies between T_a and T_b.

Since the exact distribution of possible locations is not known,

a Gaussian density function f(z) was chosen (Fig. 8c) with 99.9% of its area falling between the dimensionless positions +1 and -1. The Gaussian density function is given by:

$$f\left(\frac{x_1 - \bar{x}_1}{r}\right) = \frac{1}{S\sqrt{2\pi}} \; e^{-\left(\frac{x_1 - \bar{x}_1}{r}\right)^2 \frac{1}{2S^2}}$$

where S is the standard deviation obtained from:

$$\int_{-1}^{+1} f\left(\frac{x_1 - \bar{x}_1}{r}\right) d\left(\frac{x_1 - \bar{x}_1}{r}\right) = 0.999$$

This integral is tabulated in terms of S [20] and yields S = 0.31. The interpretation of this standard deviation is as follows: 68% of all possible measurements lie in the range $(x_1 - \bar{x}_1)/r = \pm 0.31$.

7.4 Distribution of Possible Wall Temperature Measurements

The distribution of temperature measurement errors at each hole and the distribution of error resulting around $\bar{T}_w$ are shown schematically in Fig. 9. The actual temperature profile in the block is known from the Fourier conduction equation. Both in the holes and at the wall, the experimental errors are symmetrical about the actual temperature existing at that location. Using the same grouping of variables as given in Fig. 8c, the distribution of $\left(\frac{T_w - \bar{T}_w}{\frac{q/A}{k} r}\right)$ is, according to [21], Gaussian with a mean value of zero and a standard deviation (S_w) given by:

$$S_w = S\sqrt{\frac{1}{n} + \frac{\mu^2}{\sum_{i=1}^{n} (\bar{x}_i - \mu)^2}} \qquad (7)$$

where

$$\mu = \frac{1}{n} \sum_{i=1}^{n} \bar{x}_i$$

n = number of thermocouple holes

$\bar{x}_i$ = distance of "i"th. hole from wall.

The following data were used to evaluate the distribution of wall temperature measurements for three typical systems. The "effective radius" shown is taken equal to twice the actual radius; this larger radius was assumed in an attempt to account conservatively for the distortion of isotherms around a hole. For a hole across which no heat is transferred, the distortion of isotherms causes a temperature difference across the hole equal to twice the difference which would exist if no distortion occurred. The "effective radius" is used in all of the following calculations.

System (Material: k)	Hole	Distance to Wall-Inches	Effective Radius Inches
Present (Copper:210)	1	0.1675	0.046
	2	0.4169	
	3	0.6670	
	4	0.9176	
	5	1.1670	
	6	1.4183	
Kroger [13] (Nickel:28)	1	0.0625	0.062
	2	0.3750	
	3	0.6875	
Meyrial [12] (St.Steel:12)	1	0.125	0.062
	2	0.375	
	3	0.625	

The standard deviation for $\left(\frac{T_1 - \bar{T}_1}{\frac{q/A}{k} r}\right)$ is equal to the standard deviation for $\frac{x_1 - \bar{x}_1}{r}$, namely S. Both S_w, the standard deviation of $\left(\frac{T_w - \bar{T}_w}{\frac{q/A}{k} r}\right)$, and S are given below for the three systems.

System	At Each Hole S	At the Wall S_w(Eq.(7))
Present	0.31	0.26
Kroger [13]	0.31	0.31
Meyrial [12]	0.31	0.37

With the present system of 6 thermocouple holes the possible temperature measurement error at the wall is less than the temperature measurement error in any hole; however, the opposite is true for Meyrial's [12] system of three thermocouple holes. As one would expect, a large number of holes spaced far apart reduces the possible error in the extrapolated temperature at the wall. The comparison shows less than a 50% difference between the three systems from the effects of number and position of holes. The variable $\left(\frac{T_w - \bar{T}_w}{q/A}\right)$ is, however, the meaningful comparison of the three systems. The standard deviation for the variable $\left(\frac{T_w - \bar{T}_w}{q/A}\right)$ is shown below:

System	Standard Deviation of $\left(\frac{T_w - \bar{T}_w}{q/A}\right)$
Present	4.8×10^{-6} (°F)/(BTU/hr ft^2)
Kroger [13]	5.8×10^{-5}
Meyrial [12]	1.6×10^{-4}

Figure 10 shows the resulting distributions for the three systems. The profound differences between the systems are primarily due to the conductivities of the material used in the condensing block. The

present system used copper (k = 210); Kroger used nickel (k = 28); Meyrial used stainless steel (k = 12).

Figure 11 shows that the drop across the condensate $(\overline{T}_s - \overline{T}_w)$ is a very weak function of pressure; therefore, the distribution of temperature errors at the surface of the condensate is identical to the distribution at the wall.

As the pressure increases, the magnitude of $(\overline{T}_v - \overline{T}_s)/(q/A)$ decreases (Fig. 11). Clearly when the probable error in the determination of $(T_w - \overline{T}_w)/(q/A)$ and hence in $(T_s - \overline{T}_s)/(q/A)$ is equal to the magnitude of $(\overline{T}_v - \overline{T}_s)/(q/A)$, the limit of meaningful measurement has certainly been reached. Taking the standard deviation from Fig. 10 as the measure of probable error in $(T_s - \overline{T}_s)/(q/A)$ and equating this to the magnitude of $(\overline{T}_v - \overline{T}_s)/(q/A)$, the upper limit of P_v where meaningful measurements can be made is read from Fig. 11. For the three sets of experiments discussed, this limit is as follows:

Experimenter	"Probable" Error (Fig. 10)	Corresponding P_v (Fig. 11)
Wilcox	4.8×10^{-6} (°F)/(BTU/hr ft^2)	0.27 atm.
Kroger	5.8×10^{-5}	0.011
Meyrial	1.6×10^{-4}	0.0034

Since Kroger [13] and Meyrial's [12] data falls above 0.01 atmospheres, the accuracy of their data as well as any other data which was obtained without exceptional concern with the measurement of T_w is very questionable.

7.5 Exclusion of Data Indicating $T_s > T_v$; Calculation of $E(T_w)$, $E(\sigma)$

A value of unity is now assigned to the actual condensation coefficient $(\overline{\sigma})$. This will be justified a posteriori. One could argue

that the possible experimental error shown in Fig. 10 should simply cause scatter in the data points around a condensation coefficient of unity. However, if all data for which $T_s > T_v$ is assumed to remain unreported, the reported data will yield magnitudes of σ which scatter around a number less than unity. This is shown in Fig. 12 where the magnitude of $\overline{T}_v$ lies within the range of possible magnitudes of T_s. Then the Expected Value of T_s, $E(T_s)$ is not $\overline{T}_s$ but a value somewhat less than $\overline{T}_s$. $E(T_s)$ is determined by dividing the remaining area of the density function below $\overline{T}_v$ in two equal parts as indicated by the vertical line labelled $E[T_s/(q/A)]$ in Fig. 12. Associated with $E(T_s)$ and $\overline{T}_v$ is an Expected Value of the condensation coefficient $E(\sigma)$. It follows that the published data should scatter about $E(\sigma)$ even though $\overline{\sigma} = 1$.

Figure 13 was formulated for the variables in Fig. 12 by using the tabulated properties of a Gaussian density function. Note in Fig. 13 that the higher the precision of one's system (lower magnitude of standard deviation), the closer $E(T_s)$ is to $\overline{T}_s$.

As pressure increases, $(\overline{T}_v - \overline{T}_s)/(q/A)$ decreases rapidly. In general at low pressure $T_v >> T_s$, and it is not possible to measure $T_s > T_v$. At high pressure it is very possible to measure $T_s > T_v$.

The curves of Fig. 14 present the curves of Fig. 13 in terms of the predicted Expected Value of σ, $E(\sigma)$, for the three test systems. $E(\sigma)$ is obtained by evaluating and equating the right hand side of Eq. (3) for the following two sets of conditions: $\sigma = 1$ at $(\overline{P}_v - \overline{P}_s)$ and $\sigma = E(\sigma)$ at $E(\overline{P}_v - P_s)$. This yields:

$$\frac{2E(\sigma)}{2 - E(\sigma)} \; E(\overline{P}_v - P_s) = \frac{2}{2 - 1} (\overline{P}_v - \overline{P}_s)$$

For small differences of $(T_s - \overline{T}_s)$

$$\frac{\overline{P}_v - \overline{P}_s}{\overline{P}_v - P_s} = \frac{\overline{T}_v - \overline{T}_s}{\overline{T}_v - T_s}$$

then

$$\frac{E(\sigma)}{2 - E(\sigma)} = \frac{\overline{T}_v - \overline{T}_s}{E(\overline{T}_v - T_s)} = \frac{\left(\frac{\overline{T}_v - \overline{T}_s}{q/A}\right)}{E\left(\frac{\overline{T}_v - T_s}{q/A}\right)}$$

The curves in Fig. 14 show a strong effect of pressure on $E(\sigma)$ resulting simply from the assumption that data indicating $T_s > T_v$ remain unreported. It is interesting to note that the arguments which have led to $E(\sigma)$ are essentially equivalent to claiming a fixed error in $(\overline{T}_v - T_s)/(q/A)$ for an experimenter. This is readily seen from the approximately horizontal lines shown for [12] and [13] in Fig. 13.

By considering both the distribution of possible wall temperature measurements that remain after the area (Fig. 12) where $T_s > T_v$ is eliminated and the relationship between σ and $(\overline{T}_v - T_s)$, one can estimate where the condensation coefficient data should be concentrated. Figure 15 shows this result for Meyrial's [12] system at two pressures. The probability that data will fall between any two given values of the condensation coefficient is given by the area under the curve between the two values of interest. It follows that the total area under the curve must equal unity. A unit area results for the curves shown if a unit distance on the abscissa is taken as the linear distance between $\sigma = 1$ and $\sigma = 2$. Note that at high pressures one should not expect the remaining data to yield a condensation coefficient close to unity. For example, the curve shown at $P_v = 0.3$ atm. has only 10% of its area

in the range $0.35 \leq \sigma \leq 2.0$. A comparison shows that Meyrial's data (Fig. 14) in the vicinity of $P_v = 0.3$ atm. appear to be concentrated as one would expect using the distribution of Fig. 15.

VIII. EFFECT OF CONDENSING FLUID

A similar error analysis leading to $E(\sigma)$ vs. P_v curves (Fig. 16) for various liquid metals was made for the condensing block geometry and material of Fig. 3 and those of Kroger [13] and of Meyrial [12]. It is observed that the differences between the liquid metals are not very great. Note also that the curves for nickel and stainless steel for the various liquid metals group together as do the data in Fig. 6 taken with stainless steel and nickel blocks. The effect of the hole size and spacing used by the various experimenters would move the predicted curves somewhat; however, the effect of variation in hole size and spacing used by various experimenters would probably not be large compared with the effect of block conductivity.

Since many experimenters are interested in the condensation coefficient of water, this analysis was also run for water. Even with a copper condensing block, Fig. 17 shows the available precision to be marginal. Considering the fact that with water the Nusselt film resistance is approximately 10 to 100 times greater than the interphase resistance for the range and systems shown in Fig. 16, meaningful measurements of the condensation coefficient for water using a standard film condensation experiment appear to be almost impossible to obtain.

IX. EXPERIMENTS USING SECOND CONDENSER

It has been shown (Kroger [22]) that traces of non-condensable gas in a condensing test system tend to collect at the cold surface and drastically reduce the heat transfer at the condensing surface. Experiments were run to determine whether minute quantities of non-condensable gas were accumulating at the test surface and affecting the experimental results. In these experiments, the second condenser (Fig. 2) was cooled with silicone oil and the net heat extracted was calculated. Since this vapor passed through the test section on its way from the boiler to the second condenser, a net velocity was generated over the test surface. This velocity would tend to sweep away the non-condensable gas and minimize its accumulation at the test surface. If the results with and without this net vapor flow are the same, one may conclude that there is probably no non-condensable gas collected at the test surface.

A similar method of preventing accumulation of non-condensable gas was used successfully by Citakoglu and Rose [8] in the study of drop condensation. In the present investigation, data were taken at a P_v of approximately 0.02 atm as shown in Fig. 18. For the data shown at approximately 900 BTU/hr, the "average" velocity through the test section is calculated to be approximately 15 feet/second. No measured effect of vapor flow and hence of non-condensable gas was observed.

X. DISCUSSION

The error analysis presented here is limited to errors resulting in the determination of T_w (and hence T_s and $(T_v - T_s)$) deduced from extrapolation of the readings of thermocouples placed in the cold block at various distances from the condensing surface. It shows clearly the requirement for high precision in the determination of T_s at higher pressures. As pressure is increased the actual magnitude of $\overline{T}_v - \overline{T}_s$ decreases and above some limiting pressure for any system becomes less than the measuring precision of the particular system. The magnitude of this measuring precision is affected by the thermal conductivity of the condensing block material and the thermocouple hole size and spacing. Since hole size and spacing do not vary greatly among test systems, the major effect is that of thermal conductivity.

The analysis shows that above the precision limited pressure, it is possible that T_s can be determined from the measurements to be greater than $\overline{T}_v$. Assuming that such data would not be reported, the Expected Value of σ, $E(\sigma)$, should be less than unity even though the actual value $\overline{\sigma} = 1.0$. Reliance, therefore, should be placed only on those data obtained below the precision limited pressure.

It is interesting to note that the actual magnitude of the heat flux has practically no effect on the precision of the determination of σ. Since for small differences $(P_v - P_s)$ is approximately linear with $(T_v - T_s)$, then from Eq. (3) and Eq. (4) $(T_v - T_s)$ varies linearly with (q/A). In Section 7.4, it is shown that the error $(T_s - \overline{T}_s)/(q/A)$ is a function of only the condenser block design; therefore, the error $(T_s - \overline{T}_s)$ is linear in (q/A) for a given design. The ratio of

$(T_s - \overline{T}_s)/(T_v - T_s)$ is, therefore, independent of q/A. It follows that $E(\sigma)$ is independent of q/A for this analysis.

Although all of the experimenters of Fig. 6 did not determine the wall or condensate surface temperature by placing thermocouples in holes drilled in a condensing block, the requirement of high precision in the determination of the temperature T_s and hence T_w are just as stringent. While the details of the error analysis would differ for the various systems, the results would all suggest curves for $E(\sigma)$ vs. P_v similar to those of Fig. 14.

XI. CONCLUSIONS

1. An error analysis suggests that for each condensing test system there exists an upper limit of pressure above which the precision of measurement required to determine the condensation coefficient (σ) exceeds that of the apparatus.

2. For systems in which the wall surface temperature is determined from measurements within the condensing block, such as in Fig. 3, the precision of measurement depends on the thermal conductivity of the block and the thermocouple hole size and spacing. For the various test systems used, the strongest effect on precision is the thermal conductivity of the test block with high precision resulting from the use of a high thermal conductivity material.

3. Assuming that the actual value of the condensation coefficient is unity ($\overline{\sigma} = 1.0$) and assuming that any data indicating the condensate surface temperature to be higher than the vapor temperature would not be reported, an error analysis of any condensing system would lead to a curve of Expected Value of σ vs. vapor pressure (P_v) which would be unity at low pressures and decreasing below unity at increasing pressures.

4. Experimental data for potassium presented here for a copper condensing block and data previously obtained for a stainless steel block [12] and a nickel block [13] scatter around the curves of $E(\sigma)$ vs. P_v (Fig. 14) predicted by the error analysis which uses an actual value of the condensation coefficient of unity at all pressures.

5. The actual value of the condensation coefficient equals unity for liquid metals at all pressures.

REFERENCES

1. Nusselt, W., Zeitsch. d. Ver. deutsch. Ing., 60, 541 (1916).

2. Schrage, R. W., A Theoretical Study of Interphase Mass Transfer, Columbia University Press, New York (1953).

3. Rohsenow, W. M. and Choi, H. Y., Heat, Mass and Momentum Transfer, Prentice-Hall Inc. (1961).

4. Adt, R. R., "A Study of the Liquid-Vapor Phase Change of Mercury Based on Irreversible Thermodynamics", Ph.D. Thesis, M.I.T., Cambridge, Massachusetts (1967).

5. Bornhorst, W. J., and Hatsopoulos, G. N., "Analysis of a Liquid Vapor Phase Change by the Methods of Irreversible Thermodynamics", ASME Journal of Applied Mechanics, 34E, p. 840, December (1967).

6. Wilhelm, Donald J., "Condensation of Metal Vapors: Mercury and the Kinetic Theory of Condensation", Argonne National Report #6948 (1964).

7. Mills, A. F., "The Condensation of Steam at Low Pressures", Ph.D. Thesis, Technical Report Series No. 6, Issue No. 39, Space Science Laboratory, University of California, Berkeley (1965).

8. Citakoglu, E. and Rose, J. W., "Dropwise Condensation - Some Factors Influencing the Validity of Heat-Transfer Measurements", Int. J. Heat Mass Transfer, 2, p. 523 (1968).

9. Weatherford, W. D., Tyler, J. C., Ku, P. M., Properties of Inorganic Energy-Conversion and Heat-Transfer Fluids for Space Applications, Wadd Technical Report 61-96 (1961).

10. Lemmon, A. W., Deem, H. W., Hall, E. H., and Walling, J. P., "The Thermodynamic and Transport Properties of Potassium," Battelle Memorial Institute.

11. Subbotin, V. I., Ivanovskii, M. N., Sorokin, V. P., and Chulkov, V. A., Teplophizika Vysokih Temperatur, No. 4, p. 616 (1964).

12. Meyrial, P. M., Morin, M. L., and Rohsenow, W. M., "Heat Transfer During Film Condensation of Potassium Vapor on a Horizontal Plate", Report No. 70008-52, Engineering Projects Laboratory, Mass. Inst. of Technology, Cambridge, Mass. (1968).

13. Kroger, D. G., and Rohsenow, W. M., "Film Condensation of Saturated Potassium Vapor", Int. Journal of Heat and Mass Transfer, 10, December (1967).

14. Subbotin, V. I., Bakulin, N. V., Ivanoskii, M. N., and Sorokin, V. P., Teplofizika Vysokih Temperatur, Vol. 5 (1967).

15. Subbotin, V. I., Ivanovskii, M. N., and Milovanov, A. I., "Condensation Coefficient for Mercury", Atomnaya Energia, Vol. 24, No. 2 (1968).

16. Sukhatme, S. and Rohsenow, W. M., "Film Condensation of a Liquid Metal", ASME Journal of Heat Transfer, Vol. 88c, pp. 19-29, February (1966).

17. Misra, B., and Bonilla, C. F., "Heat Transfer in the Condensation of Metal Vapors: Mercury and Sodium up to Atmospheric Pressure", Chem. Engr. Prog. Sym., Ser. 18 52(7) (1965).

18. Barry, R. E., and Balzhiser, R. E., "Condensation of Sodium at High Heat Fluxes", in the Proceedings of 3rd Int. Heat Transfer Conference, Vol. 2, p. 318, Chicago, Illinois (1966).

19. Aladyev, I. T., Kondratyev, N. S., Mukhin, V. A., Mukhin, M. E., Kipshidze, M. E., Parfentyev, I. and Kisselev, J. V., "Film Condensation of Sodium and Potassium Vapor", 3rd Int. Heat Transfer Conference, Chicago, Illinois, Vol. 2, p. 313 (1966).

20. C. R. C. Standard Mathematical Tables, Chemical Rubber Publishing Company, (1961).

21. Hald, A., Statistical Theory with Engineering Application, John Wiley & Sons, Inc., p. 536 (1952).

22. Kroger, D. G., and Rohsenow, W. M., "Condensation Heat Transfer in the Presence of a Non-Condensable Gas", Int. J. Heat Mass Transfer, Vol. 10 (1967).

23. Technical Survey-OFHC Brand Copper, American Metal Climax, Inc. (1961).

24. Kroger, D. G., Mech. E. Thesis, M.I.T. (1965).

25. Roeser, W. F., "Thermoelectric Thermometry," Temperature-Its Measurement and Control in Science and Industry Vol. 1, American Institute of Physics (1941).

26. Potts, J. F. and McElroy, D. L., "The Effects of Cold Working, Heat Treatment, and Oxidation on the Thermal emf of Nickel-Base Thermoelements", Temperature-Its Measurement and Control in Science and Industry Vol. 3-Pt. 2, American Institute of Physics (1941).

27. Potts, J. F. and McElroy, D. L., "Thermocouple Research to 1000 °C-Final Report", Oak Ridge National Laboratory, Oak Ridge, Tenn. (Available from Clearinghouse for Federal Scientific and Technical Information under ORNL #2773).

28. Dahl, A. I., "The Stability of Base-Metal Thermocouples in Air from 800 to 2200 °F", Temperature-Its Measurement and Control in Science and Industry-Vol. 1, American Institute of Physics (1941).

29. Wadsworth, G. P. and Bryan, J. G., Introduction to Probility and Random Variables, McGraw Hill Book Company, Inc., p. 154 (1960).

30. Kreith, F., Principles of Heat Transfer, International Textbook Company, p. 49 (1959).

APPENDIX A

Description of Equipment

A new apparatus was designed and fabricated for this thesis. The apparatus previously used for film condensation experiments with potassium at M.I.T. is described in [12] and [13]. The design objectives for the new apparatus were:

1. increase the accuracy of the condensing wall temperature measurement by one order of magnitude,
2. reduce both the size of the apparatus and the quantity of potassium required thereby making the equipment more manageable and safer, and
3. include the ability to generate a net vapor velocity through the test section. This velocity permitted studies on the possible existence of non-condensable gas in the system.

Basic Loop-General

The final design is shown schematically in Fig. 2 and photographically in Fig. A1. Figure A2 shows the "loop" in an early stage of development. As shown, the natural convection loop consists of a boiler, superheater (in photographs only), test section, second condenser, and return line. The superheater was not used in any of the experiments and will, therefore, not be discussed. Figure A3 shows the relative sizes of the old and new apparatus. The new apparatus requires only 2.5 lbs. of potassium vs. 20 lbs. for the apparatus described in [12]. The basic loop was fabricated from seamless, type 304 stainless steel tubing by Atomic Welding and Fabricating of Cambridge. All welds were made using the

Heliarc Welding Technique. The flanges shown in Fig. 2 could be opened by grinding through the weld. This technique had previously been demonstrated to produce an inexpensive, leak-tight joint. Where it was necessary to use fittings, Swagelok fittings of type 316 stainless steel were employed.

Boiler

The boiler consisted of 6 Watlow, cartridge heaters each rated at 2500 watts at 240 volts. As shown in Fig. 2, the heaters were arranged in two rows with three per row. The three heaters in each row were connected in parallel and connected via a switch to a Variac power supply. Since only one Variac was used for both rows, one could not vary the voltage independently for each row but merely control which row or rows received power. The author, however, always supplied power to both rows. During operation, the maximum voltage required was 80 volts.

A layer of weld metal was deposited on the top of the tube holders as shown in Fig. 2 to promote nucleation. This weld distorted the tubes making it difficult to obtain a good fit between the cartridge heaters and the tubes. Although no problems were encountered with the heaters, future designs should substitute a "sand blast" or other roughening technique for the weld metal approach.

Test Condenser

The test condenser is the most critical element in the system. As discussed in the main part of the thesis, the ability to accurately measure the temperature of the condensing wall is of critical importance and a function of the design of the test section.

The elements making up the test condenser are shown in Fig. 3 and

Fig. A4. The OFHC brand copper and the 304 stainless steel elements were brazed together in a vacuum furnace. The one inch thick block of stainless steel was used to obtain a reasonable heat flux. Figure A5 shows the test section after brazing. The front surface was then ground to a finish of 16AA. The positions of the holes into which the six thermocouples were inserted were measured on a traversing microscope both before brazing and again after the grinding. The positions of the holes relative to the ground, copper surface are given below:

Hole Number	Distance to Ground Copper Surface
1	0.1675 (inches)
2	0.4169
3	0.6670
4	0.9176
5	1.1670
6	1.4183

The thermal conductivity of OFHC brand copper, obtained from [23], is as follows:

Temperature (°F)	k(BTU/hr ft °F)
775.	213.
890.	207.
1042.	203.

A curve was fit to this data. "k" was then evaluated for each "Run" at the mean temperature of the condensing block and used in calculating the heat flux (q/A).

The test section was plated with nickel; however, only the thickness of the nickel plate on the front, copper surface was specified as

critical. This was measured at 0.0017 inches with a Magne-Gage. The Magne-Gage had been calibrated against standards, and the measurement is considered to be accurate within ±10%. The nickel plate was required only to prevent corrosion of the copper by the potassium. The plating of the additional copper in the test section eliminated oxidation of the copper at high temperatures. Hydrogen was outgassed from the nickel plating by heating the test section in air to a level of 600 °F at the rate of 100 deg. F/hour. The thermal conductivity of the nickel plating was obtained from [24]. Thermal conductivity of Nickel = 17.58 + 0.01278(T °F) where T > 690 °F. The nickel conductivity was evaluated at the temperature of the copper-nickel interface. The test section was mounted by welding the stainless steel holder to the stainless steel loop. In operation, the test condenser was cooled by passing silicone oil through a 1/4 inch copper tube which was copper welded to the short copper block shown in Fig. 3. The short copper block insured that the stainless steel resistance block would see a heat sink of uniform temperature. Flow rate of the silicone oil was measured with a 1/2" Fisher-Porter Rotameter, and the inlet and outlet oil temperatures were recorded with thermocouples. These data were used as a rough check on the heat flux obtained from the gradient in the copper block.

A tube was mounted in the loop directly opposite the condensing surface. This tube could be opened with a tubing cutter thus allowing one to visually inspect the condition of the nickel plating. This inspection could be performed with potassium in the loop by maintaining a net flow of argon out the open tube. Upon completion of the inspection, the tube was then welded closed. The nickel plating was inspected after each "Series" and found in excellent condition.

Second Condenser

In order to generate a net velocity of potassium vapor over the condensing surface, a second condenser was employed. This condenser consisted simply of a stainless steel tube welded to the far leg of the loop. When silicone oil was passed through the tube, condensation resulted. The potassium vapor required for the second condenser was generated in the boiler and passed over the test condenser on its way to the second condenser. The flow rate of silicone oil was measured with a 1/4" Fisher-Porter Rotameter. The inlet and outlet temperatures of the silicone oil were obtained from thermocouples. With the properties of the silicone oil, one could calculate the net heat being extracted through the second condenser and thereby obtain the net condensation rate of potassium at the second condenser.

Thermocouple Wells

All thermocouple wells were fabricated from 3/16 O.D. x 0.042 inch wall or 3/32 O.D. x 0.020 inch wall, type 304 stainless steel tubing. The lengths varied as shown in EPL drawing 20119-2.

Argon Supply

Except during experiments, the loop was maintained under 20 psig of dry argon. 99.996% argon (welding grade) was dried by passing it through a molecular sieve bed containing pellets of alkali metal aluminasilicate maintained at liquid nitrogen temperature before exposing it to the loop.

Vacuum System

Before running an experiment, it was necessary to evacuate the

loop. This was accomplished with a Duo Seal, mechanical vacuum pump capable of yielding an absolute pressure of less than 0.1 microns. Inert gas which was being evacuated from the loop passed through a Hoke Bellows Valve-Type 4333V8Y and through a water cooled condenser to the vacuum pump. To avoid plugging problems encountered by other experimenters, a 3/4 inch O.D. x .049 inch wall exhaust line was used between the loop and external condenser. The Bellows Valve had a 5/16 inch orifice and was capable of operation at 1200 °F. Plugging of both smaller orifice valves and valves sealed with Teflon (max. temperature limit of 500 °F) caused previous investigators many problems.

The water cooled condenser condensed any potassium vapor that was drawn out of the loop. Since the valve remained open while the system was being brought up to temperature, potassium vapor did enter the external condenser.

Approach to Auxiliary Equipment

All auxiliary equipment lines were supplied to the loop through a stationary top as shown in Fig. A6. This approach significantly improved the flexibility of the equipment. After all heaters, thermocouples, insulation, etc. were in place (Fig. A7), a protective drum was hoisted into position and bolted to the stationary top (Fig. A8). In addition to protecting against any leakage of potassium, the drum permitted an environment of argon to be charged between the drum and loop. The argon would be useful in eliminating oxidation of the loop at high temperatures.

Cleaning the System

The original system was cleaned as described in [12].

Charging the Apparatus with Potassium

In order to charge the apparatus, the supply port of a potassium supply reservoir was connected through a feed line to the supply port at the base of the apparatus. The apparatus was heated to 400 °F. The feed line was heated to 300 °F by wrapping it with heating tapes. The reservoir was heated to 240 °F with band heaters. During the heating period, the apparatus was maintained under vacuum, and the reservoir was held under 5 psig of argon. After these temperatures were obtained, the supply port valve on the reservoir was opened. Thermocouple #1 of Fig. 2 was monitored. When the potassium, which was 160 deg. F colder than the apparatus, reached the level of thermocouple #1, the reading from this thermocouple dropped quickly. Thermocouple #2 was then monitored until the same phenomena occurred. When the potassium reached the level of thermocouple #6, the valve was closed. It took 3 hours to reach the desired temperatures and 5 minutes to supply the 2.5 lbs. of potassium desired.

The loop was then charged with argon. After the system had reached room temperature, the reservoir was disconnected from the apparatus and the supply port on the apparatus was capped.

APPENDIX B

Tabulated Data and Results

TABLE I

TABULATED RESULTS

Series No.	Run No.	T_v (°F)	T_s (°F)	T_w (°F)	$T_{cu\text{-}ni}$ (°F)	q/A BTU/hr ft^2	σ	P_v (atm)	P_s (atm)	$q_{2nd\ cond}$ (BTU/hr)
1	1	853.76	851.66	851.41	851.21	39,941	0.873	0.0178	0.0174	0.
	2	843.01	841.01	840.77	840.58	38,185	0.920	0.0159	0.0155	818.
	3	856.57	853.81	853.46	853.21	51,687	0.855	0.0183	0.0178	959.
	4	988.32	987.15	986.68	986.39	62,915	0.882	0.0633	0.0626	0.
	5	963.94	962.87	962.44	962.16	59,388	0.981	0.0512	0.0507	940.
	6	981.19	979.98	979.54	979.26	59,754	0.864	0.0595	0.0589	0.
	7	977.61	976.60	976.16	975.88	59,602	0.964	0.0577	0.0572	1523.
	8	864.23	861.99	861.67	861.43	48,799	0.897	0.0198	0.0193	0.
2	9	846.02	843.57	843.28	843.06	44,633	0.885	0.0164	0.0160	0.
	10	852.45	850.09	849.82	849.61	43,100	0.859	0.0175	0.0171	752.
	11	850.71	848.56	848.28	848.07	43,084	0.912	0.0172	0.0168	1010.
	12	853.04	850.38	850.00	849.73	54,884	0.917	0.0176	0.0172	0.
	13	789.11	785.18	784.85	784.60	49,431	0.959	0.0088	0.0084	0.
	14	761.31	756.55	756.25	756.01	47,017	0.975	0.0063	0.0060	0.
	15	915.53	913.65	913.21	912.93	59,815	0.882	0.0328	0.0322	0.
	16	973.07	971.71	971.23	970.93	63,917	0.867	0.0554	0.0548	0.
	17	854.57	852.35	852.07	851.85	44,301	0.894	0.0179	0.0175	0.
3	18	842.26	839.89	839.60	839.37	45,424	0.926	0.0157	0.0154	0.
	19	922.60	920.83	920.51	920.27	48,654	0.785	0.0351	0.0345	0.
	20	990.94	989.88	989.52	989.28	51,719	0.825	0.0647	0.0641	0.
	21	989.38	988.56	988.20	987.96	51,725	0.957	0.0638	0.0634	1091.
	22	1098.18	1097.30	1096.87	1096.61	57,992	0.655	0.1516	0.1506	0.

TABLE II

TABULATED DATA - SHEET I

Series No.	Run No.	Data From Test Condenser (°F)						Data From Vapor (°F)					
		TC1	TC2	TC3	TC4	TC5	TC6	TC7	TC8	TC9	* TC10	* TC11	* TC12
1	1	848.60	844.39	840.61	836.83	832.11	828.75	854.00	854.00	853.28			
	2	838.19	834.02	830.32	826.96	822.29	819.18	843.29	843.29	842.44			
	3	850.00	844.31	839.21	834.79	828.45	824.20	856.81	856.85	856.04			
	4	982.53	975.35	969.19	963.12	955.81	950.67	988.65	988.52	987.80			
	5	958.53	951.78	945.96	940.35	933.29	928.58	964.27	964.14	963.42			
	6	975.61	968.81	962.91	957.17	950.21	945.40	981.51	981.39	980.66			
	7	972.25	965.50	959.55	953.82	946.89	942.17	977.95	977.82	977.05			
	8	858.59	852.94	848.26	843.63	837.97	834.28	864.41	864.41	863.86			
2	9	840.06	835.13	831.60	827.05	822.29	817.44	845.33	845.75	846.99			
	10	846.82	841.89	838.40	834.15	829.56	824.88	851.79	852.21	853.36			
	11	845.20	840.35	836.91	832.75	828.03	823.26	849.92	850.39	851.83			
	12	846.09	840.06	835.51	829.98	823.99	818.42	852.30	852.85	853.96			
	13	781.47	775.81	771.86	766.97	761.69	756.59	788.44	788.87	790.01			
	14	752.97	747.70	744.00	739.32	734.30	729.41	760.63	761.10	762.20			
	15	909.03	902.15	897.30	891.23	884.82	878.44	914.81	915.32	916.47			
	16	966.77	959.34	954.07	947.57	940.60	933.89	972.25	972.85	974.12			
	17	848.98	843.88	840.40	835.89	831.21	826.45	853.96	854.26	855.49			
3	18	836.02	832.31	827.26	822.42	818.38	813.58	842.33	842.29	841.95	842.50	842.04	842.42
	19	916.74	912.49	907.14	902.05	897.51	892.37	922.92	922.84	922.38	922.71	922.16	922.42
	20	985.52	980.93	975.17	969.70	964.86	959.40	991.03	991.07	990.65	991.15	990.61	991.15
	21	984.09	979.71	973.91	968.40	963.52	958.05	989.47	989.47	989.09	989.55	989.18	989.51
	22	1092.31	1087.18	1080.50	1074.40	1068.86	1062.63	1098.32	1098.03	1097.86	1098.36	1097.82	1098.66
Distance**		0.1675	0.4169	0.6670	0.9176	1.1670	1.4183						

* Additional vapor thermocouples installed after Run 17

** Distance from copper-nickel interface (inches)

TABLE III

TABULATED DATA - SHEET 2

Data from Second Condenser (Silicone Oil Coolant)

Run Number	Outlet Temperature (°F)	Inlet Temperature (°F)	Flow Rate lbm/hr	Specific Heat BTU/lbm deg.F	q BTU/hr
1	-	-	0.	0.35	0.
2	238.5	71.5	14.		818.
3	137.5	71.5	41.5		959.
4	-	-	0.		0.
5	280.0	74.0	14.0		940.
6	-	-	0.		0.
7	187.0	74.0	38.5		1523.
8	-	-	0.		0.
9	-	-	0.		0.
10	247.5	71.5	12.2		752.
11	124.5	72.5	55.5		1010.
12	-	-	0.		0.
13	-	-	0.		0.
14	-	-	0.		0.
15	-	-	0.		0.
16	-	-	0.		0.
17	-	-	0.		0.
18	-	-	0.		0.
19	-	-	0.		0.
20	-	-	0.		0.
21	185.5	69.0	27.2		1091.
22	-	-	0.		0.

APPENDIX C

Thermocouple Preparation and Use

The voltage developed by a thermocouple of homogeneous metals is a function of the temperature of its junctions. It is important, therefore, that the "hot junction" and the "cold (reference) junction" actually be at the temperature of the environment to be measured and that the thermocouple be homogeneous.

Depth of Immersion of Junctions

All thermocouples were made by spot welding Leeds & Northrup, 28 gage chromel-alumel thermocouple wire. Each individual wire was insulated with asbestos, and the two wires were jacketed together with glass braid. Since chromel and alumel have high thermal conductivities, it is necessary to insure that conduction down the leads doesn't significantly cool (or heat) the junctions. If conduction down the leads is a problem, the temperature of the junction will be seriously affected by the depth of immersion of the thermocouple. A test was first run to determine if cooling of the hot junction would be a problem in the 2 inch wide test condenser.

A copper block (1" x 2" x 5") was used for this test. A 0.046 inch diameter hole was drilled through the 2 inch wide block. The copper block was then insulated on all but one side, and the non-insulated side was exposed to the inside of a high temperature oven. After heating the block to 750 °F, the output of a homogeneous thermocouple was recorded as the thermocouple was traversed through the hole in the block. If conduction down the leads was a problem, the recorded thermocouple temperature would increase as the thermocouple was traversed

deeper into the block. Figure C1 shows that the effect of conduction cooling of the hot junction is insignificant except within 1/2 inch of the edge of the block. The six thermocouples used in the test condenser were, therefore, inserted 1.1 inches for all experiments.

The "hot junctions" used to measure the vapor temperature were inserted in wells which varied in length from 1.6 to 4.5 inches. Based on the previously described test with the copper block, no immersion problem was anticipated. Since no consistent difference was observed between temperature readings from the 1.6 and 4.5 inch wells, no immersion problem existed.

The "cold junctions" were maintained at the melting temperature of ice. The "cold junctions" were inserted tightly in glass tubes which were then inserted 9 inches into a bath of crushed ice and distilled water. No immersion problem was encountered with the "cold junctions".

Homogeneity

A homogeneous thermocouple is one whose emf output is only a function of the temperature of its junctions; whereas, the emf output for an inhomogeneous thermocouple depends also on the temperature distribution encountered by the inhomogeneous portion of the wires. Figure C2 shows the response obtained for two "as received" chromel-alumel thermocouples which were simultaneously traversed through two neighboring holes in the previously described copper block. The thermocouples were stationary in the 750 °F block for several hours before being traversed. Note in Fig. C2 that the deeper the thermocouples were traversed into the block, the lower the temperature reading that resulted! In addition, analysis of Fig. C2 implies that two temperature

profiles existed simultaneously in the well insulated, copper block!

The basic explanation for this anomaly is that the "as received" wires were not homogeneous. The portion of the wire that remained above approximately 500 °F received a stabilizing heat treatment which made it homogeneous. When the thermocouples were traversed in the block, the composition of the wire in the temperature gradient changed and, therefore, the emf output also changed. The wire always passes through a temperature gradient since it must go from the hot, copper block to the ice bath. Although the data is not included here, similar inhomogenities were encountered with tests on Conax, sheathed thermocouples.

One can visualize an inhomogeneous wire as one that is composed of short sections of wires of different compositions. Each junction between these hypothetical wires acts like a thermocouple. As long as all the junctions are at the same temperature, no emf is generated. Once the junctions assume different temperatures, an emf is generated. Both a temperature gradient and inhomogeneous wire are required to cause a spurious emf. Since corrections for inhomogeneities are impractical, it is necessary to minimize or eliminate the inhomogeneities. Much work has been performed in this general area. Some of the results of these studies as well as some general information which the author found particularly helpful are presented below.

Fundamental Laws of Thermoelectric Thermometry from [25]:

"1. The Law of the Homogeneous Circuit. An electric current cannot be sustained in a circuit of a single homogeneous metal, however varying in section, by the application of heat alone.

2. Law of Intermediate Metals. If in any circuit of solid conductors

the temperature is uniform from any point P through all the conducting matter to a point Q, the algebraic sum of the thermoelectromotive forces in the entire circuit is totally independent of this intermediate matter, and is the same as if P and Q were put in contact.

3. Law of Successive or Intermediate Temperatures. The thermal emf developed by any thermocouple of homogeneous metals with its junctions at any two temperatures T_1 and T_3 is the algebraic sum of the emf of the thermocouple with one junction at T_1 and the other at any other temperature T_2 and the emf of the same thermocouple with its junctions at T_2 and T_3."

Effect of Cold Working

An extensive study on the effect of cold working was undertaken by Potts and McElroy [26]. The following are quotations for [26]:

"An inhomogeneity may be due to a variation of the mechanical state or of the chemical composition of a wire along its length."

"Commercial thermocouple wire in the as-received state was found to be cold worked to the extent of 2 to 5%, causing an error of 3 °C at 300 °C."

"Proper heat treatment of Chromel-P-Alumel will yield thermocouples stable to within ±1/2 °C at 400 °C."

"These results indicate that the heat-treated wire is stable at a maximum temperature not exceeding the heat-treating temperature..."

"The temperature ranges for recovery and recrystallization were found to be 250 to 450 °C and 500 to 750 °C, respectively, for the alloys studied."

"In the temperature range of interest for the alloys under study,

both recovery and recrystallization of cold-worked metal occur. Both phenomena are nucleation and growth processes and their completion is dependent on time, temperature, and the original amount of cold work for each material."

"Effects attributable to cold working, recovery, recrystallization and alloying were studied by measuring hardness, electrical resistivity, and thermal emf."

The following quotations are from a more detailed report [27] written by Potts and McElroy on the same work described in [26]:

"Two notable metallurgical processes involved in producing a homegeneous mechanical state in a metal in the temperature range of interest are the recovery and recrystallization of the cold worked metal. Recovery is characterized by a restoration of the electrical and magnetic properties of the cold-worked metal to those of an annealed metal, with no observed change in the metal microstructure or other mechanical properties."

"The recrystallization of a cold-worked metal begins at a higher temperature than recovery does. It is characterized by the growth of new strain-free grains in partially recovered metal with a restoration of the mechanical properties characteristic of the annealed metal."

"Heat treatment designed to produce the recovered state in originally cold worked material causes a recovery of nearly 90% of the error induced by cold working in Chromel-P and somewhat less in Alumel, principally because the initial change in Alumel is less."

Effect of Oxidation

According to data presented by Dahl [28], oxidation of chromel-

alumel thermocouples at temperatures below 1000 °F for exposures of 24 hours is insignificant; however, Dahl shows that higher temperatures and longer exposures can cause changes in the calibration of chromel-alumel thermocouples. The following quotations are from [28]:

"All base metal thermocouples become inhomogeneous with use at high temperatures."

"The results of the immersion tests emphasize the importance of never decreasing the depth of immersion of a thermocouple after it has once been placed in service. The practice of using a single base-metal thermocouple for high-temperature measurements in a number of different installations should be avoided. It is even difficult to obtain consistent and accurate results by using a thermocouple in a single installation if the couple is withdrawn and replaced between periods of service. The results obtained by removing a used base-metal couple from an installation to determine the corrections to the original calibration by testing it in a laboratory furnace are unreliable. The temperature gradients in the two furnaces usually differ widely, and hence the results will not be applicable to the actual service conditions."

Based on information available in the literature and on testing, all chromel-alumel thermocouples were heat treated at 750 °F in air for 1 to 1-1/2 hours. The 750 °F temperature is well within the recovery range (480-840 °F) for chromel-alumel. The objective of obtaining thermocouples which were homogeneous was approached by:

(1) taking all thermocouple wire from the same roll thus obtaining uniform chemical composition,

(2) giving all thermocouples the same recovery heat treatment,

(3) handling all thermocouples carefully to avoid additional cold working of the wires, and

(4) avoiding aging (oxidation) effects by replacing thermocouples after each test series. Each of the three series lasted 24 hours; therefore, exposure time was short.

Since most of the data was to be taken between 700 °F and 1000 °F, a "crude" test was run to insure that chromel-alumel wires heat treated at 750 °F for 1 hour were homogeneous at 1000 °F. As shown on the abscissa in Fig. C3, a series of wires were heat treated in air for 1 hour at various temperatures. The wires were then checked for homogeneity at 1000 °F using the test arrangement shown in Fig. C4. Note in Fig. C4 that although the thermocouple passes through the 1000 °F furnace, all junctions are in ice baths. Since with a homogeneous thermocouple the emf developed is a function of the temperature of the junctions and not of the gradients through which the wire passes, the potentiometer would, with a homogeneous thermocouple, always read zero.

Each wire was left as shown in Fig. C4 for approximately 1/2 hour. The wires at Point 1 were then pulled out of the furnace a distance of 3 inches. This replaced the original wires which were in the temperature gradient at Point 1 with wires which had been exposed to 1000 °F. The emf measured after pulling the wires a distance of 3 inches minus the emf measured immediately before pulling the wires is a measure of the inhomogeneity of the original wires. This difference is plotted on the ordinate of Fig. C3. The emf recorded before pulling the wire always corresponded to less than 1/2 deg. F. Due to the symmetry of the temperature gradients at Points 1 and 2, one would not expect a

larger effect.

The average emf at 1000 °F resulting from inhomogeneity for wire heat treated at 750 °F was 8. microvolts (0.3 deg. F) vs. 122. microvolts (5.3 deg. F) for "as received" wire. The 750 °F heat treatment was chosen since it is suitable for use at 1000 °F and since the insulation on the thermocouples was only weakened but not destroyed at 750 °F. A more meaningful measure of the accuracy obtainable from these heat treated thermocouples can be obtained by comparing the measured values of the vapor temperature.

Three thermocouples were used to measure T_v in both Series 1 and 2. Six thermocouples were used in Series 3. At approximately 850 °F, the following typical data was obtained:

Series	Run	Vapor Temperatures					
		TC7	TC8	TC9			
1	1	854.00	854.00	853.28			
2	12	852.30	852.85	853.96	TC10	TC11	TC12
3	18	842.33	842.29	841.95	842.50	842.04	842.42

From the above data, the greatest uniformity was obtained from Series 3 with a maximum variation of ±0.27 deg. F. This was followed by a maximum variation of ±.36 deg. F for Series 1 and ±0.83 deg. F for series 2. Calculation of the condensation coefficient was based on the average vapor temperature. No data was excluded in obtaining the average. As one would expect, the condensation coefficients obtained using the average vapor temperature was 0.90 ±0.03. Kroger [13] reports a condensation coefficient of 0.45 at approximately the same pressure that existed during Runs 1, 12 and 18. Converting this difference to a corresponding

temperature, the average vapor temperature reported for Runs 1, 12 and 18 would have to be in error by approximately 4. deg. F to account for the difference.

It is the author's opinion that Series 2 thermocouples did not receive a complete heat treatment. Whereas the insulation on wires from Series 1 and 3 was uniformly white after the heat treatment, the insulation on wires for Series 2 was not. The exposure time in the furnace was increased to 1-1/2 hours for Series 3.

Extra thermocouples were heat treated and sent to Conax Corporation for calibration. The resulting correction was of the order of 7 deg. F at 850 °F. Since this correction was to be applied to all thermocouples, it had a small effect on the calculated value of the condensation coefficient; however, the correction was included for completeness.

APPENDIX D

Simplified Derivation of Temperature Distribution at Wall

In the body of this thesis, the distribution of possible wall temperature measurements for the condensing block is presented assuming a Gaussian distribution of temperature measurements at each thermocouple hole. To demonstrate the steps required to obtain the wall temperature distribution, the following solution was derived for a condensing block with two holes. A cosine function, with its finite limits, was assumed for the distribution of possible temperature measurements in each hole. The cosine function was chosen because it is easier to handle than the Gaussian function.

Equation for T_w as a function of (T_1, T_2, x_1, x_2)

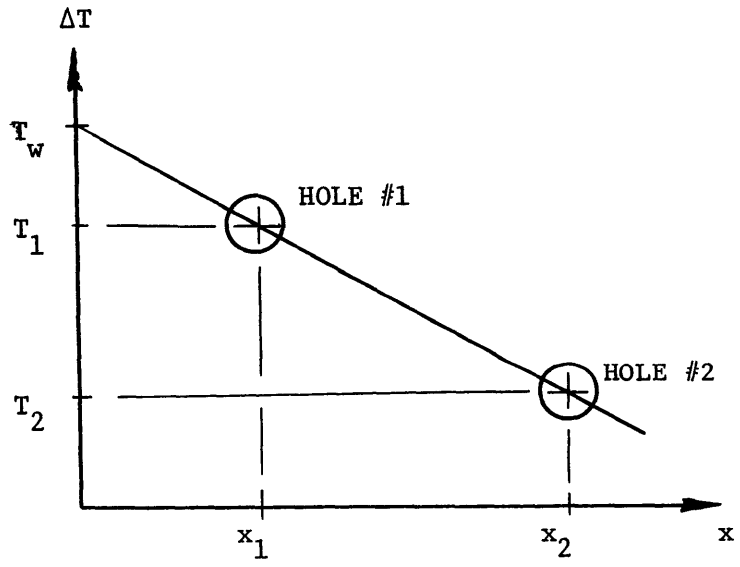

Knowing that the equation for the line shown must be of the form $T = T_w + mx$, one can solve for T_w:

$$T_w = \frac{T_1 x_2 - T_2 x_1}{x_2 - x_1} \qquad \text{(D-1)}$$

Density Function of Possible Errors in Hole #1

By assuming both a linear temperature drop across hole #1 and a cosine density function for the temperature readings at hole #1, one obtains the density function $f_1(T_1)$ as given by (D-2). This density function will also be referred to as the marginal density function of T_1. The limits were obtained by applying the well known Fourier Equation with $\overline{T}_1$ equal to the undisturbed temperature at the centerline of hole #1.

$$f_1(T_1) = \frac{\pi}{4(\frac{q/A}{k})r} \cos\left[\frac{\pi(T_1 - \overline{T}_1)}{2(\frac{q/A}{k})r}\right] \qquad \text{(D-2)}$$

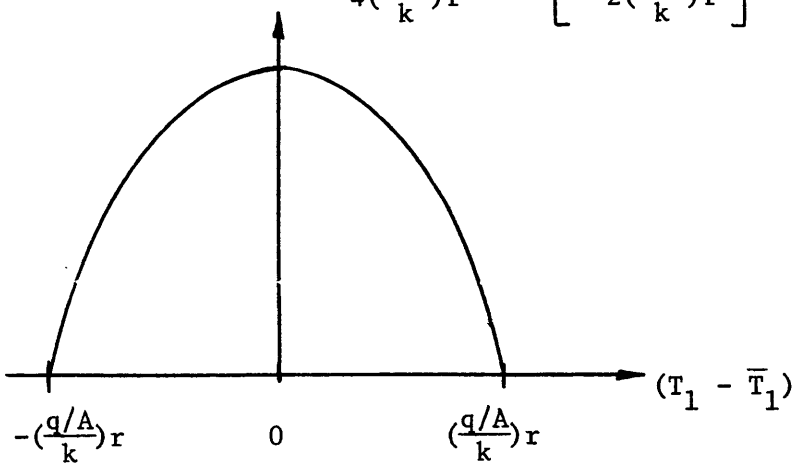

Marginal Density Function of Possible Error at Wall

Setting x_1 and x_2 equal to the known locations of the hole centerlines, the density function $f_3(T_w)$ is obtained by using the approach of [29]. With x_1 and x_2 as constants and T_1 and T_2 as independent variates with known marginal density functions, one imagines T_2 to be held fixed while T_1 varies from $\overline{T}_1 - \frac{(q/A)r}{k}$ to $\overline{T}_1 + \frac{(q/A)r}{k}$. The conditional probability of T_w given T_2, $\phi(T_w \mid T_2)$, is given by:

$$\phi(T_w|T_2) = f_1(T_1)\left|\frac{\partial T_1}{\partial T_w}\right| \qquad \text{(D-3)}$$

From (D-1):

$$T_1 = \frac{T_w(x_2 - x_1) + T_2 x_1}{x_2} \qquad \text{(D-4)}$$

$$\left| \frac{\partial T_1}{\partial T_w} \right| = 1 - \frac{x_1}{x_2} \quad \text{where } x_2 > x_1 \geq 0 \tag{D-5}$$

$$\phi(T_w \mid T_2) = \frac{\pi}{4(\frac{q/A}{k})r} \cos\left[\frac{\pi[T_w(1 - \frac{x_1}{x_2}) + T_2 \frac{x_1}{x_2} - \overline{T}_1]}{2(\frac{q/A}{k})r} \right] (1 - \frac{x_1}{x_2}) \tag{D-6}$$

The joint probability of T_w and T_2 is g (T_w, T_2) which is given by:

$$g\ (T_w, T_2) = \phi(T_w \mid T_2)\ f_2(T_2) \tag{D-7}$$

where

$$f_2(T_2) = \frac{\pi}{4(\frac{q/A}{k})r} \cos\left[\frac{\pi(T_2 - \overline{T}_2)}{2(\frac{q/A}{k})r} \right] \tag{D-8}$$

A map of permissible values of T_2 and T_w is shown below. $\overline{T}_2$ is the undisturbed temperature at the centerline of hole #2, and $\overline{T}_w$ is the actual wall temperature.

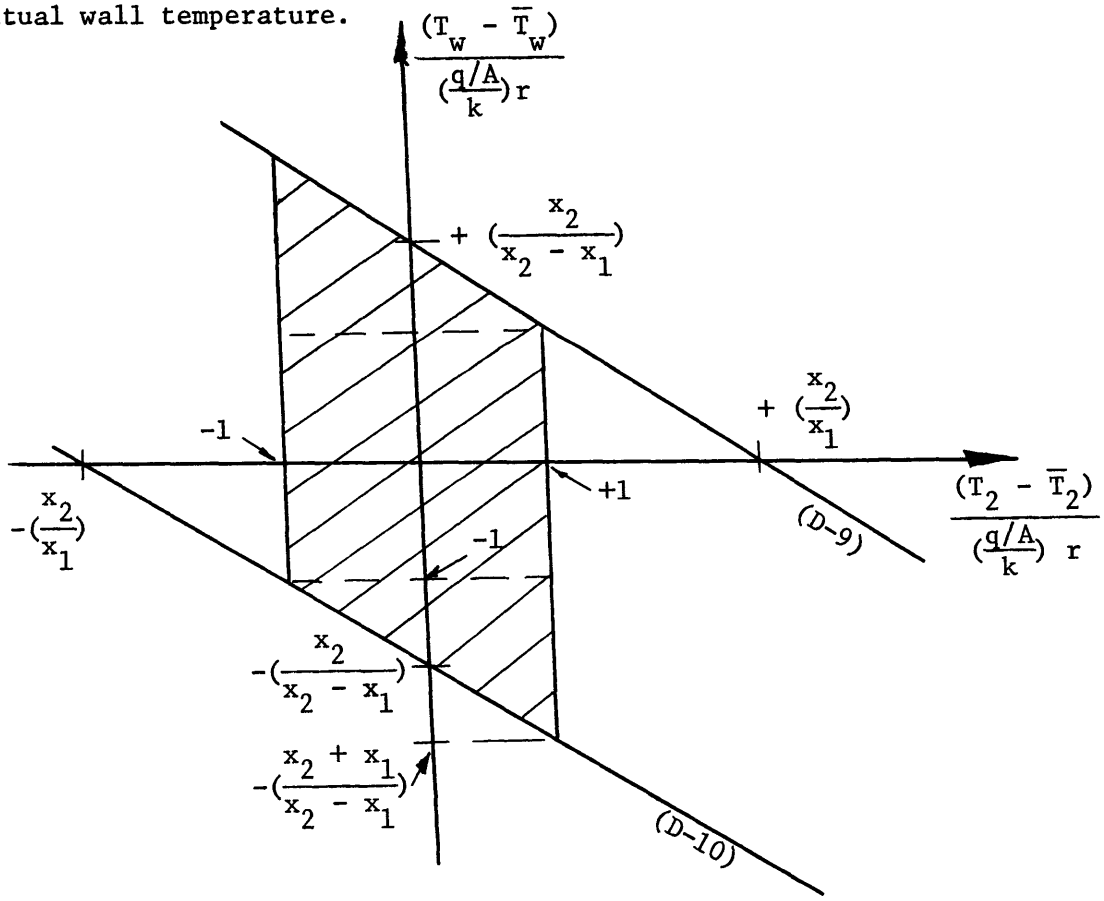

$$\frac{(T_w - \overline{T}_w)}{(\frac{q/A}{k})r} = \frac{x_2}{x_2 - x_1} - (\frac{x_1}{x_2 - x_1}) \frac{(T_2 - \overline{T}_2)}{(\frac{q/A}{k})r} \qquad \text{(D-9)}$$

$$\frac{(T_w - \overline{T}_w)}{(\frac{q/A}{k})r} = \frac{-x_2}{x_2 - x_1} - (\frac{x_1}{x_2 - x_1}) \frac{(T_2 - \overline{T}_2)}{(\frac{q/A}{k})r} \qquad \text{(D-10)}$$

(D-9) was obtained by inserting the maximum permissible value of T_1, namely $\overline{T}_1 + (\frac{q/A}{k})r$, in (D-1) and noting that $\overline{T}_1 = \overline{T}_w - (\frac{q/A}{k})\, x_1$ and that $\overline{T}_2 = \overline{T}_w - (\frac{q/A}{k})\, x_2$. Likewise, (D-10) represents the minimum permissible value of T_1, namely $\overline{T}_1 - (\frac{q/A}{k})r$.

To obtain the marginal density function $f_3\,(T_w)$, one integrates the joint density function $g(T_w, T_2)$ with respect to T_2.

$$f_3(T_w) = \int_{(T_2)_{min.}}^{(T_2)_{max.}} g(T_w, T_2)\, dT_2 \qquad \text{(D-11)}$$

As can be seen from the previous map of permissible values of T_2 and T_w, $f_3\,(T_w)$ can be obtained by performing two integrations and recognizing that $f_3\,(T_w)$ must be symmetrical about $T_w = \overline{T}_w$.

For the following range of $(T_w - \overline{T}_w)$

$$-(\frac{x_2 + x_1}{x_2 - x_1})(\frac{q/A}{k})r \leq (T_w - \overline{T}_w) \leq -(\frac{q/A}{k})r$$

the limits on the integration are

$$\left[(\frac{q/A}{k})r\,\frac{x_2}{x_1} - (\frac{x_2 - x_1}{x_1})(T_w - \overline{T}_w)\right] \leq (T_2 - \overline{T}_2) \leq + (\frac{q/A}{k})r$$

and the results of the integration yield:

$$f_3(T_w) = \left[\frac{\pi}{8r(\frac{q/A}{k})(1 + \frac{x_1}{x_2})}\right]\left(\cos\frac{\pi}{2}\left[\frac{x_1}{x_2} + (\frac{T_w - \overline{T}_w}{\frac{q/A}{k}\,r})(1 - \frac{x_1}{x_2})\right]\right.$$

$$\left. - \frac{x_1}{x_2}\cos\frac{\pi}{2}\left[\frac{x_2}{x_1} - (\frac{T_w - \overline{T}_w}{\frac{q/A}{k}\,r})(1 - \frac{x_1}{x_2})\right]\right) \qquad \text{(D-12)}$$

For the following range of $(T_w - \overline{T}_w)$

$$-(\frac{q/A}{k})r \leq (T_w - \overline{T}_w) \leq 0$$

the limits on the integration are

$$-(\frac{q/A}{k})r \leq (T_2 - \overline{T}_2) \leq +(\frac{q/A}{k})r$$

and the results of the integration yield:

$$f_3(T_w) = \left[\frac{\pi}{4r(\frac{q/A}{k})(1 + \frac{x_1}{x_2})}\right]\cos(\frac{\pi}{2}\frac{x_1}{x_2})\cos\frac{\pi}{2}\left[(1 - \frac{x_1}{x_2})(\frac{T_w - \overline{T}_w}{\frac{q/A}{k}\,r})\right] \qquad \text{(D-13)}$$

It is very interesting to note that wherever T_w appears in (D-12) and (D-13) it appears as part of the dimensionless group $(\frac{T_w - \overline{T}_w}{\frac{q/A}{k}\,r})$. This same group results from the analysis used in the body of this thesis. The following figures show the marginal density function assumed at hole #1 and the resulting marginal density function at the wall. Both are plotted using dimensionless groups. Simply by multiplying (D-12) and (D-13) by $(\frac{q/A}{k}\,r)$, these equations were converted from a function of the variable T_w to a function of the variable $(\frac{T_w - \overline{T}_w}{\frac{q/A}{k}\,r})$.

$$f_1\left(\frac{T_1 - \bar{T}_1}{\frac{q/A}{k} r}\right) = \frac{\pi}{4} \cos\left[\frac{\pi}{2}\left(\frac{T_1 - \bar{T}_1}{\frac{q/A}{k} r}\right)\right]$$

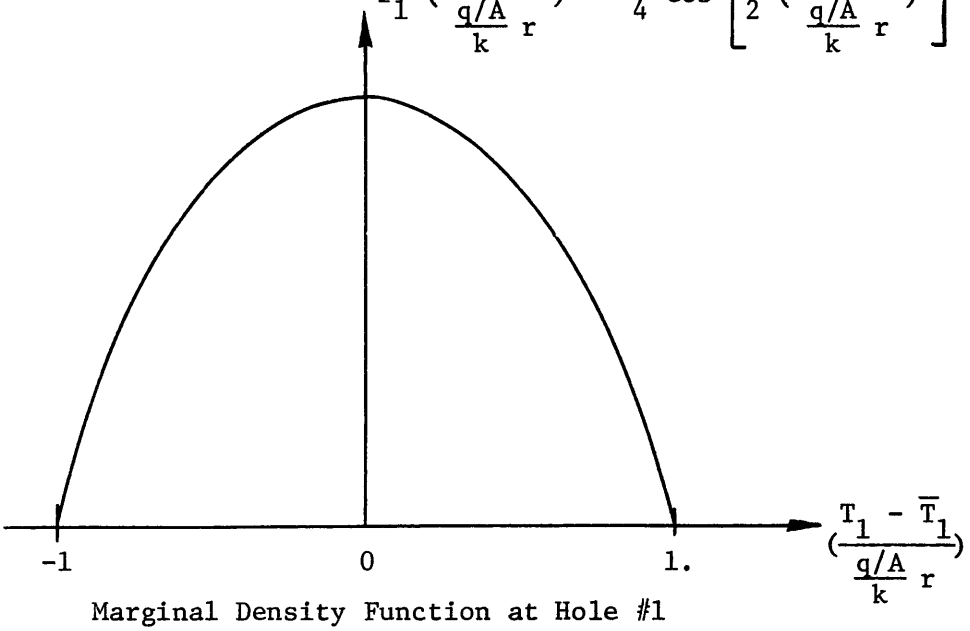

Marginal Density Function at Hole #1

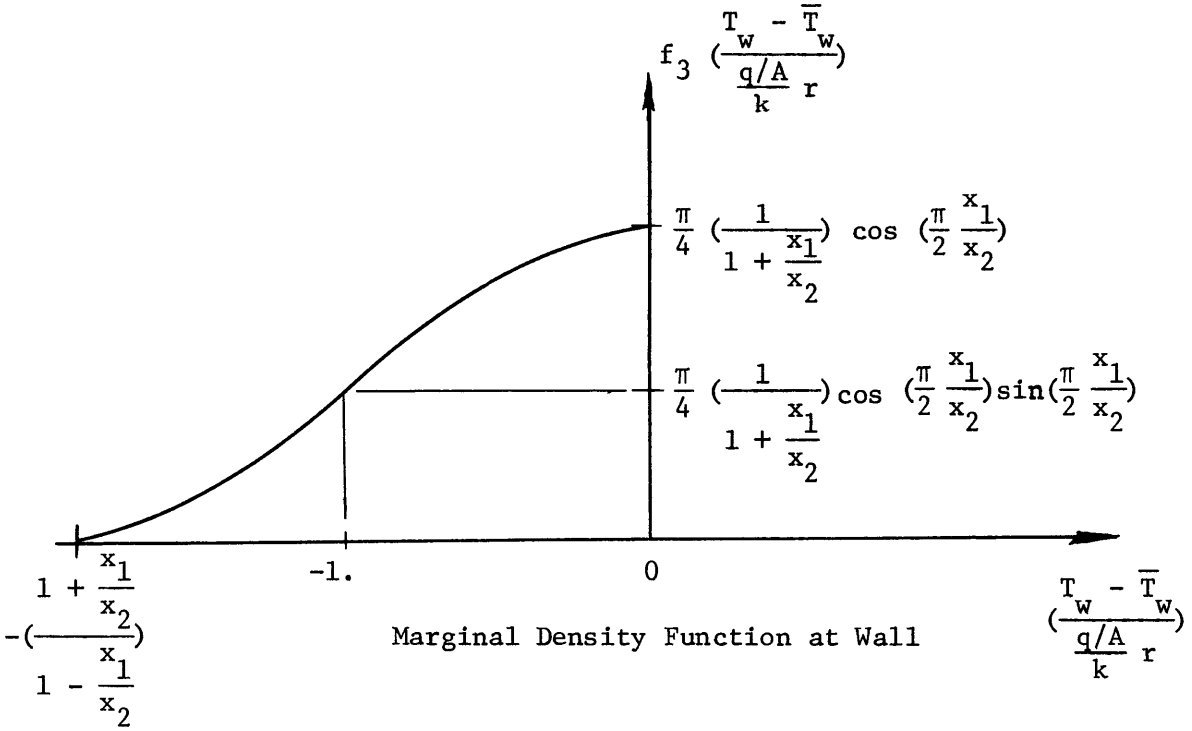

Marginal Density Function at Wall

From the previous limits, one gets:

$$\left|\frac{T_w - \bar{T}_w}{\frac{q/A}{k} r}\right|_{max.} = \frac{1 + \frac{x_1}{x_2}}{1 - \frac{x_1}{x_2}} \qquad \text{(D-14)}$$

From (D-2), one gets:

$$\left|\frac{T_1 - \bar{T}_1}{\frac{q/A}{k} r}\right|_{max.} = 1 \qquad \text{(D-15)}$$

Unless $(\frac{x_1}{x_2}) = \infty$, the maximum error in temperature measurement at the wall is greater than that assumed in a hole at x_1 or x_2. It follows that the first thermocouple hole should be as close to the wall as possible ($x_1 \to 0$) and that the last thermocouple hole should be as far from the wall as possible ($x_2 \to \infty$). By rewriting (D-14) as follows, the powerful effects of material conductivity and hole radius are seen:

$$\left|\frac{T_w - \bar{T}_w}{q/A}\right|_{max.} = \left[\frac{1 + \frac{x_1}{x_2}}{1 - \frac{x_1}{x_2}}\right]\frac{r}{k} \qquad \text{(D-16)}$$

For example, simply by converting to copper (k = 210) from stainless steel (k = 12), one can reduce the possible error in the wall temperature measurement by 1650. %.

Knowing the marginal density function at the wall, one can obtain any statistical parameters of interest. If one had been concerned only with the standard deviation at the wall, this could have been obtained for this linear case without calculating $f_3\ (T_w)$.

Standard Deviation at the Wall

For the linear case, it is easier to obtain the standard deviation

at the wall indirectly by obtaining the standard deviation in a hole and then applying the formula for the variance of a linear function than to obtain it directly by making the necessary integrations using (D-12) and (D-13). The variance of $\left(\frac{T_1 - \bar{T}_1}{\frac{q/A}{k} r}\right)$ is obtained as follows:

$$\text{Variance of } \left[\frac{T_1 - \bar{T}_1}{\frac{q/A}{k} r}\right] = \frac{\pi}{4}\int_{-1}^{1}\left[\frac{T_1 - \bar{T}_1}{\frac{q/A}{k} r}\right]^2 \cos\left[\frac{\pi}{2}\ \frac{T_1 - \bar{T}_1}{\frac{q/A}{k} r}\right] d\left[\frac{T_1 - \bar{T}_1}{\frac{q/A}{k} r}\right] = 0.19$$

By rewriting (D-1) as follows:

$$\left[\frac{T_w - \bar{T}_w}{\frac{q/A}{k} r}\right] = \frac{x_2}{x_2 - x_1}\left[\frac{T_1 - \bar{T}_1}{\frac{q/A}{k} r}\right] - \frac{x_1}{x_2 - x_1}\left[\frac{T_2 - \bar{T}_2}{\frac{q/A}{k} r}\right]$$

the variance at the wall is easily obtained using the formula for the variance of a linear function [29]. This yields:

$$\text{Variance of } \left[\frac{T_w - \bar{T}_w}{\frac{q/A}{k} r}\right] = \left[\frac{x_2}{x_2 - x_1}\right]^2 (\text{Variance}_{\text{Hole 1}}) + \left[\left(\frac{x_1}{x_2 - x_1}\right)\right]^2 (\text{Variance}_{\text{Hole 2}})$$

$$= \frac{1 + \left(\frac{x_1}{x_2}\right)^2}{\left(1 - \frac{x_1}{x_2}\right)} (0.19)$$

$$\text{The standard deviation of } \left[\frac{T_w - \bar{T}_w}{q/A}\right] = \frac{\sqrt{1 + \left(\frac{x_1}{x_2}\right)^2}}{\left(1 - \frac{x_1}{x_2}\right)} (0.436)\ \frac{r}{k} \qquad \text{(D-17)}$$

This result could have been obtained using Eq. (7) from the main body of this thesis with S = 0.436. To apply (D-17) to a condensing block with more than two holes, set x_1 of (D-17) equal to $x_{min.}$ for the

block of interest and set $x_2 = x_{max.}$. Using the information tabulated in Section 7.4 of the body of the thesis, (D-17) was evaluated for the present system and the systems of [12] and [13]. Once again, the "effective radius", which is equal to twice the actual radius, was used to correct for the distortion of isotherms around the hole. The results from (D-17) are compared to the complete results as given in the body of the thesis in the following table. As shown in the table, (D-17) is an excellent approximation to the complete result and is an acceptable estimate of the possible experimental error in wall temperature measurement.

$$\left(\frac{T_w - \bar{T}_w}{q/A}\right) \text{ at 1 St. Dev.}$$

System	2 Hole Result (D-17)	All Hole Result (Eq. 7)
Wilcox	9.1×10^{-6} °F/(BTU/hr ft^2)	4.8×10^{-6}
Kroger [13]	9.2×10^{-5}	5.8×10^{-5}
Meyrial [12]	2.4×10^{-4}	1.6×10^{-4}

APPENDIX E

Additional Analysis of Error

From experiment, the temperature of the cold wall (T_w), the temperature of the saturated vapor far from the condensate (T_v), and the heat flux (q/A) are determined. From these measured quantities, the temperature at the free surface of the condensate (T_s) and the condensation coefficient (σ) are calculated. It has been stated that T_w, which is measured by extrapolation, is generally subject to the greatest experimental error. Since measured temperature differences ($T_v - T_w$) are very small, errors in T_w have a large effect on the calculated condensation coefficient.

Error in Vapor Temperature Measurement Due to Fin Effect

It obviously follows that errors in T_v also have a large effect on the calculated condensation coefficient. Since T_v was measured by inserting a thermocouple into a well which protruded into the vapor, the recorded T_v is actually the temperature of the far end of the well. To compare the temperature at the far end of the well with the temperature of the vapor, the thermocouple well can be modeled as a pin fin protruding from a surface. Neglecting the heat transfer from the end of the fin, [30] gives the following relation between the pertinent variables:

$$\frac{T_v - \bar{T}_v}{T_{w.w.} - \bar{T}_v} = \frac{1}{\cosh(m\ell)} \qquad \text{(E-1)}$$

where T_v = measured temperature from thermocouple in the well

$\bar{T}_v$ = actual vapor temperature

$T_{w.w.}$ = temperature of wall at base of thermocouple well

$m^2 = (h' P') / (k' A')$

h' = heat transfer coefficient between vapor and well

P' = perimeter of well

k' = conductivity of well

A' = cross-sectional area of well

ℓ = length of well

Thermocouples were spot welded to the outside surface of the loop. These thermocouples were located at the base of thermocouple wells which were used to measure the vapor temperature. From these readings, $(T_v - T_{w.w.})_{max.} < 2$ deg. F. For this case (E-1) can therefore be written as follows:

$$(\overline{T}_v - T_v)_{max} < \frac{2}{\cosh(m\ell) - 1} \qquad \text{(E-2)}$$

Since no auxiliary heaters were present in the test section, condensation did take place on the stainless steel wells and, therefore, the applicable h' is that associated with condensation ($h' \sim 20{,}000$ BTU/hr ft^2 °F). Applying (E-2) to the thermocouple wells used in the measurement of the vapor temperature, one obtains a measure of the error $(\overline{T}_v - T_v)$ associated with the fin effect:

Stainless Steel Thermocouple Wells	$(\overline{T}_v - T_v)$ deg. F
3/16 O.D. x 0.042 wall x 1.6 inches	10^{-43}
3/32 O.D. x 0.020 wall x 4.0 inches	10^{-162}

One obviously concludes that the ends of both thermocouple wells are at the actual vapor temperature. This is consistent with the fact

that measured vapor temperatures from the two designs are the same. For the work reported in this thesis, the error in the vapor temperature measurement due to the "fin effect" is completely negligible.

If the walls of the test section had been heated with auxiliary heaters to a temperature above $\overline{T}_v$, the applicable h' to use in (E-1) would not have been that associated with condensation. The applicable h' would have been $\sim$2. BTU/hr ft^2 °F. Using (E-1), a significant wall temperature influence would have been calculated, and a meaningful difference would exist between the two designs.

(q/A) Error - Condensing Block

The actual temperature profile in the block in terms of the formulation of Eq. (7) is:

$$\frac{\overline{T} - \overline{T}_w}{\frac{q/A}{k} r} = -\frac{\overline{x}}{r}$$

where the slope is $(\frac{-1}{r})$. A distribution of "measured slopes" will result from the uncertainty of the temperature measured in a hole as described in Section 7.3. Analysis of the distribution of possible measured slopes resulting from this uncertainty yields, according to [21], that the standard deviation of the slope =

$$S \sqrt{\frac{1}{\sum_{i=1}^{n} (\overline{x}_i - \mu)^2}}$$

where $\mu = \frac{1}{n} \sum_{i=1}^{n} \overline{x}_i$

$\overline{x}_i$ = distance of "i" the hole from wall

n = number of holes

S = standard deviation of distribution in hole.

Using this standard deviation as a measure of the "probable" error, one gets:

$$\text{Probable Error in } (q/A)\ (\%) = \frac{S\sqrt{\frac{1}{\sum_{i=1}^{n} (\bar{x}_i - \mu)^2}}}{\frac{1}{r}} \times 100. \qquad \text{(E-3)}$$

Since the hole positions were measured on a traversing microscope and since the thermal conductivity for OFHC brand copper is well established, assuming these variables to be free from error is reasonable.

For the present system with S = 0.31 and "r" equal to the "effective" radius of 0.046 inches, (E-3) yields a "probable" error in q/A of 1.4%. Roughly speaking, a 1.4% error in (q/A) will cause a (1.4/2)% error in the calculated value of the condensation coefficient. The effect of the (q/A) error for the author's system is not significant.

Temperature Level Error

The effect that would result from a uniform error in all temperature readings due to inaccurate thermocouple wire calibration will now be analyzed. Throughout this thesis it has been argued that accurate measurement of $(T_v - T_s)$ is the key to meaningful data. The following calculated results show the small effect on the condensation coefficient resulting from a 10 deg. F error in the recorded level of all temperatures. Note that $(T_v - T_s)$ remains constant for each set of examples. The heat flux for all nine calculations was 60,000 BTU/hr ft^2. Compare this relatively small effect to the large change in σ from variations in $(T_v - T_s)$ as recorded in Fig. 7. Since the error in temperature level is estimated at less than 1 deg. F, the resulting error in the determination of σ is less than 0.005 due to this effect.

T_v(°F)	T_s(°F)	$(T_v - T_s)$	σ
740.00	733.47	6.53	1.05
750.00	743.47	6.53	1.00
760.00	753.47	6.53	0.95
890.00	888.32	1.68	1.04
900.00	898.32	1.68	1.00
910.00	908.32	1.68	0.96
1140.00	1139.67	0.33	1.03
1150.00	1149.67	0.33	1.00
1160.00	1159.67	0.33	0.97

Nusselt Analysis-Errors

As can be seen from Fig. 11, the resistance of the liquid film is small compared to the interphase resistance except at the highest pressure (0.15 atm.) considered in the author's experiments. At 0.15 atm., the two resistances are equivalent. It follows that minor inaccuracies in the Nusselt analysis will have a very small effect when the Nusselt resistance is small compared to the interphase resistance. Minor modifications of the Nusselt analysis are possible. For example, the effect of momentum and shear stress evaluated according to [3] would increase the resistance of the film by $\sim$1%. Although this and other modifications are possible, the greatest uncertainty appears to be the correct boundary condition to apply at the top of the condensing surface. The Nusselt analysis assumes the film thickness to be zero at the top of the condensing surface. Since in the present equipment

condensation does take place on the walls, the film thickness is not zero at the top of the condensing surface. To avoid having such inaccuracies in the film analysis seriously affect the calculated condensation coefficient, experiments were curtailed at 0.15 atm.

Effect of Variation of T_v on the Condensation Coefficient

As is discussed in Appendix C, there was some variation in the individual vapor temperature readings for each "Run". The magnitude of this variation, which is probably due primarily to the remaining inhomogeneity of the thermocouple wire, seemed to depend on the effectiveness of the heat treatment given to the wires. New thermocouples were fabricated, heat treated and installed for each of the three Series which were run. To show the effect of these variations in T_v, σ was calculated using the individual readings of T_v. The temperature at the surface of the liquid film obtained for the Run was used in the calculations. Figures E1, E2, and E3 show the results from these calculations and the result obtained using the average T_v. The "circled" points in the figures are individual data points, and the "slash" represents the average vapor temperature for the Run. The average vapor temperature was used in the results reported in the body of the thesis. The three figures refer to the three Series which were run.

The sensitivity to accurate determination of T_v or $(T_v - T_s)$ is very evident in the figures. To obtain high confidence in experimental data, one should use the average from a number of thermocouples which measure T_v. In addition, one should have the ability to replace all thermocouples between Series. The variations in σ shown in Fig. E-2 cause little concern because the averaged results agree with the higher

precision results shown in Fig. E1 and E3. Three thermocouple wells were used to measure T_v for Series #1 and #2. Three additional wells were installed after Series #2, and therefore six values of T_v were obtained in Series #3. The resulting σ obtained using the average T_v agree for all three Series.

General Comment on Error

Of all errors, those associated with the measurement of T_w are, in general, predominate. For the author's system, the uncertainty due to the effect of inhomogeneities in the thermocouples is of the same order of magnitude as the uncertainty in the wall temperature measurement (neglecting inhomogeneity). For others who used nickel or stainless steel condensing blocks, the lack of precision in the measurement of T_w dwarfs the inhomogeneity effect; therefore, the effect of inhomogeneity was not discussed in general in the body of the thesis.

APPENDIX F

Additional Information on Effect of Second Condenser

The second condenser (Fig. 2) was used as described in the main body of this thesis to determine whether non-condensable gas was accumulating at the test condenser and significantly affecting the experimental data. In addition to the data taken at ∿0.02 atm. (Fig. 18), data were also taken at ∿0.06 atm. (Fig. F1). Note in Fig. F1 that as the heat extracted at the second condenser increased, the condensation coefficient increased from ∿0.86 to ∿0.96. For the "Runs" shown this corresponds to a change in $(T_v - T_s)$ of less than 0.25 deg. F. Since the effect shown in Fig. F1 is small and since no effect is shown in Fig. 18, it is simply concluded that the effect of non-condensable gas in these experiments was not significant.

APPENDIX G

Listing of Computer Programs

```
PAGE   2                  DATA ANALYSIS PROGRAM NO. 1 (WILCOX)

C      THIS PROGRAM WRITTEN TO PERFORM THE FOLLOWING JOBS
C      CONVERT MILLIVOLT TC OUTPUT TO DEGREE F
C      MAKE LEAST SQUARES FIT STRAIGHT LINE OF TEMP IN BLOCK.
C      COMPUTE HEAT FLUX, SURFACE TEMP,HEAT TRANS COEFF.

       REAL MVLT(40)
       DIMENSION DEV(40),POTC(40),TMP(40),DATA(40),CALB(40),DIST(40)
       DIMENSION Y(40)
       IR=2
       IW=3

C      DATA INPUT

       READ(IR,91) NOPT,NO
 91    FORMAT(2I2)
       DO 10 I=1,NOPT
 10    DIST(I)=0.
       READ(IR,9) (DIST(I),I=1,NO)
 5     READ(IR,9) (MVLT(I),I=1,NOPT)
 9     FORMAT (7F10.0)
       IF(MVLT(1)) 99,99,8
 8     CONTINUE

C      CONVERSION OF MILLIVOLT TC OUTPUT TO DEGREE F

       DO 15 I=1,NOPT
       DATA(I)=MVLT(I)
       MUNIT=MVLT(I)/10.
       VLT=(MVLT(I)/10.)-MUNIT
       CORF=-0.101E- 02+0.100E- 01*VLT-0.272E- 03*VLT**2
      1  +0.315E-03*VLT**3-0.126E- 03*VLT**4
C  POTC IS CORRECTION FOR SLIDE WIRE CALIBRATION ON POTENTIONMETER
       POTC(I)=CORF*10.
       MVLT(I)=(MVLT(I)/10. + CORF)*10.
       TMP(I)= 55.40606 + 42.55409*MVLT(I) -0.00515*(MVLT(I)**2.)
C  NEXT CARD CORRECTS FOR CALIBRATION OF WIRE
       CALB(I)= -1.*(1.7768594 + 0.0063321*TMP(I) )
       TMP(I)=TMP(I) + CALB(I)
 15    CONTINUE

C      LEAST SQUARES FIT OF STRAIGHT LINE TEMP GRADIENT

       DO 18 I=1,NOPT
 18    Y(I)=TMP(I)
       CALL JSHLS(NO,DIST,Y,POIN,SLEP)
       DO 20 I=1,NOPT
       DEV(I) = TMP(I) - (POIN + SLEP*DIST(I))
 20    CONTINUE

C      COMPUTAYION OF HEAT FLUX, SURFACE TEMP,HEAT TRANS COEFF
```

```
      COND=230.42105 - 0.026316*TMP(3)
      HTFX= -12.*COND*SLEP
C     CALCULATES TWALL AND TSAS(SURFACE TEMPERATURE)
      XNCON=(211. + 0.1534*POIN )/12.
      TWALL= POIN - SLEP*0.0017*COND/XNCON
      DENL=52.1666 - 0.007666*TWALL
      DENVA=2.71828**(.00768*TWALL-13.82)
      VISL=0.80197 - 0.0003733*TWALL
      CONDL= 29.2094 - 0.008066*TWALL
      CPLW=0.183
      XLEN=0.0825
       HFG=991.2854-0.101428*TWALL
      TSAS=TWALL+((HTFX   /0.943)**1.333)*((XLEN*VISL/(DENL*4.17312E8*
     1(DENL-DENVA)*(CONDL**3.)*HFG))**.333)
      HFGC=HFG+CPLW*(TSAS-TWALL)*0.375
      TSAS=TWALL+((HTFX   /0.943)**1.333)*((XLEN*VISL/(DENL*4.17312E8*
     1(DENL-DENVA)*(CONDL**3.)*HFGC))**.333)
      DTMP= TMP(NO + 1) - TWALL
      HTC=HTFX/DTMP

C     DATA OUTPUT

      WRITE(IW,33) HTFX,DTMP,HTC
 33   FORMAT (1H1,40X'RUN NO  ', // 10X'HEAT FLUX=',F9.1,10X'TEMP DIF=',
     1F4.2,10X'HEAT TRANS COEFF=',F9.1 // 1X'POSITION NO',5X'DISTANCE',7
     2X'DATA',7X'CORRECTION',3X'MILLIVOLT',8X'CALB(F)',3X'    TEMP(F)
     3 DEVIATION')
      DO 31 I=1,NOPT
 31   WRITE(IW,34) I,DIST(I),DATA(I),POTC(I),MVLT(I),CALB(I),TMP(I),DEV(
     1I)
 34   FORMAT(I7,1F16.4,3(7X,1F7.3),6X,F8.2,6X,F8.2,6X,F8.2)
      WRITE(IW,35) SLEP,POIN
 35   FORMAT (//10X'TEMP = ',F8.2,' X DIST  + ',F8.2)
      WRITE(IW,36) TWALL,XNCON,COND
 36   FORMAT(/10X'TWALL= ',F8.2,10X'NICKEL CONDUCTIVITY=',F8.2,10X'COPPE
     1R CONDUCTIVITY=',F8.2)
      WRITE(IW,37) TSAS ,DENVA,DENL,CONDL,VISL,HFG,HFGC,CPLW
 37   FORMAT(/10X'TSAS=',F8.2,10X'VAPOR DENSITY=',F8.5,10X'LIQUID DENSIT
     1Y= ',F8.2,//10X'CONDUCTIVITY LIQUID=',F5.2,31X'VISCOSITY LIQUID=',
     2F5.3,//10X'HFG=',F8.2,12X'HFG+CP EFFECT=',F8.2,10X'CP LIQUID=',F8.
     35)
      GO TO 5
 99   CALL EXIT
      END

FEATURES SUPPORTED
 IOCS
```

```
PAGE   2                DATA ANALYSIS PROGRAM NO. 2 (WILCOX)

C    THIS PROGRAM WRITTEN TO PERFORM THE FOLLOWING JOBS
C    CALCULATE CONDENSATION COEFFICIENT USING PSAV AND PSAS
C    AND ALSO CALCULATE  A 'COEFFICIENT' USING PSAI AND PSAS.

C   TSAV=TEMP. OF SAT. VAPOR AT 'V'(F)--PSAV=ABS. PRES. OF SAT. VAPOR AT 'V'(ATM)
C   TSAI=TEMP. OF SAT. VAPOR AT 'I'(F)--PSAI=ABS. PRES. OF SAT. VAPOR AT 'I'(ATM)
C   TSAS=TEMP. OF SAT. VAPOR AT 'S'(F)--PSAS=ABS. PRES. OF SAT. VAPOR AT 'S'(ATM)
C   CONDQ=BTU/(HR FT**2)    CONDW=LBM/(HR FT**2)        HFG=BTU/LBM
C   CPSAV=BTU/(LBM F)       VSAV=LBM/(FT HR)            XKSAV=BTU/(HR FT F)
C   GSAI=DIMENSIONLESS      XMSAI=MOLECULAR WEIGHT AT I
C   PATH=PATH LENGTH AT 'I' IN CENTIMETERS   DFET AND DTHEO ARE IN CENTIMETERS
C SIGMA-KROG=SIGMA CALCULATED WITH PV AND PS.
C   SIGMA=SIGMA CALCULATED WITH PI AND PS.
C   ALL VAPOR PROPERTIES ARE FROM WEATHERFORD.  PATH IS FROM HIRSCHFELDER.

      IR=2.                                                                1130
      IW=3.                                                                1130
    9 READ(IR,10) TSAS,TSAV,CONDQ,RUN
   10 FORMAT(4F10.3)
      IF(TSAV) 898,898,11
   11 CONTINUE
       PSAS=10.**(4.185-(7797.6/(TSAS+460.)))                               K
       PSAV=10.**(4.185-(7797.6/(TSAV+460.)))                               K
       CPSAV=0.01463061+0.0002701871*TSAV-8.979*TSAV*TSAV*(1.E-8)           K
      XKSAV=0.00457429 + (0.00000252857*TSAV)                               K
      XMSAV=37.00084+0.003154*TSAV                                          K
       VSAV=0.0261286 + (0.0000148571*TSAV)                                 K
       HFG=991.2854-0.101428*TSAV                                           K
       CONDW=CONDQ/HFG
      SIGMA=(8.527009E5)*(PSAV-PSAS)*((XMSAV/(TSAV+460.))**0.5)/CONDW     1 OF 2
      SIGMA=2./(1.+SIGMA)
      DPVSS=(PSAV-PSAS)/PSAS
      WRITE(IW,19)
   19 FORMAT(///,' RUN      TSAV       TSAS       CONDQ')
      WRITE(IW,20) RUN,TSAV,TSAS,CONDQ
   20 FORMAT(1F5.0,2F10.3,1F10.1,/)
      WRITE(IW,21)
   21 FORMAT(9X,4HPSAV,6X,4HPSAS,6X,5HCPSAV,5X,4HVSAV,6X,5HXKSAV,4X,3HHF
     1G,6X,5HCONDW,4X,10HSIGMA-KROG,3X,5HDPVSS)
      WRITE(IW,22) PSAV,PSAS,CPSAV,VSAV,XKSAV,HFG,CONDW,SIGMA,DPVSS
   22 FORMAT(5X,5F10.5,1F10.2,3F10.5,//)

C    IF DATA SWITCH 1 IS UP, THE PROGRAM ALSO CALCULATES USING PSAI AND PSAS.
C    XN= NUMBER OF PATH LENGTHS IN TEMPERATURE JUMP EQUATION.
      XN=10.
      TSAI=TSAS
      CALL DATSW(1,IEXIT)
      IF(IEXIT-1.5)102,102,9
  102 CONTINUE
      CPSAI=0.01463061+0.0002701871*TSAI-8.979*TSAI*TSAI*(1.E-8)            K
```

```
PAGE   3                DATA ANALYSIS PROGRAM NO. 2 (WILCOX)

      XKSAI=0.00457429+ (0.00000252857*TSAI)                                  K
      PSAI=10.**(4.185-(7797.6/(TSAI+460.)))                                  K
      XMSAI=37.00084+0.003154*TSAI                                            K
       VSAI=0.0261286+ (0.0000148571*TSAI)                                    K
       GSAI=1.718142-0.000075714*TSAI                                         K
      XNOMO=(1.320497E22)*(PSAI)/(TSAI+460.)
      AMOL=((1.51000E-18)*(XMSAI*(TSAI+460.))**0.5)/VSAI
       PATH=0.707/(AMOL*XNOMO)
       DFET=XN*PATH
       DTHEO=2.*GSAI*PATH*XKSAI/(CPSAI*VSAI*(GSAI+1.))
       TI=CONDW*CPSAI*(DTHEO+DFET)*(0.03281)/XKSAI                        1 OF 2
      TI=(TSAV)*(1./(1.+(1./TI)))+(TSAS)*(1./(1.+TI))                     2 OF 2
      IF( ABS(TI - TSAI) - 0.01)300,200,200
  200 TSAI=TI
      GO TO 102
  300 TSAI=TI
      SIGMA=(8.527009E5)*(PSAI-PSAS)*((XMSAI/(TSAI+460.))**0.5)/CONDW     1 OF 2
      SIGMA=2./(1.+SIGMA)                                                 2 OF 2
      DPISS=(PSAI-PSAS)/PSAS
      WRITE(IW,30)
   30 FORMAT('  XN       SIGMA     TSAI       PSAI       DFET       DTHEO
     1 PATH      DPISS')
      WRITE(IW,31) XN,SIGMA,TSAI,PSAI,DFET,DTHEO,PATH,DPISS
   31 FORMAT(1F5.1,2F10.3,1F10.5,3F10.6,1F10.5,/)
      WRITE(IW,32)
   32 FORMAT(10X,5HCPSAI,4X,4HVSAI,6X,5HXKSAI,5X,4HGSAI,5X,5HXMSAI)
      WRITE(IW,33) CPSAI,VSAI,XKSAI,GSAI,XMSAI
   33 FORMAT(5X,5F10.5,//)
      GO TO 9
  898 CALL EXIT
      END

FEATURES SUPPORTED
 IOCS
```

LOGGED OUT TIME USED- 3 TIME LEFT- 387 LOGIN- 8

```
PAGE   2                    CALCULATION OF EXPECTED VALUE OF SIGMA

C   CALCULATION PERFORMED FOR K=12, 28, 210.
C   DATA REQD.--RADIUS OF HOLE AND DIMENSIONLESS STD. DEV. AT WALL.
      DIMENSION F(35)
      IR=2.
      IW=3.
      READ(IR,6) (F(I),I=1,32)
 6    FORMAT(7F10.0)
 7    READ(IR,8) R,SD
 8    FORMAT(7F10.3)
      IF(R) 900,900,9

 9    CONTINUE
      XLEN=0.0825
      CPLW=0.183
      TSAV=550.
      WRITE(IW,13)
 13   FORMAT(1H1,4X'TSAV    PSAV (TV-TS)/Q/A    D     12*(C)  28*(C)  21
     10*(C) FXEE FXFF FXGG    TE     TF      TG    SIGME SIGMF SIGMG')

 50   TSAV=TSAV+50.
       PSAV=10.**(4.185-(7797.6/(TSAV+460.)))
      XMSAV=37.00084+0.003154*TSAV
       HFG=991.2854-0.101428*TSAV
      DENL=52.1666 - 0.007666*TSAV
      DENVA=2.71828**(.00768*TSAV -13.82)
      VISL=0.80197 - 0.0003733*TSAV
      CONDL= 29.2094 - 0.008066*TSAV

C   'D' IS NUSSULT RESISTANCE.  'C' IS INTERPHASE RESISTANCE.
C   CLAUSIUS CLAPERON EQUATION USED TO OBTAIN FORMAT OF 'C'.
C   ONLY 'C' (NOT D) IS USED TO OBTAIN EXPECTED VALUE OF SIGMA.

      D=(1./0.943)*((XLEN*VISL/(DENL*4.17312E8*(DENL-DENVA)*(CONDL**3.)*
     1HFG))**.25)
      C=(1.986*(TSAV+460.)*(TSAV+460.)*SQRT((TSAV+460.)/(XMSAV)))/(HFG*H
     1FG*PSAV*8.527009E5*XMSAV)

      E=12.*(C)
      FFFF=28.*(C)
      G=210.*(C)
      H=SD*(R/12.)
      EE=E/H
      FF=FFFF/H
      GG=G/H

C   CALCULATIONS FOR K=12.  (STAINLESS STEEL)
      IF(EE-3.1) 20,21,21
 20   N=EE*10.+1.
      FXEE=F(N) + (F(N+1) - F(N))*((EE*10. + 1.)-N)
      GO TO 22
```

```
PAGE   3                    CALCULATION OF EXPECTED VALUE OF SIGMA

 21    FXEE=1.
 22    RTEE=0.5*FXEE
       N=0.
 23    N=N+1.
       IF(RTEE-(1.-F(N))) 23,23,24
 24    TE= (((N-1.)/10.) - 0.1*((RTEE+F(N)  -1.)/(F(N)-F(N-1))))*H
       SE=TE/12.
       SIGME=2./((SE/C)+2.)

C    CALCULATIONS FOR K=28. (NICKEL)
       IF(FF-3.1) 30,31,31
 30    N=FF*10.+1.
       FXFF=F(N)+(F(N+1) -F(N))*((FF*10.+1.)-N)
       GO TO 32
 31    FXFF=1.
 32    RTFF=0.5*FXFF
       N=0.
 33    N=N+1.
       IF(RTFF-(1.-F(N))) 33,33,34
 34    TF= (((N-1.)/10.) - 0.1*((RTFF+F(N)  -1.)/(F(N)-F(N-1))))*H
       SF=TF/28.
       SIGMF=2./((SF/C)+2.)

C    CALCULATIONS FOR K=210. (COPPER)
       IF(GG-3.1) 40,41,41
 40    N=GG*10.+1.
       FXGG=F(N) + (F(N+1)  - F(N))*((GG*10.+1.)-N)
       GO TO 42
 41    FXGG=1.
 42    RTGG=0.5*FXGG
       N=0.
 43    N=N+1.
       IF(RTGG-(1.-F(N))) 43,43,44
 44    TG= (((N-1.)/10.) - 0.1*((RTGG+F(N)  -1.)/(F(N)-F(N-1))))*H
       SG=TG/210.
       SIGMG=2./((SG/C)+2.)

       WRITE(IW,14) TSAV,PSAV,C,D,E,FFFF,G,FXEE,FXFF,FXGG,TE,TF,TG,SIGME,
      1SIGMF,SIGMG
 14    FORMAT(3X,F7.2,F8.5,2F10.7,3F8.5,3F5.2,3F8.5,3F6.3)
       IF(1400.-TSAV) 800,50,50
 800   WRITE(IW,12) SD,R,H,XLEN
 12    FORMAT(//3X'ST. DEV. INPUT =',F9.7,3X'RADIUS OF HOLE=',F5.3,'INCHE
      1S   STD DEV FOR SURFACE=',F8.6,'FEET   LENGTH=',F6.4,'FEET')
       GO TO 7

 900   CALL EXIT
       END

FEATURES SUPPORTED
```

Values of F(I) for "Calculation of Expected Value of Sigma" are as follows:

(I)	F(I)	(I)	F(I)
1	.5000	17	.9452
2	.5398	18	.9554
3	.5793	19	.9641
4	.6179	20	.9713
5	.6554	21	.9772
6	.6915	22	.9821
7	.7257	23	.9861
8	.7580	24	.9893
9	.7881	25	.9918
10	.8159	26	.9938
11	.8413	27	.9953
12	.8643	28	.9965
13	.8849	29	.9974
14	.9032	30	.9981
15	.9192	31	.9987
16	.9332	32	1.0000

```
PAGE   2                THIS SUBROUTINE FITS A FIRST ORDER CURVE

      SUBROUTINE JSHLS (N,X,Y,A,B)
      DIMENSION X(1), Y(1),AA(2), BB(2,2)
C     SET SUMS TO ZERO
      YY=0.0
      XX=0.0
      XY=0.0
      X2=0.0
C     FORM SUMS
      DO 1  I=1,N
      XX=XX +X(I)
      YY=YY+ Y(I)
      XY=XY+X(I)*Y(I)
      X2=X2+ X(I)**2
 1    CONTINUE
C     SETUP THE INPUT FOR SIMQ
      AA(1)=YY
      AA(2)=XY
      BB(1,1)=N
      BB(1,2)=XX
      BB(2,1)=XX
      BB(2,2)=X2
C     SOLVE MATRIX
C     SIMQ IS A IBM SCIEN.SUB. PACKAGE WHICH SOLVES SIM. LIN. EQS.
      CALL SIMQ(BB,AA,2,K)
      A=AA(1)
      B=AA(2)
      RETURN
      END
```

APPENDIX H

Theoretical Effect of Non-Condensable Gas on the Condensation Coefficient

It is shown in this appendix that the pressure dependence of the condensation coefficient reported by some investigators cannot be explained as due to non-condensable gas. The effect of a constant mass of non-condensable gas in a system is shown to reduce the measured condensation coefficient (σ) to a value which is dependent only on the mass of gas present and on the molecular properties of the diffusing gases. The effect on the measured condensation coefficient is independent of vapor pressure and heat flux!

The analysis requires the following steps:

a) Obtain an expression for the partial pressure of the non-condensable gas.

b) Assuming that the actual condensation is unity (as would be measured when no non-condensable gas is present), obtain an expression for the measured condensation coefficient including the effect of the partial pressure of the non-condensable gas.

c) Combine results from (a) and (b) to obtain the effect of non-condensable gas on the measured condensation coefficient.

Expression for Partial Pressure of Non-Condensable Gas

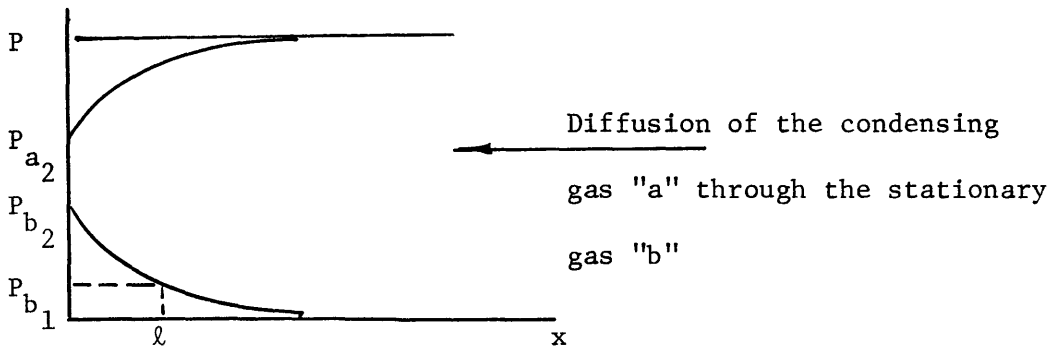

A one-dimensional, steady process at constant total pressure P and at constant temperature T is assumed. In addition, if the gases are assumed to obey the perfect gas law and if the diffusion coefficient is constant, Equation (15.41) of [3] yields:

$$\frac{P_{b_2}}{P_{b_1}} = \exp\left[\frac{\left(\frac{N_a}{A}\right)_{abs} R\ T\ \ell}{D\ P}\right] \qquad \text{(H-1)}$$

where P_{b_2} = the partial pressure of the non-condensable gas at x = 0

$\left(\frac{N_a}{A}\right)_{abs}$ = absolute molar flux of "a" = $\frac{W/A}{M_a}$

W/A = condensation rate

M_a = molecular weight of "a"

R = universal gas constant

D = diffusion coefficient

ℓ = position as shown in figure

Since the temperature is assumed constant, (H-1) can be rewritten as

$$\frac{\rho_b}{\rho_{b_2}} = e^{-c_1 x}$$

where $c_1 = \frac{(W/A)\ R\ T}{M_a\ D\ P}$.

The total mass (ψ) of non-condensable gas "b" present in the system is obtained as follows:

$$\psi = \int_0^\infty \rho_b\ A\ dx = \frac{\rho_{b_2} A}{c_1}$$

Applying the perfect gas law, the expression for the partial pressure of the non-condensable gas "b" at x = 0 (the liquid-vapor interface) is obtained:

$$P_{b_2} = \frac{\psi R^2 T^2 (W/A)}{A M_a M_b D P} \qquad \text{(H-2)}$$

The non-condensable gas is concentrated very close to the liquid vapor interface. For example, evaluation of (H-1) for typical data shows that $(P_{b_1}/P_{b_2}) \simeq 0$ for $\ell > 0.1$ inches.

Expression for Condensation Coefficient

Next an expression is obtained for the measured condensation coefficient showing the effect of the partial pressure of the non-condensable gas at x = 0. Consider a data point for which the determined condensation coefficient (σ) is less than unity, and assume that the cause of σ being < 1.0 is due to the presence of non-condensable gas.

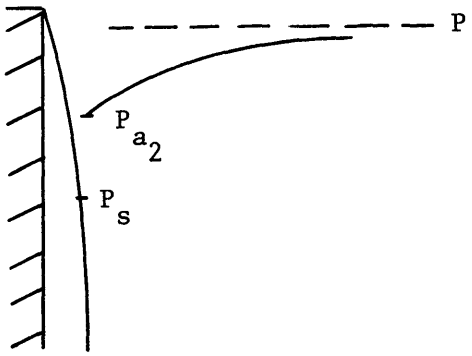

If non-condensable gas is present, the partial pressure of the vapor at the liquid interface will be reduced to P_{a_2} as shown above. However, most experimenters obtain the total pressure in the system by measuring the vapor temperature at a distance far from the interface

and relating this temperature to the saturation pressure of the condendable gas. For small quantities of non-condensable gas, the partial pressure of the non-condensable gas far from the interface is negligible. Ignoring the presence of the non-condensable gas, the experimenter will obtain the calculated condensation coefficient using the total pressure:

$$W/A = \frac{2\sigma}{2 - \sigma} \sqrt{\frac{M_a}{2\pi RT_s}} (P - P_s) \qquad \text{(H-3)}$$

If it is assumed that the actual magnitude of the condensation coefficient is unity and that the interphase mass transfer is determined by the pressure difference $(P_{a_2} - P_s)$, then:

$$W/A = \frac{2}{2 - 1} \sqrt{\frac{M_a}{2\pi RT_s}} (P_{a_2} - P_s) \qquad \text{(H-4)}$$

To show the effect of the non-condensable gas on the determined magnitude of σ, equate (H-3) and (H-4) and set $P = P_{a_2} + P_{b_2}$; then:

$$\sigma = \frac{2}{2 + \left(\frac{P_{b_2}}{P_{a_2} - P_s}\right)} \qquad \text{(H-5)}$$

Combination of Resulting Expressions

Using Equation (14.9) of [3], the diffusion coefficient in gaseous mixtures takes the form:

$$D = C_2 \frac{T^{3/2}}{P} \qquad \text{(H-6)}$$

where C_2 is a function of the molecular properties of the diffusing gases.

Substituting (H-2), (H-4) and (H-6) into (H-5), one obtains:

$$\sigma = \frac{1}{1 + \left(\frac{\psi}{A}\right)\left(\frac{R^{3/2}}{\sqrt{M_a}\, M_b\, C_2\, \sqrt{2\pi}}\right)} \qquad \text{(H-7)}$$

This equation shows that for a particular non-condensing gas and a particular condensing vapor, σ is a function of only the total mass of non-condensable gas present. If in a particular apparatus it is assumed that when the total pressure is changed the mass of non-condensable gas present remains constant, then the σ vs. P curve should be horizontal (σ independent of P). Since this is not generally observed in Fig. 6, the fall off of σ at the higher pressures should not be attributed to non-condensable gas. The uniformly low value of the condensation coefficient reported by Sukhatme [16] could, however, be explained on the basis of non-condensable gas.

Example

To show that the mass of non-condensable gas needed to reduce the condensation coefficient is minute, (H-7) will be evaluated for the following hypothetical example:

Given: (1) $\sigma = 0.5$

(2) non-condensable gas is argon ($M_b = 39.9$)

(3) condensing gas is potassium ($M_a = 39.1$)

(4) $C_2 = 0.091$ lbf/hr$(°R)^{3/2}$ from [22]

(5) A = 2.0 square inches

From (H-7),

$$\psi = A \cdot \frac{1 - \sigma}{\sigma\left(\frac{R^{3/2}}{\sqrt{M_a}\, M_b\, C_2\, \sqrt{2\pi}}\right)}$$

$$\psi = \left(\frac{2.0}{144}\right) \frac{1 - 0.5}{(0.5)\left[\frac{(1545)^{3/2}\,(3600)}{\sqrt{39.1}\,(39.9)(0.091)\sqrt{2\pi}\,\sqrt{32.2}}\right]}$$

$$\psi \simeq 10^{-8} \text{ lbm}$$

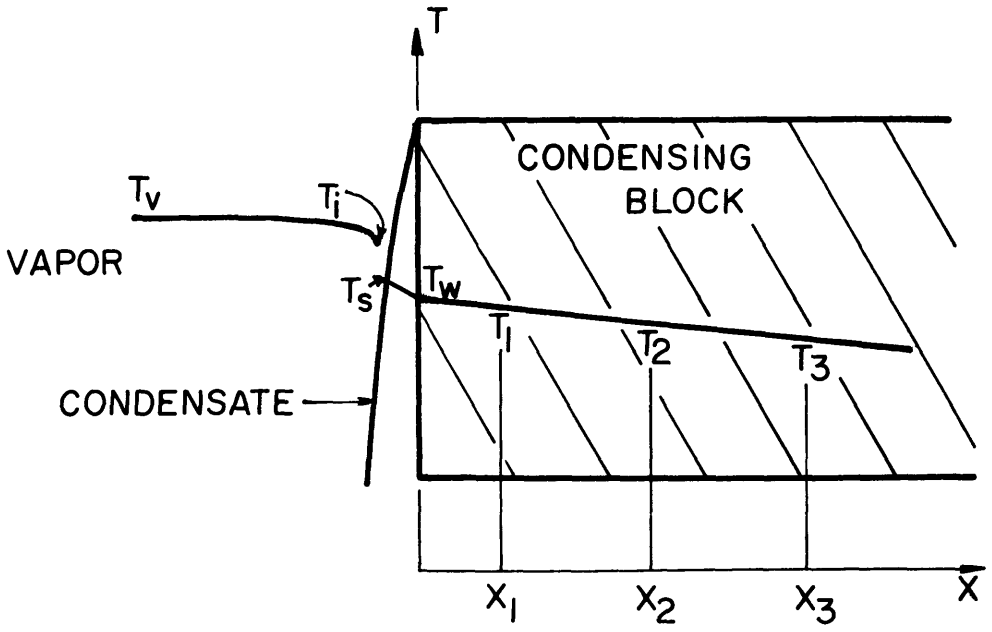

FIG. 1 FUNDAMENTAL DIAGRAM FOR FILM CONDENSATION

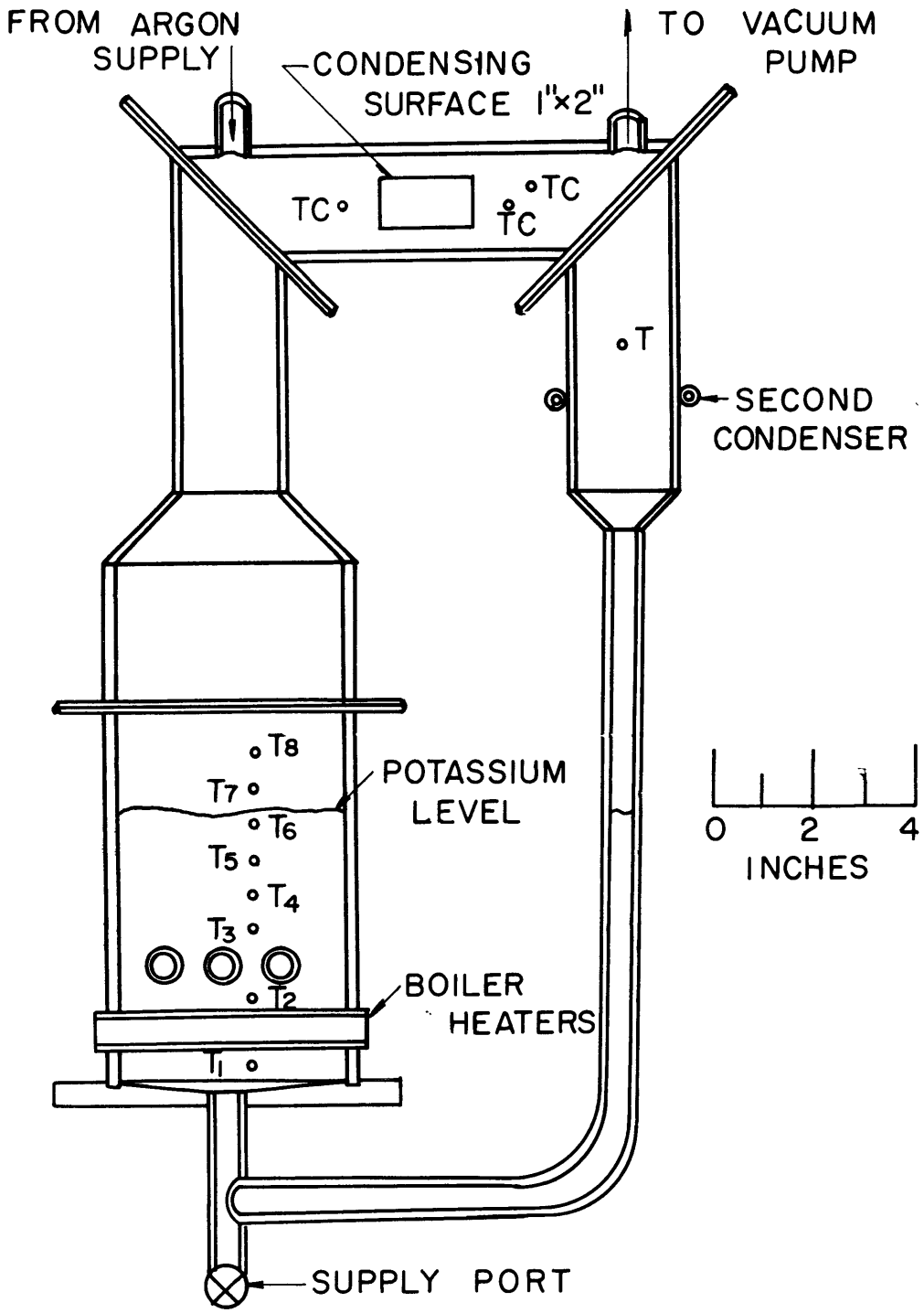

FIG 2 SCHEMATIC OF NATURAL CONVECTION LOOP

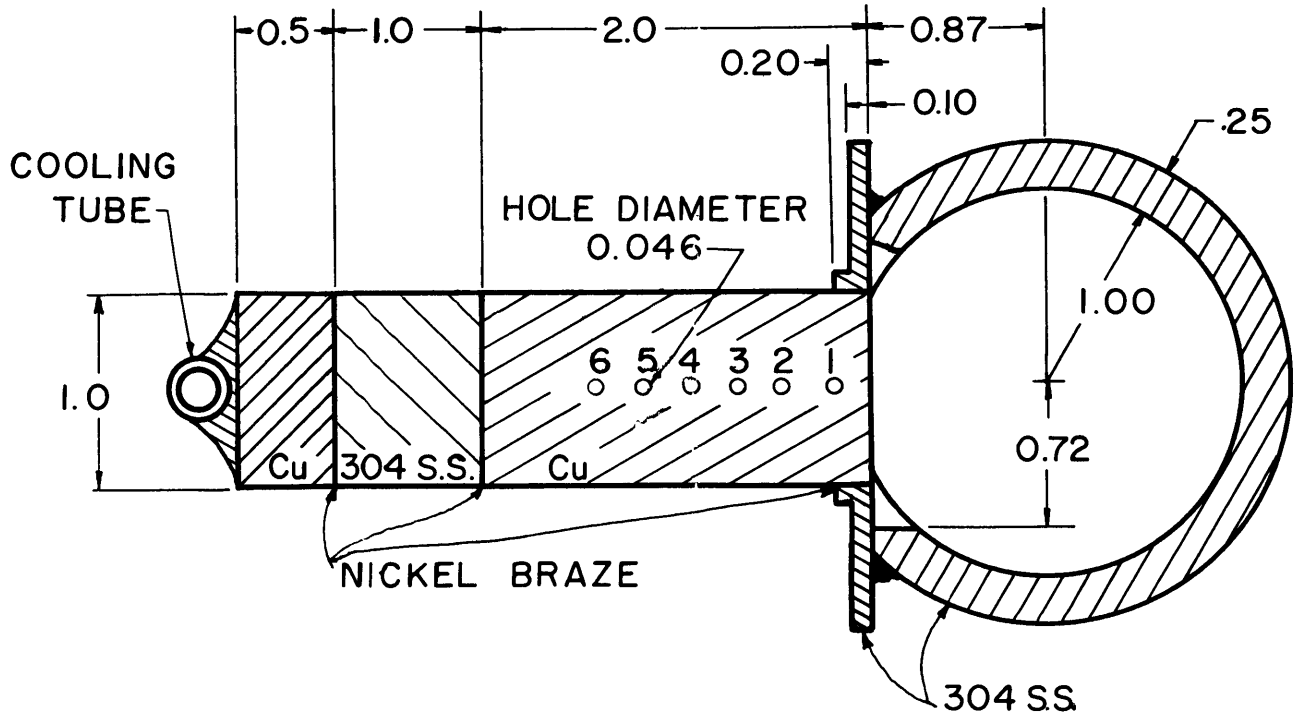

FIG. 3 SECTIONAL VIEW OF TEST CONDENSER

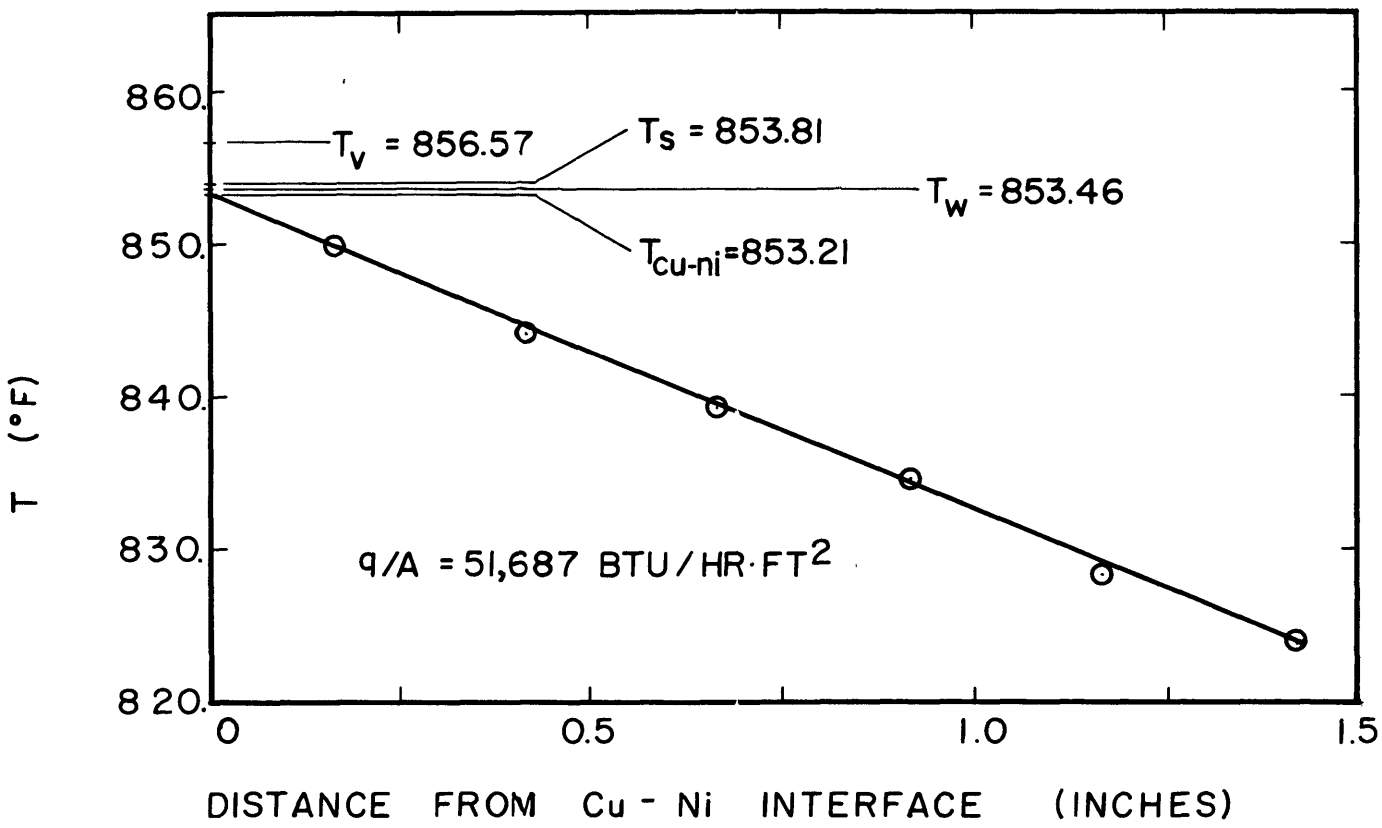

FIG. 4 DATA & RESULTS (RUN 3-SERIES 1)

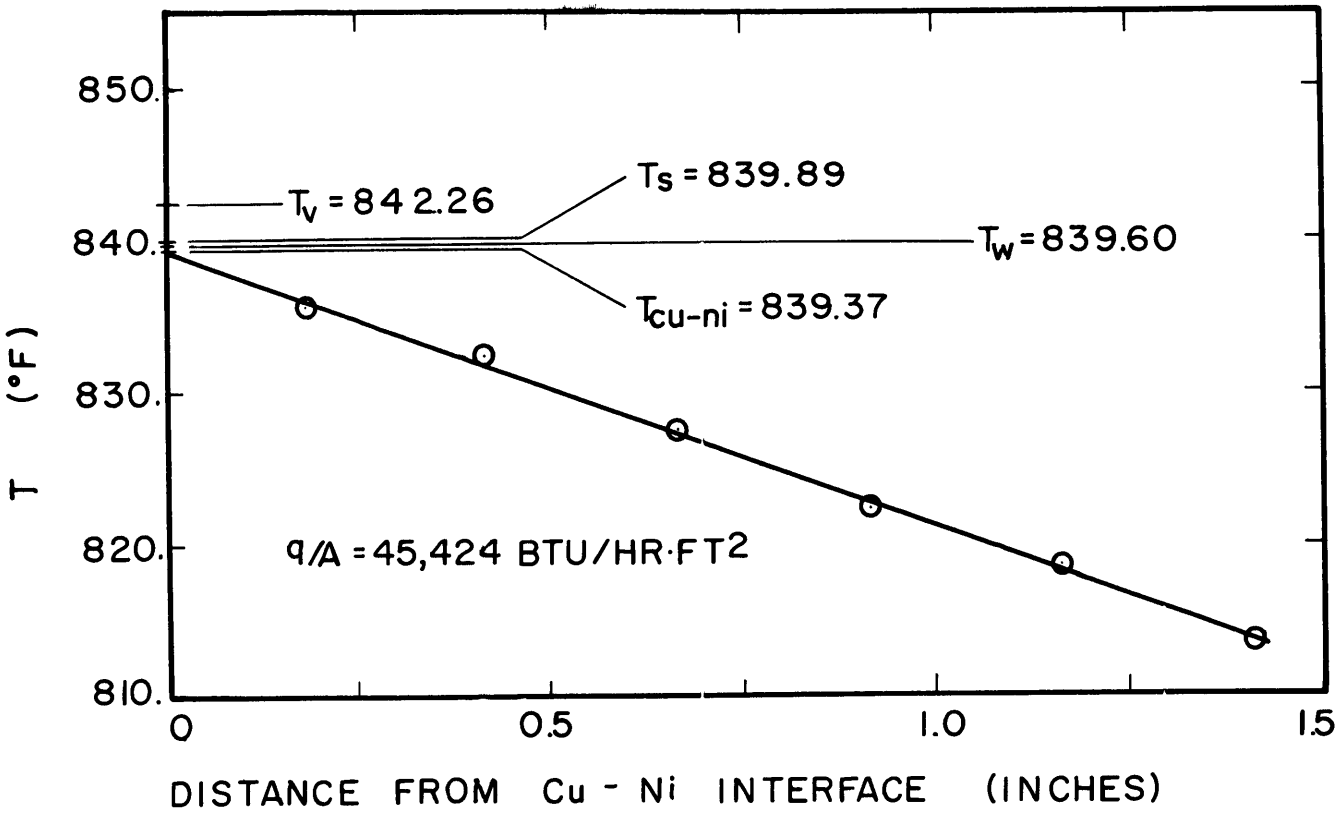

FIG. 5 DATA & RESULTS (RUN 18 - SERIES 3)

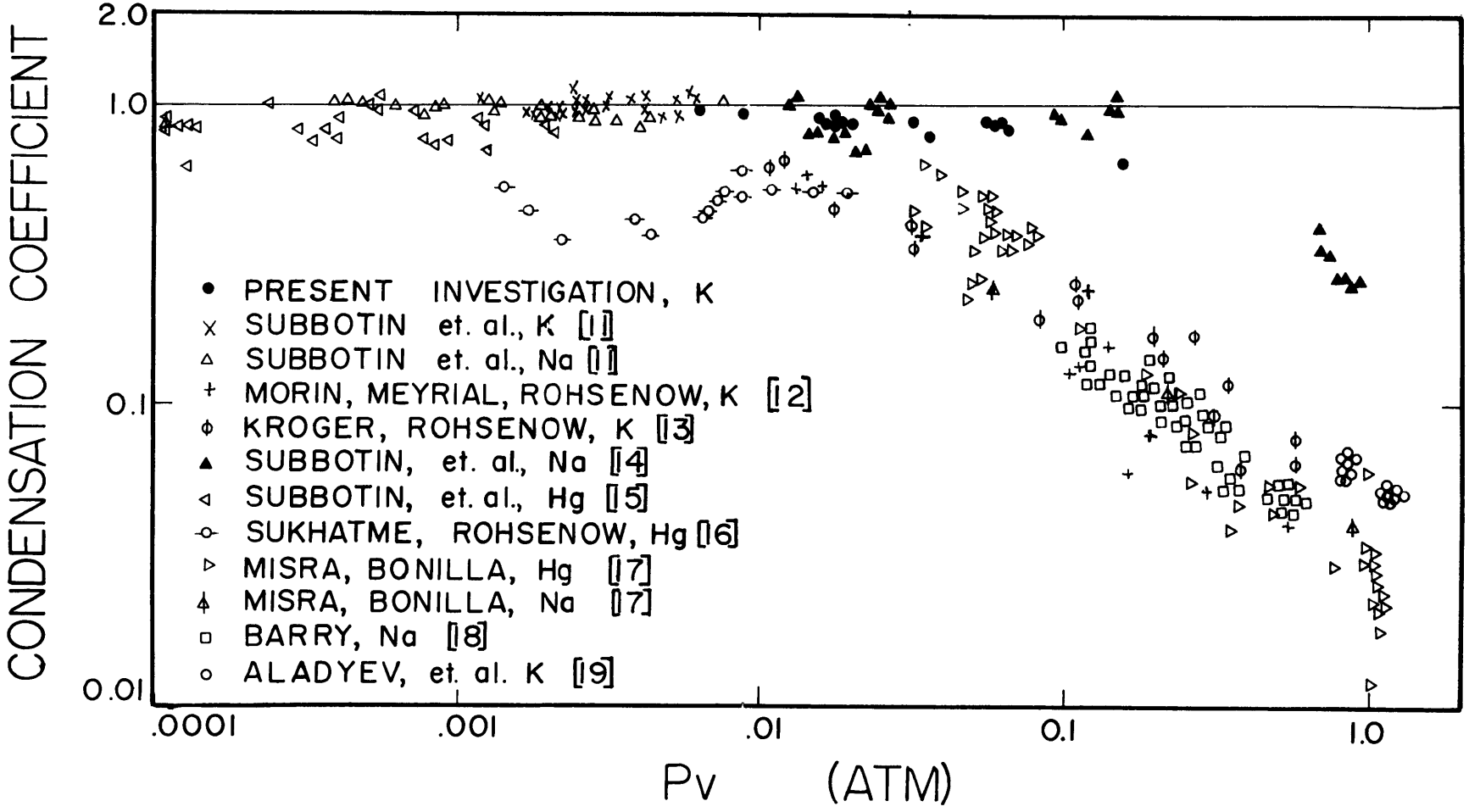

FIG. 6 SURVEY OF CONDENSATION COEFFICIENT DATA

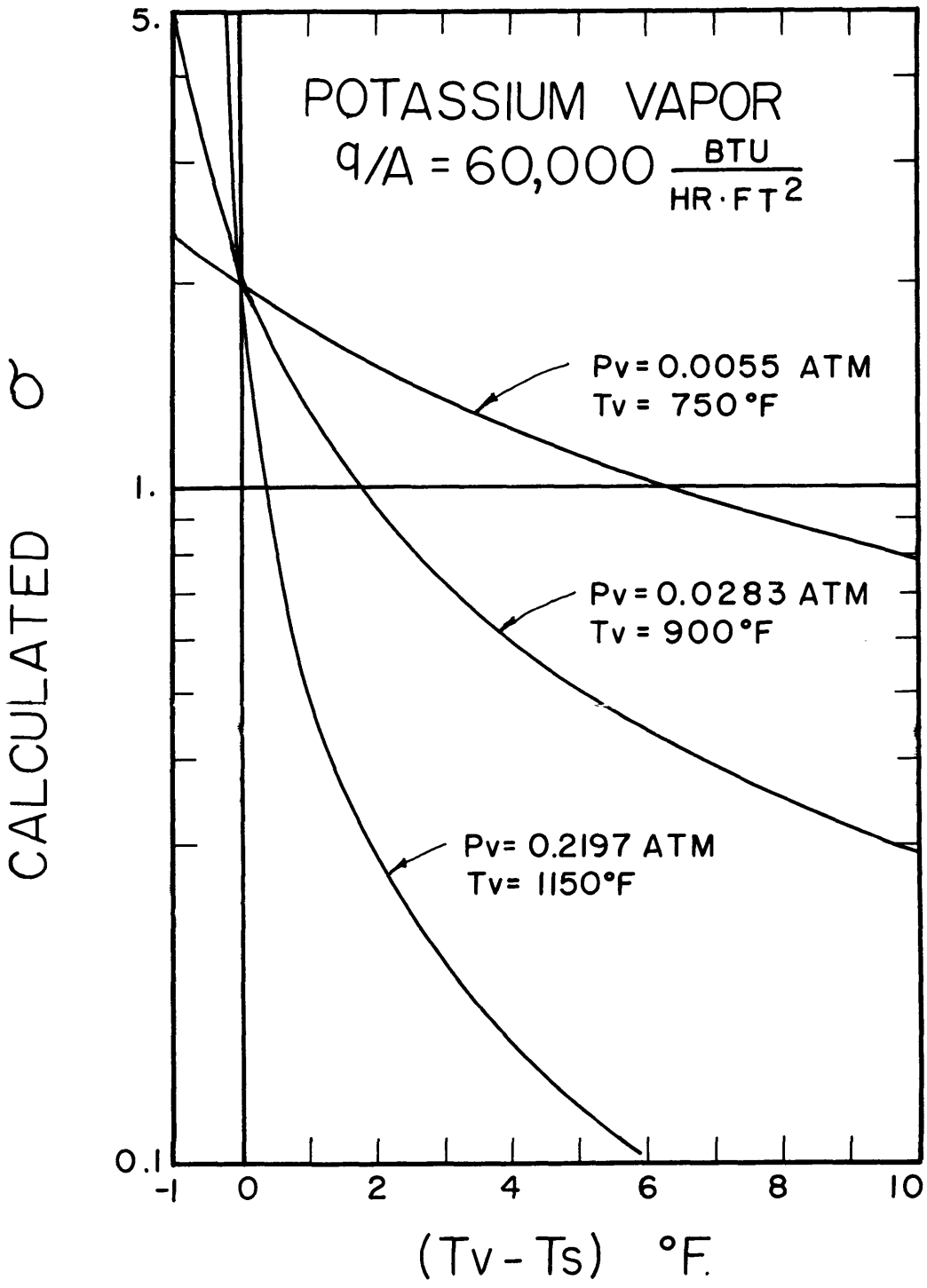

FIG.7 CONDENSATION COEFFICIENT VS. (Tv - Ts)

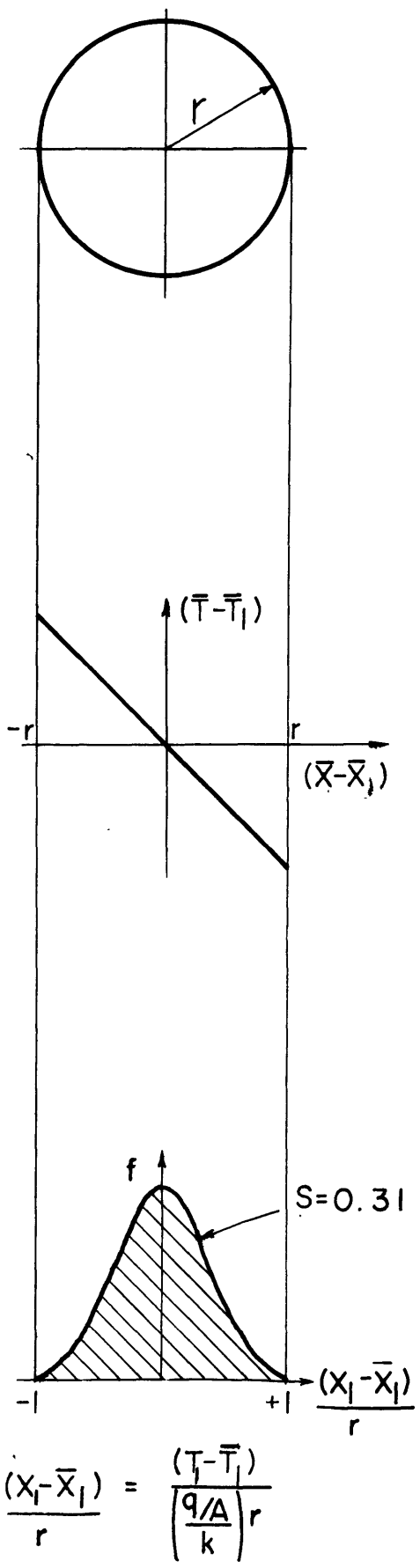

FIG. 8a

TYPICAL HOLE OF RADIUS "r"

FIG. 8b

SIMPLIFIED, LINEAR TEMPERATURE DROP IMPRESSED ACROSS HOLE

FIG. 8c

GAUSSIAN DISTRIBUTION OF TEMPERATURE MEASUREMENTS IN HOLE

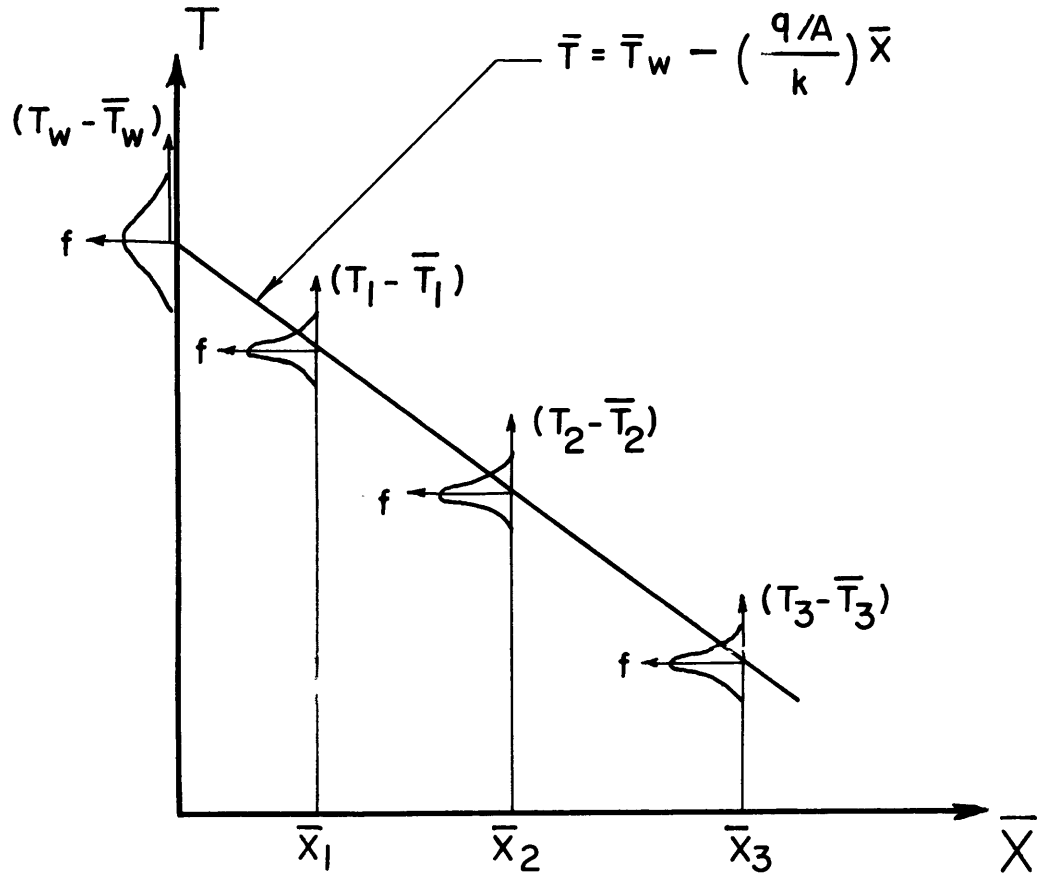

FIG. 9 SCHEMATIC REPRESENTATION OF DISTRIBUTIONS IN HOLES AND AT WALL

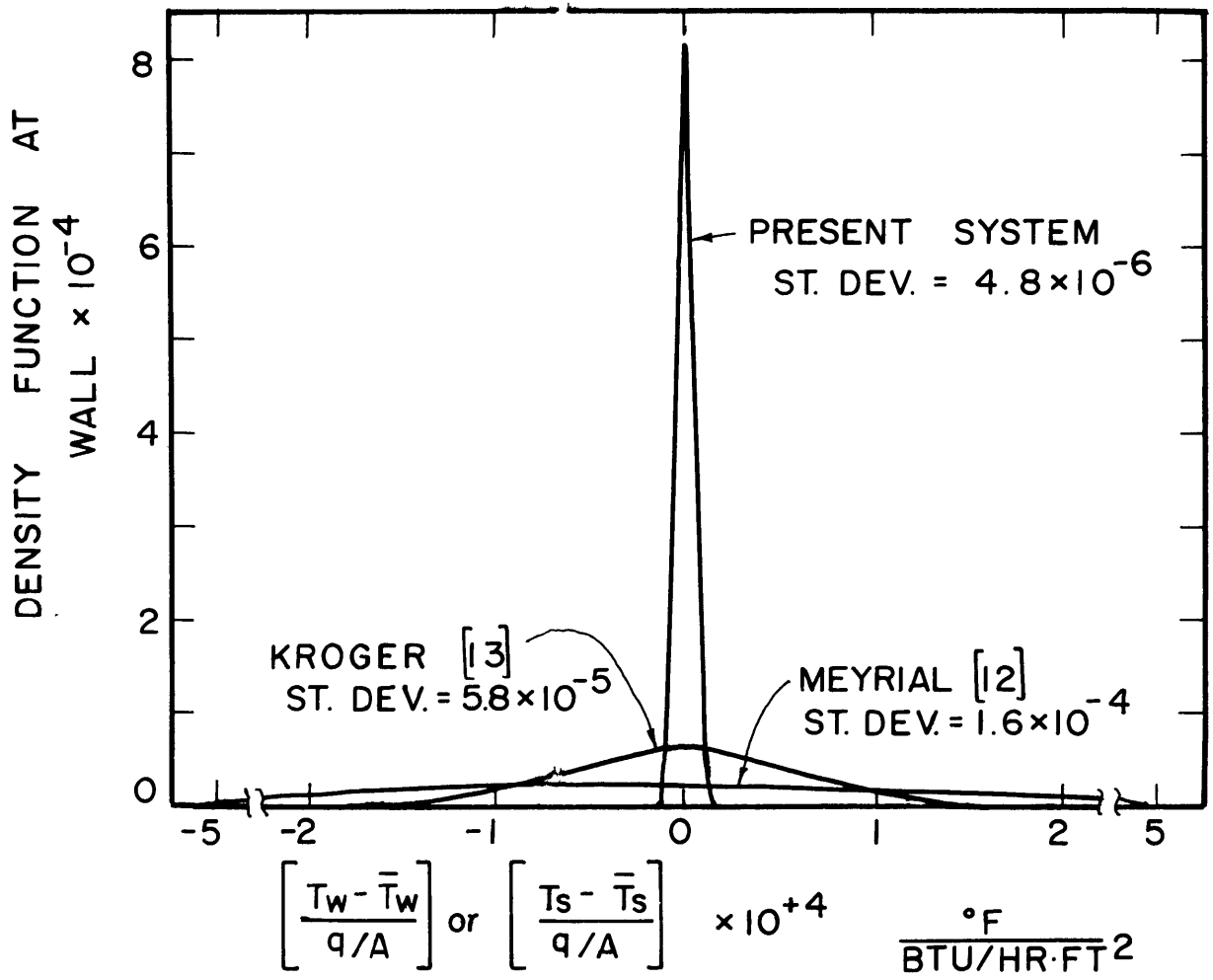

FIG. 10 PROBABILITY DENSITY FUNCTION AT WALL

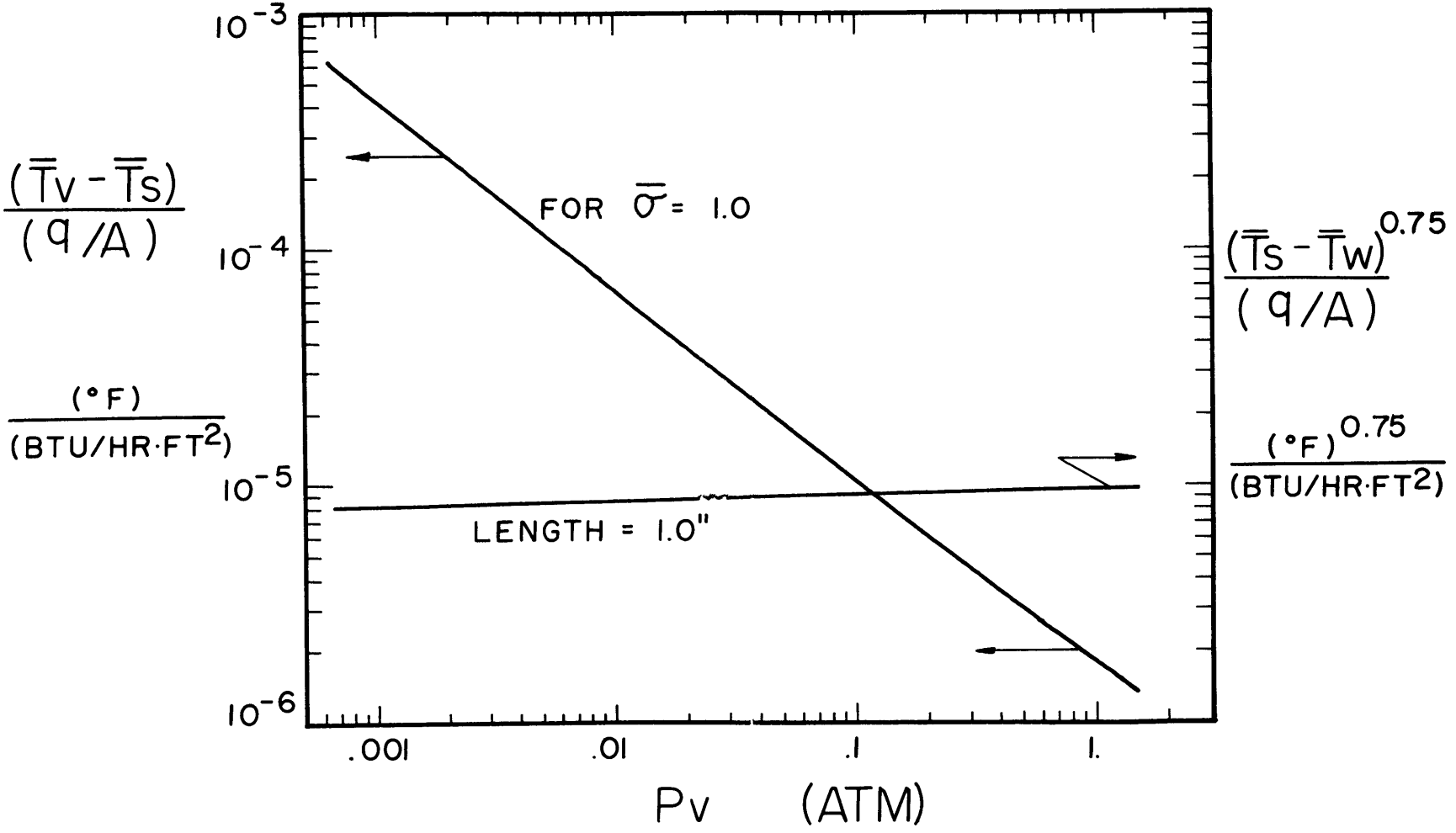

FIG. 11 EFFECT OF Pv ON $(\overline{T}v - \overline{T}s)$ & $(\overline{T}s - \overline{T}w)$ FOR POTASSIUM

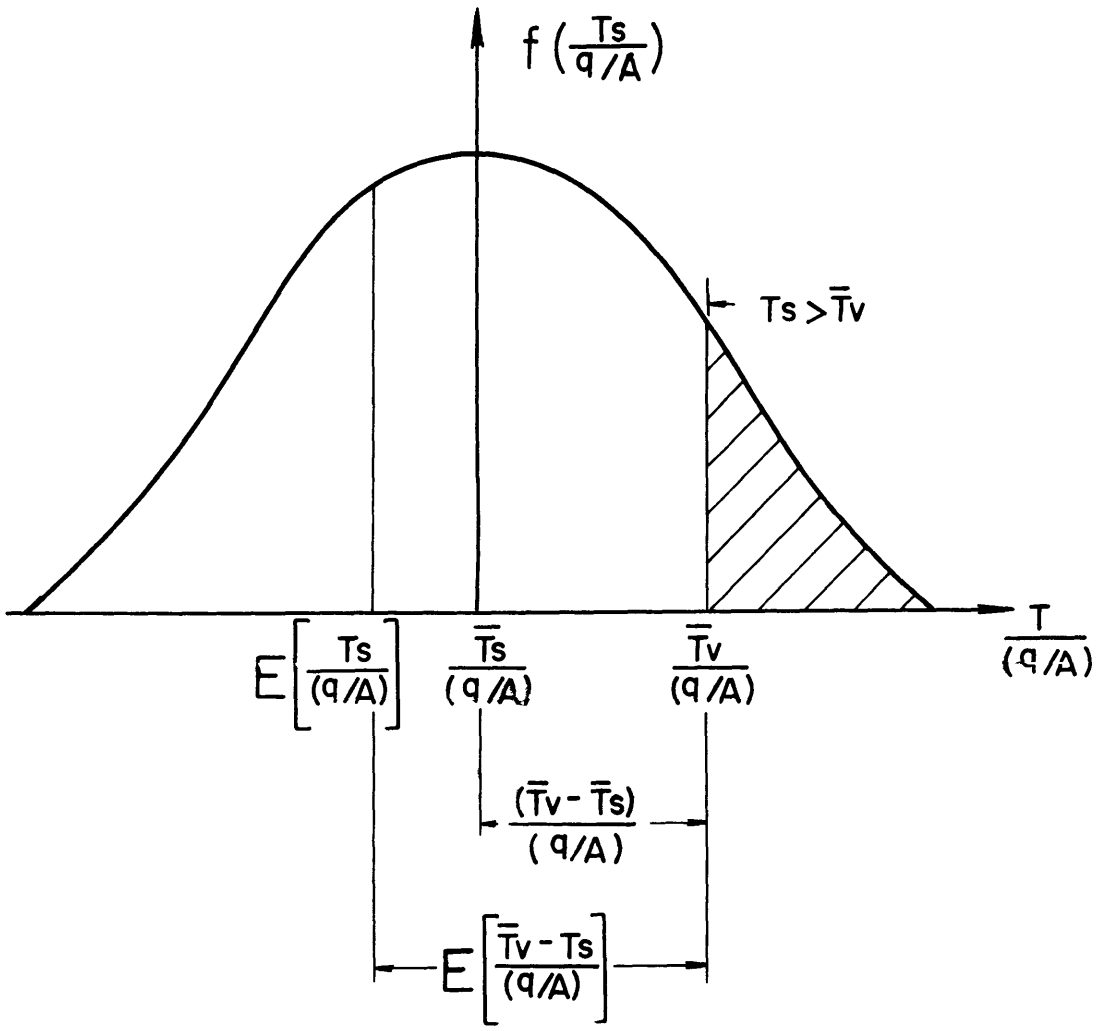

FIG. 12 DISTRIBUTION OF CONDENSATE SURFACE TEMPERATURE

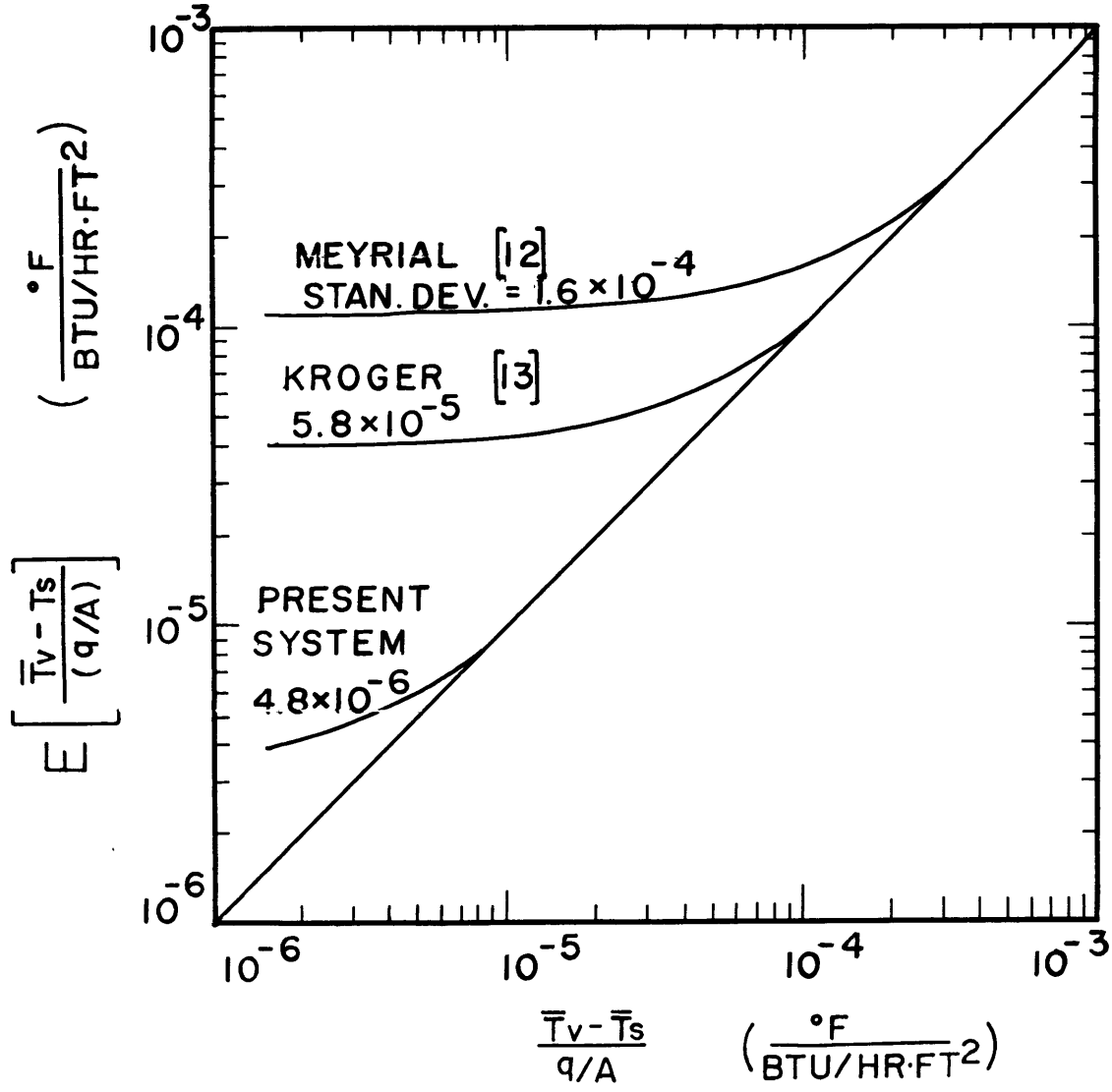

FIG.13 $E\left[(\bar{T}v - Ts)/(q/A)\right]$ vs. $(\bar{T}v - \bar{T}s)/(q/A)$

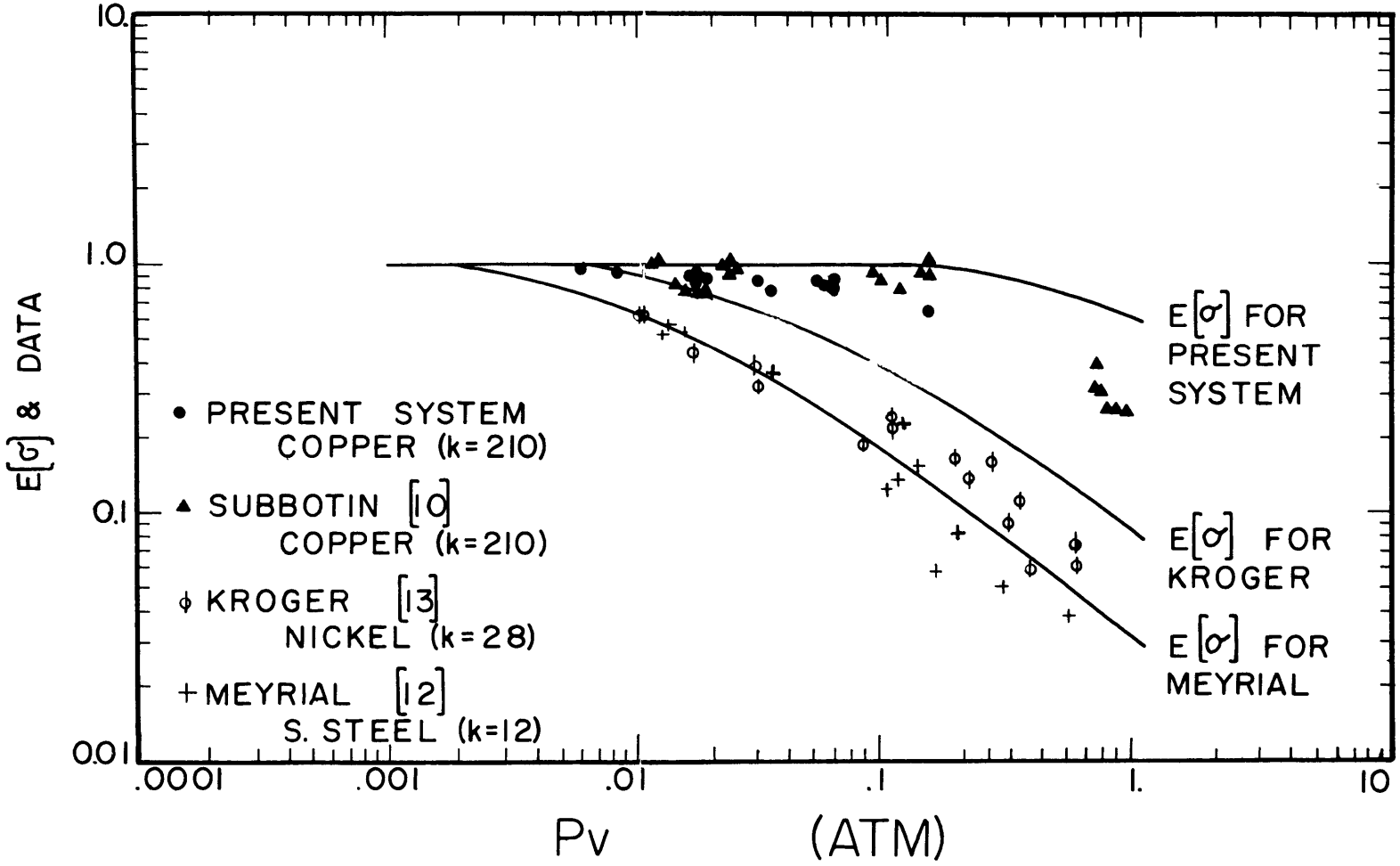

FIG. 14 E[σ] & DATA vs. Pv

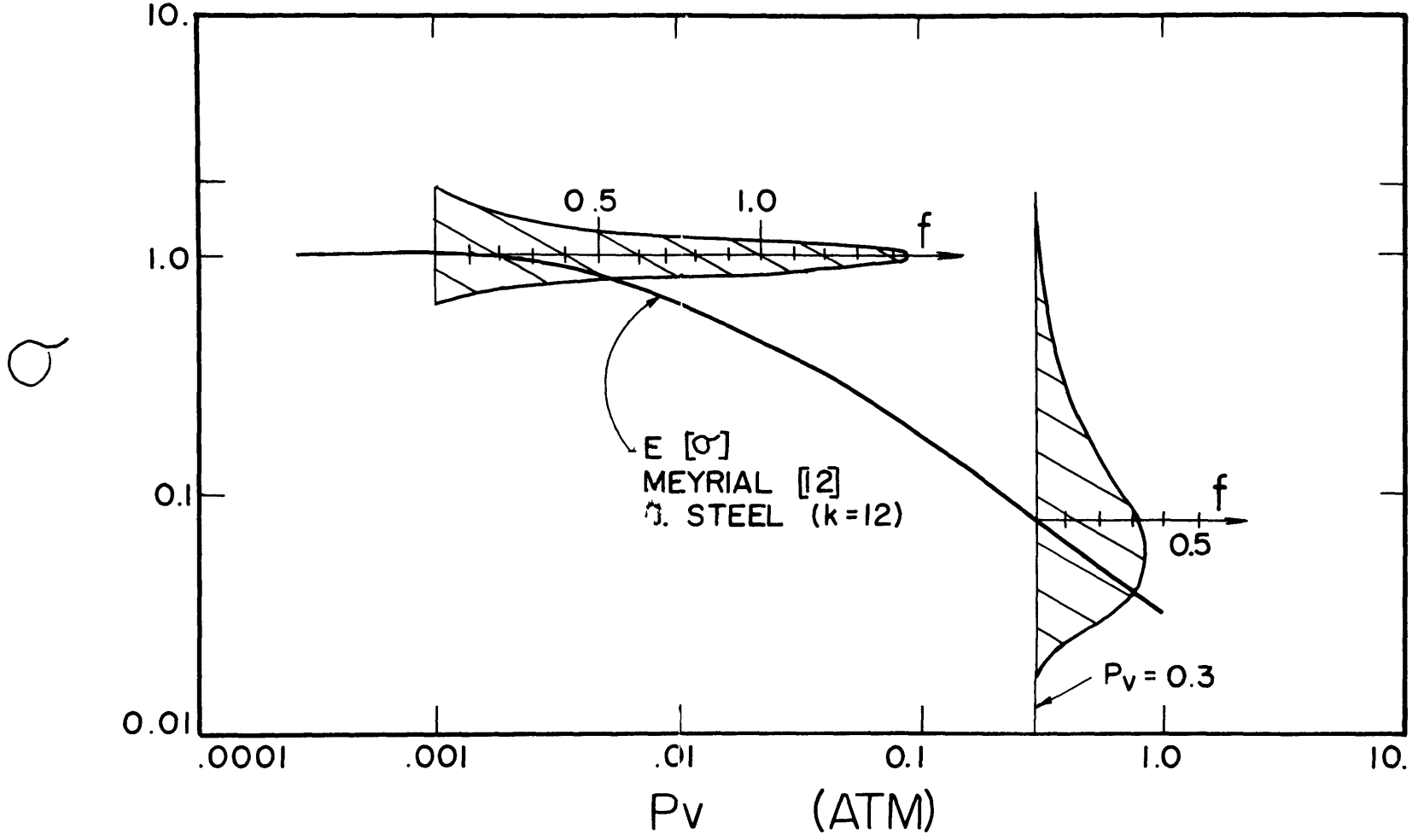

FIG. 15 PREDICTED DISTRIBUTION OF DATA

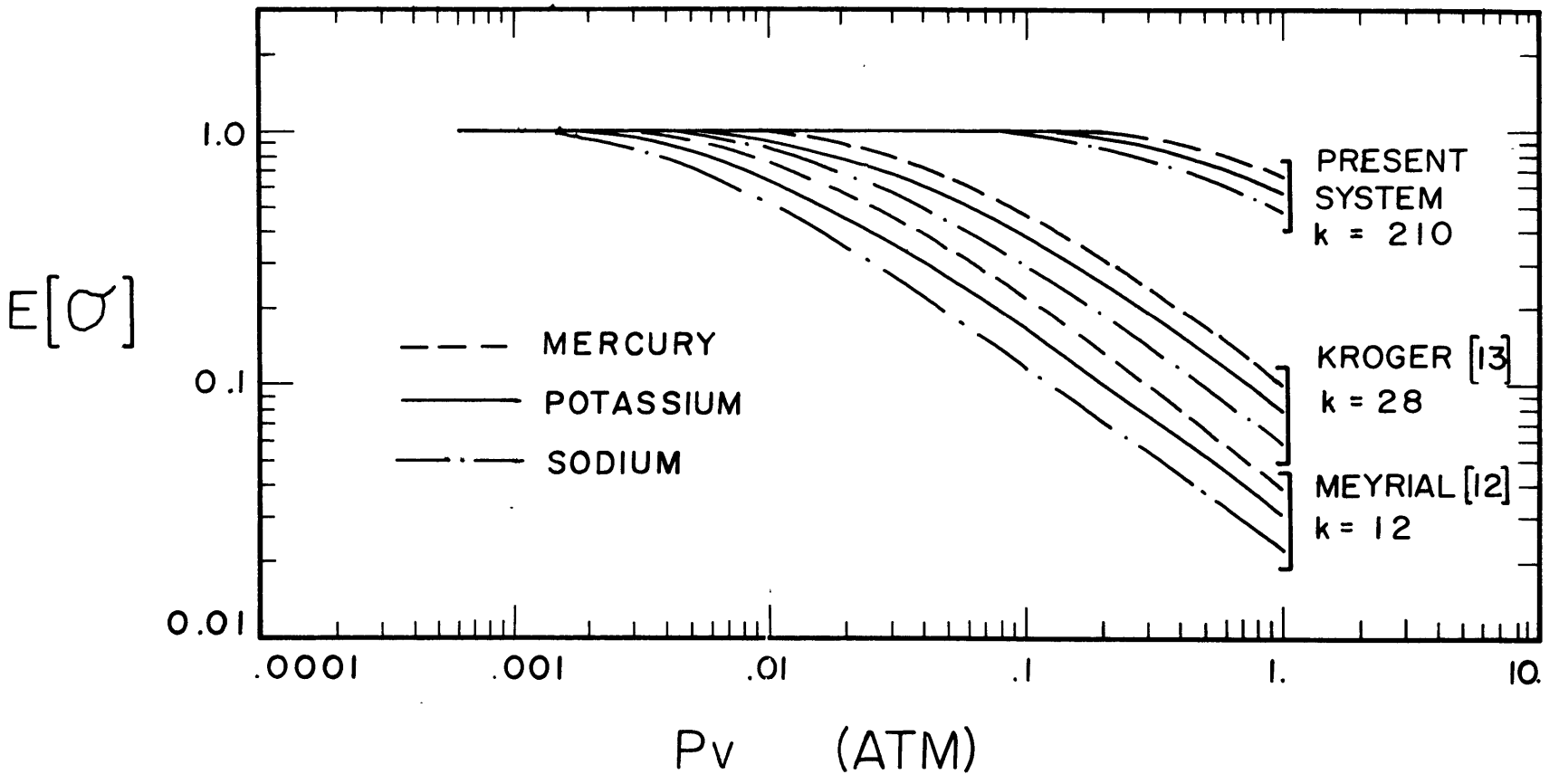

FIG. 16 EFFECT OF FLUID ON E[σ]

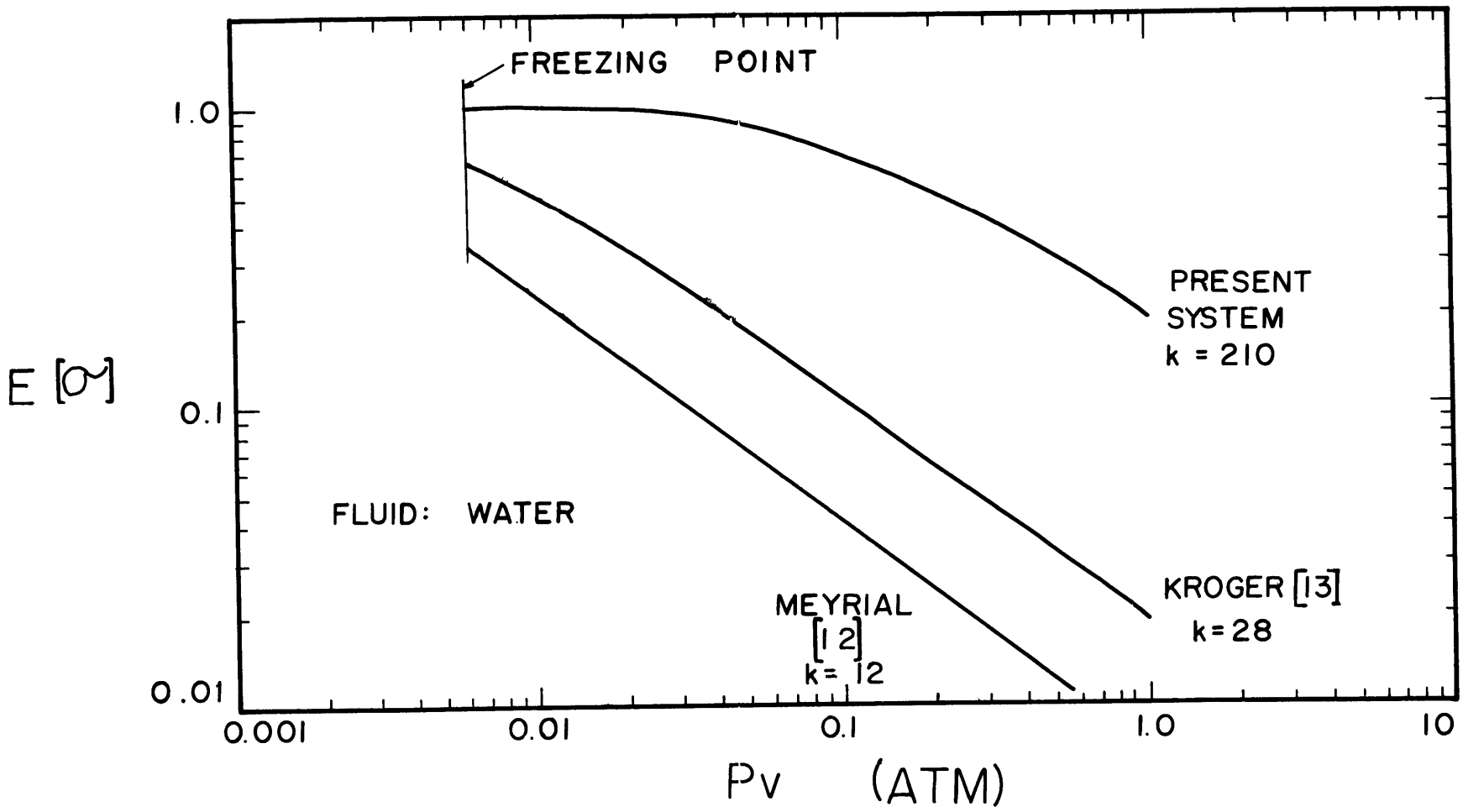

FIG.17 E [σ] VS. Pv FOR WATER

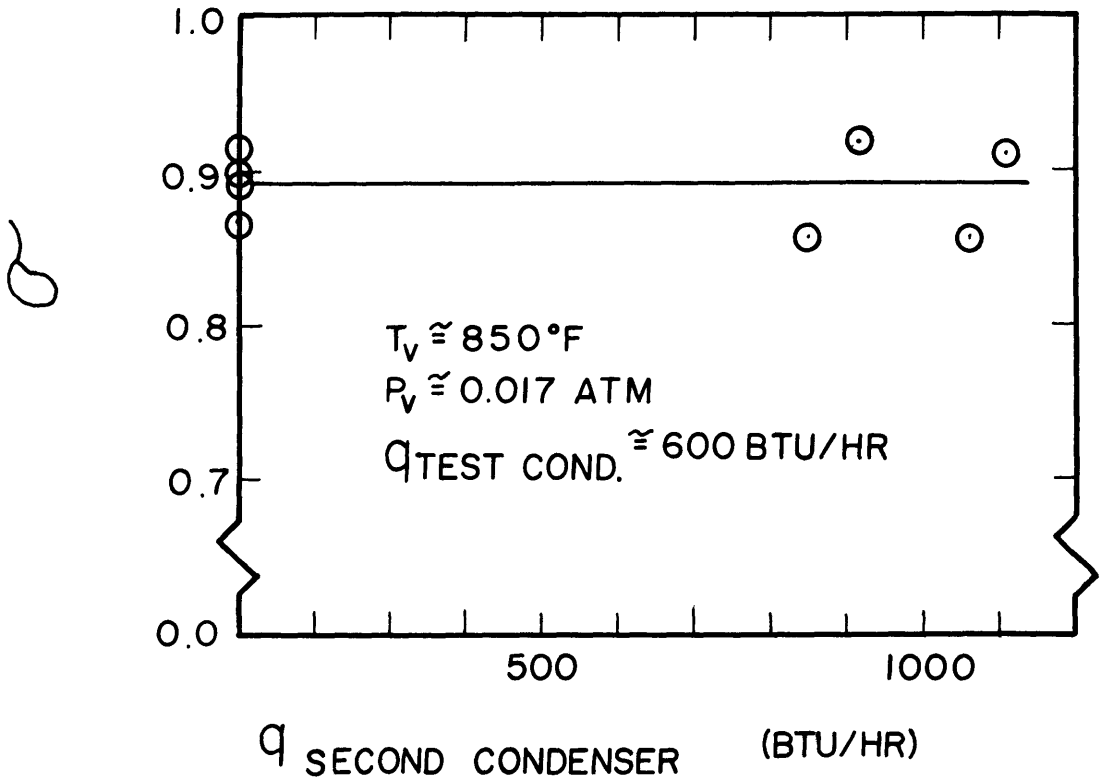

FIG. 18 EFFECT OF SECOND CONDENSER AT ~ 0.02 ATM

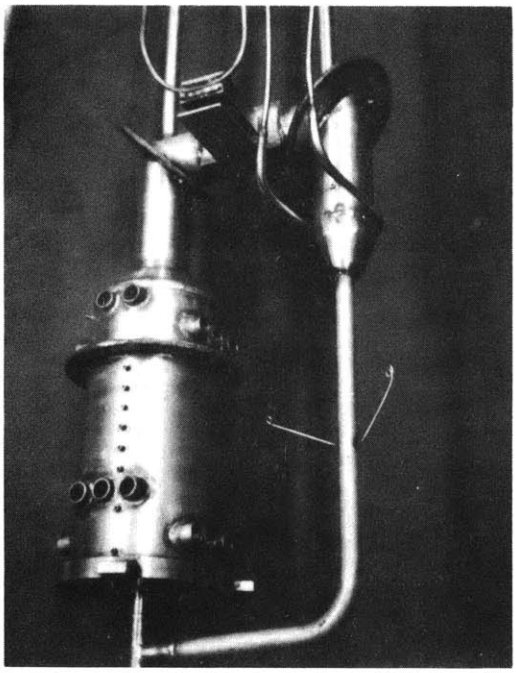

FIG. A1. NATURAL CONVECTION LOOP

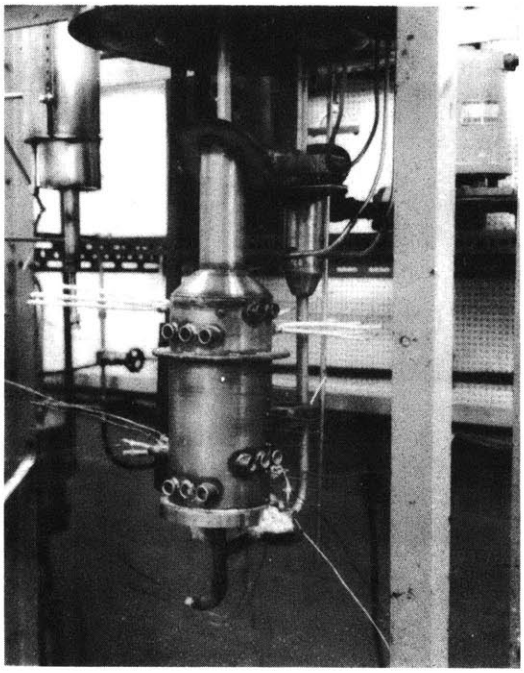

FIG. A2. LOOP DURING CONSTRUCTION

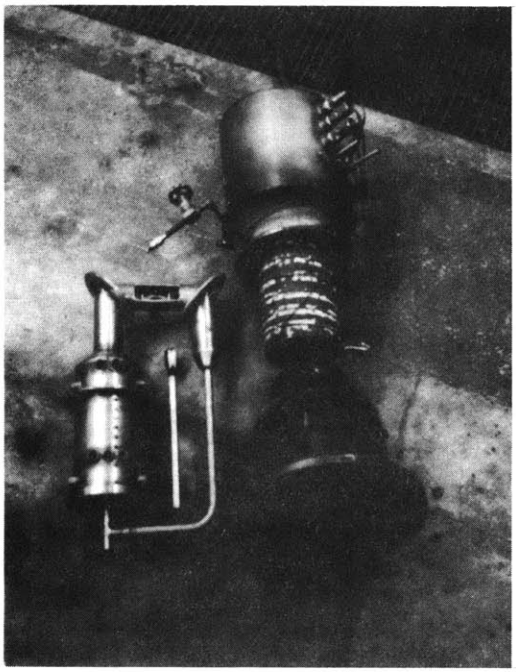

FIG. A3. OLD AND NEW APPARATUS

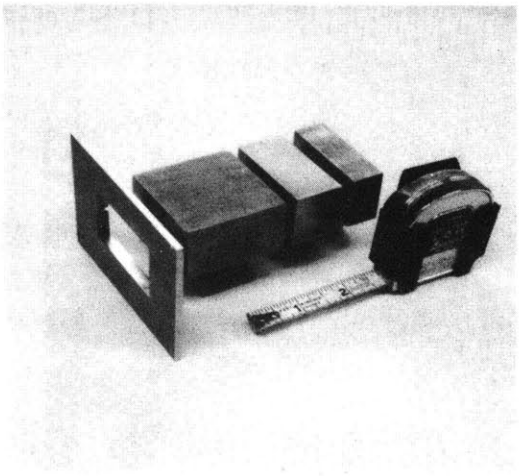

FIG. A4.ELEMENTS FOR TEST SECTION

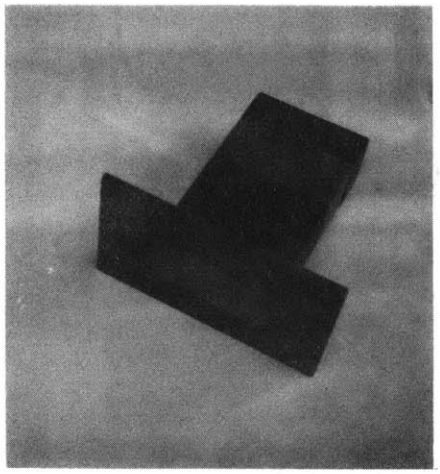

FIG. A5. TEST SECTION AFTER BRAZING

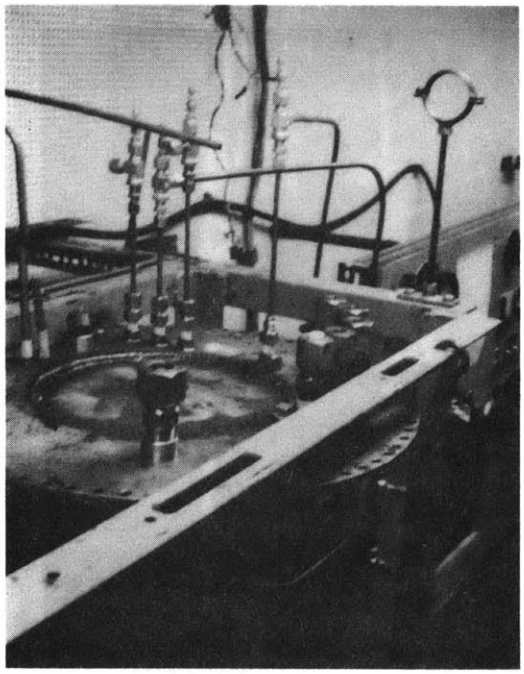

FIG. A6. ASSEMBLING OF TOP

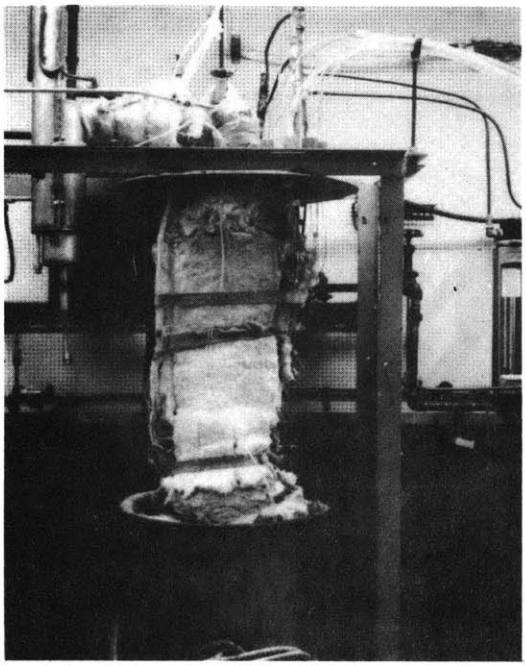

FIG. A7. LOOP WITH AUXILIARIES

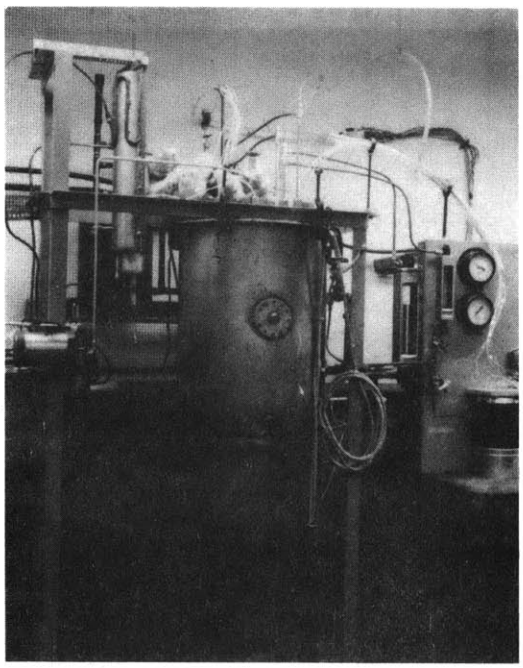

FIG. A8. PROTECTIVE DRUM IN PLACE

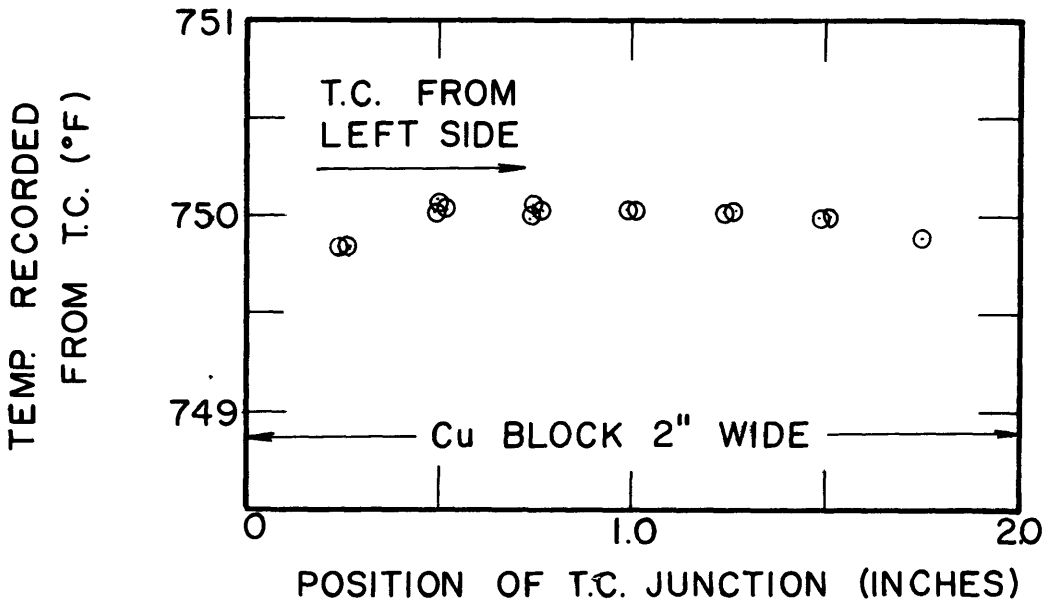

FIG. C-1 IMMERSION TEST WITH HOMOGENEOUS T.C.

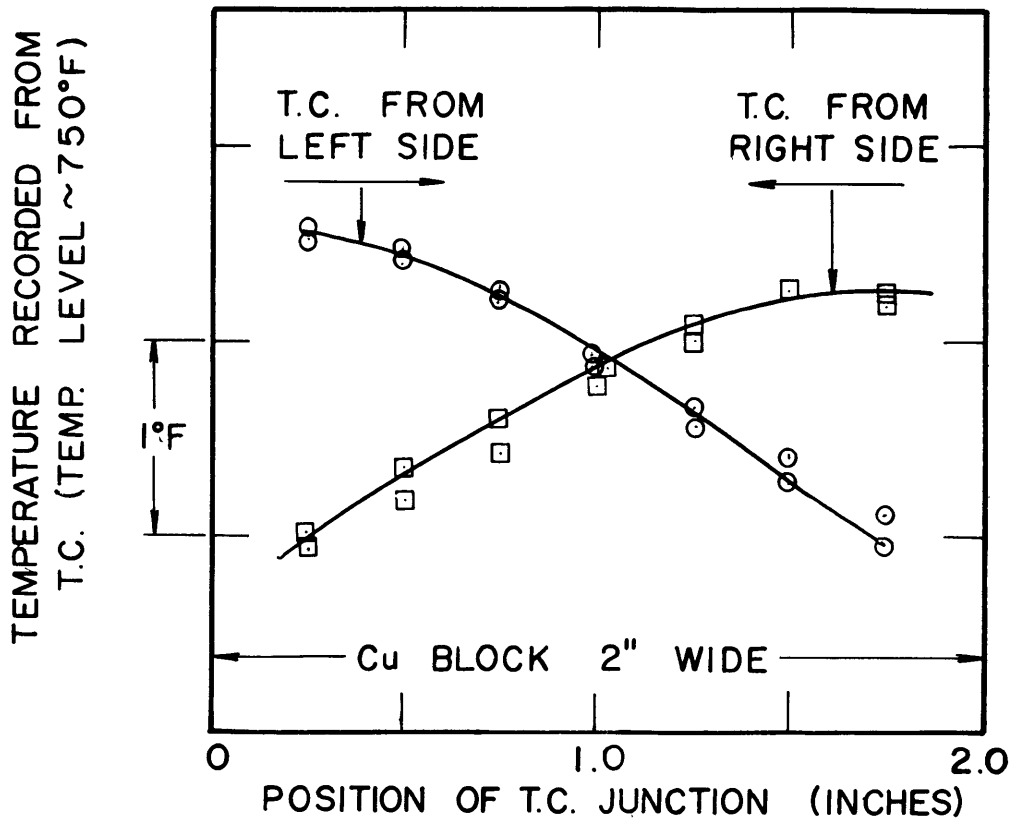

FIG. C-2 IMMERSION TEST WITH INHOMOGENEOUS T.C.

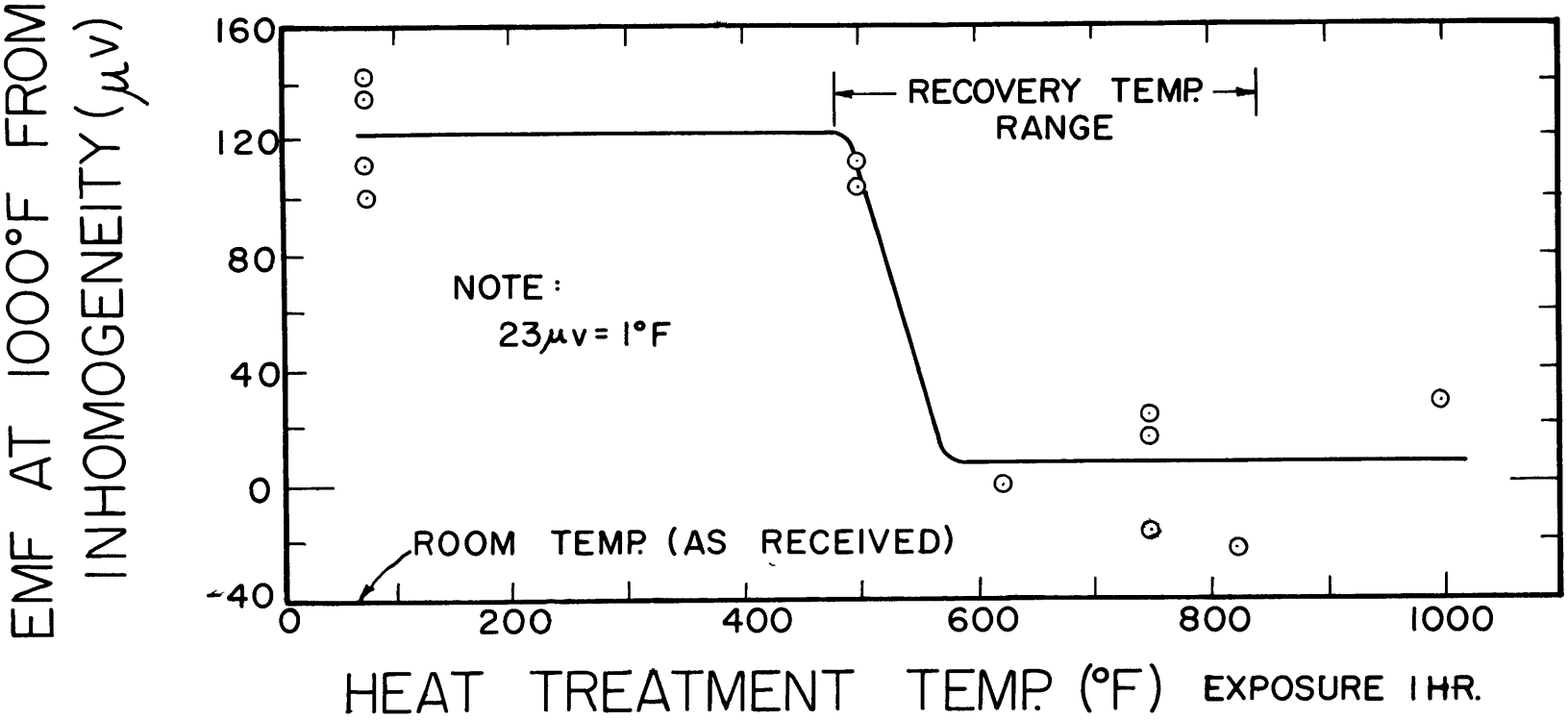

FIG. C-3 HEAT TREATMENT OF CHROMEL ALUMEL THERMOCOUPLES

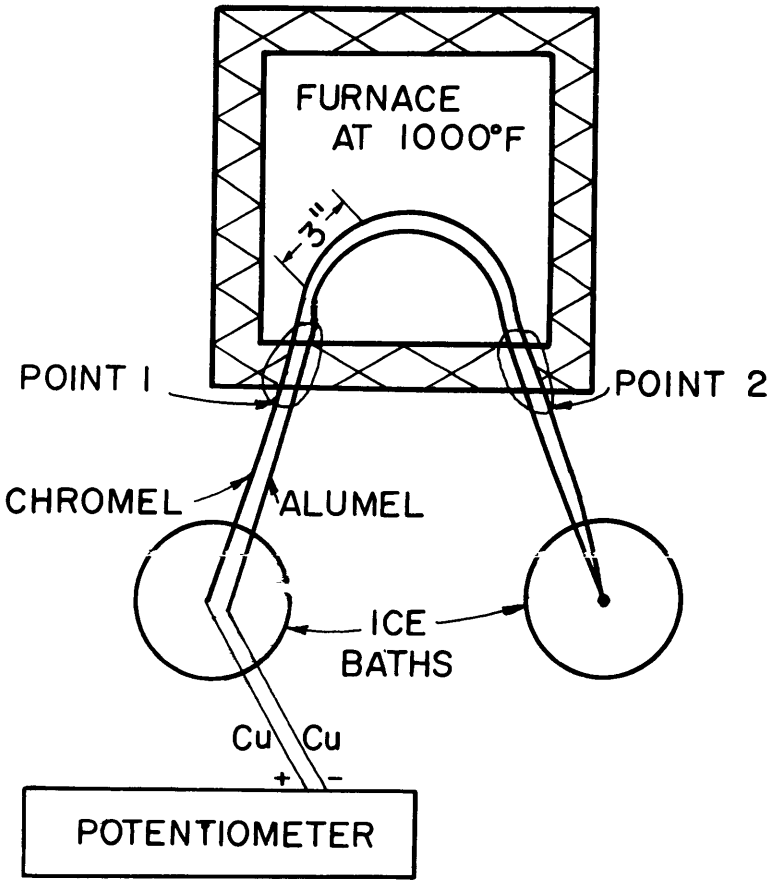

FIG. C-4 SET-UP USED IN TESTS OF HOMOGENEITY

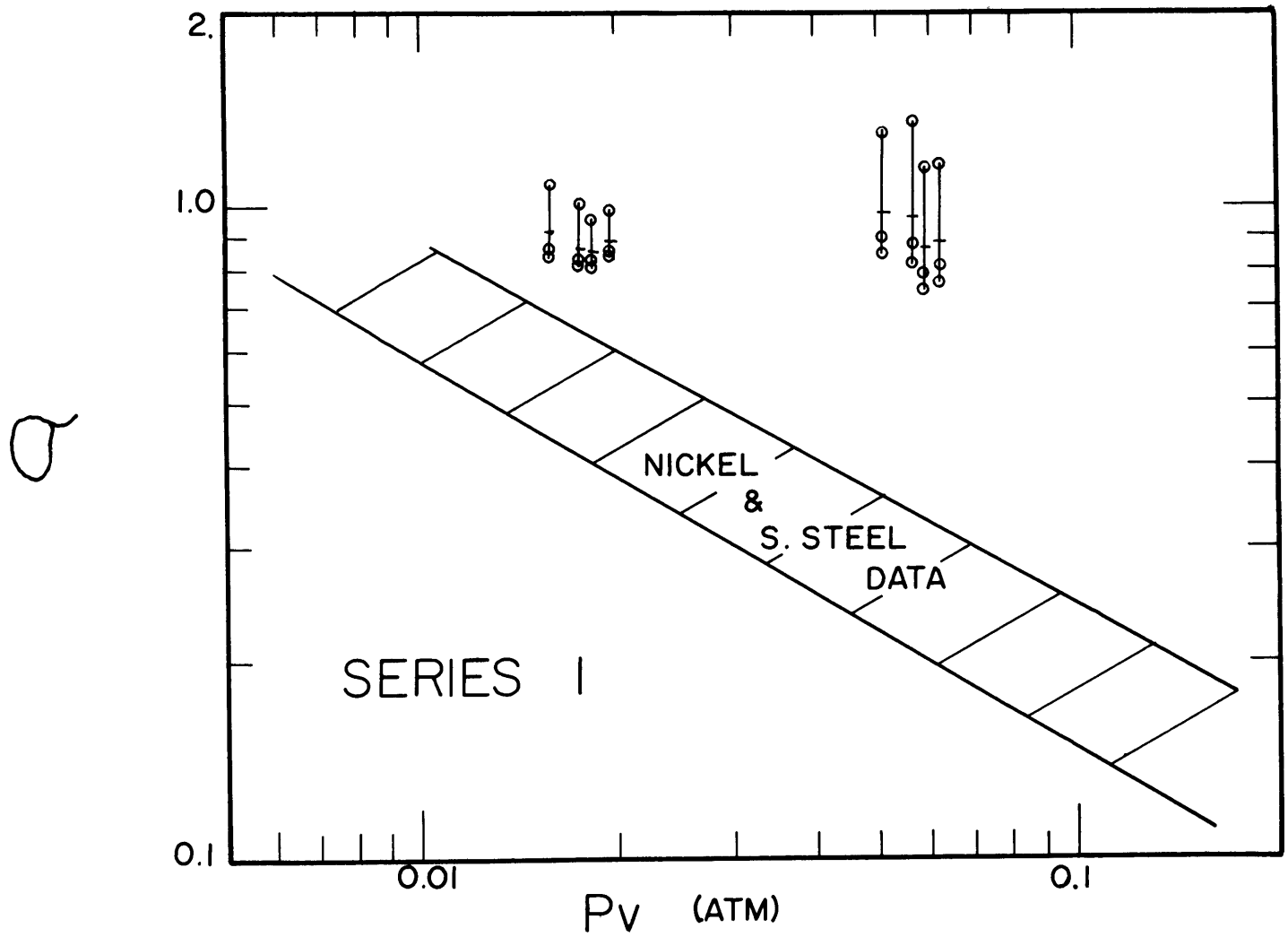

FIG. E-1 EFFECT OF Tv DATA - SERIES I

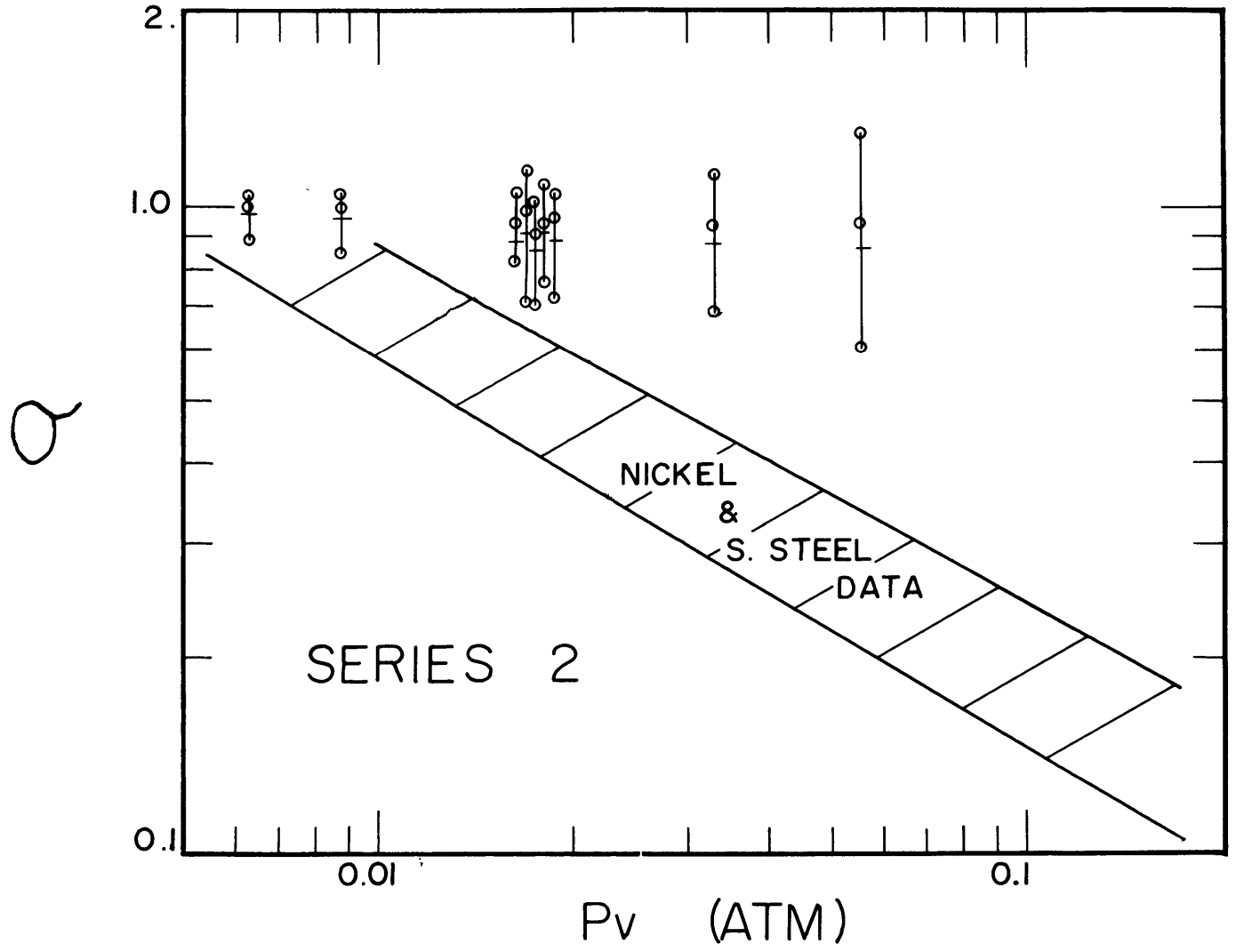

FIG. E-2 EFFECT OF Tv DATA - SERIES 2

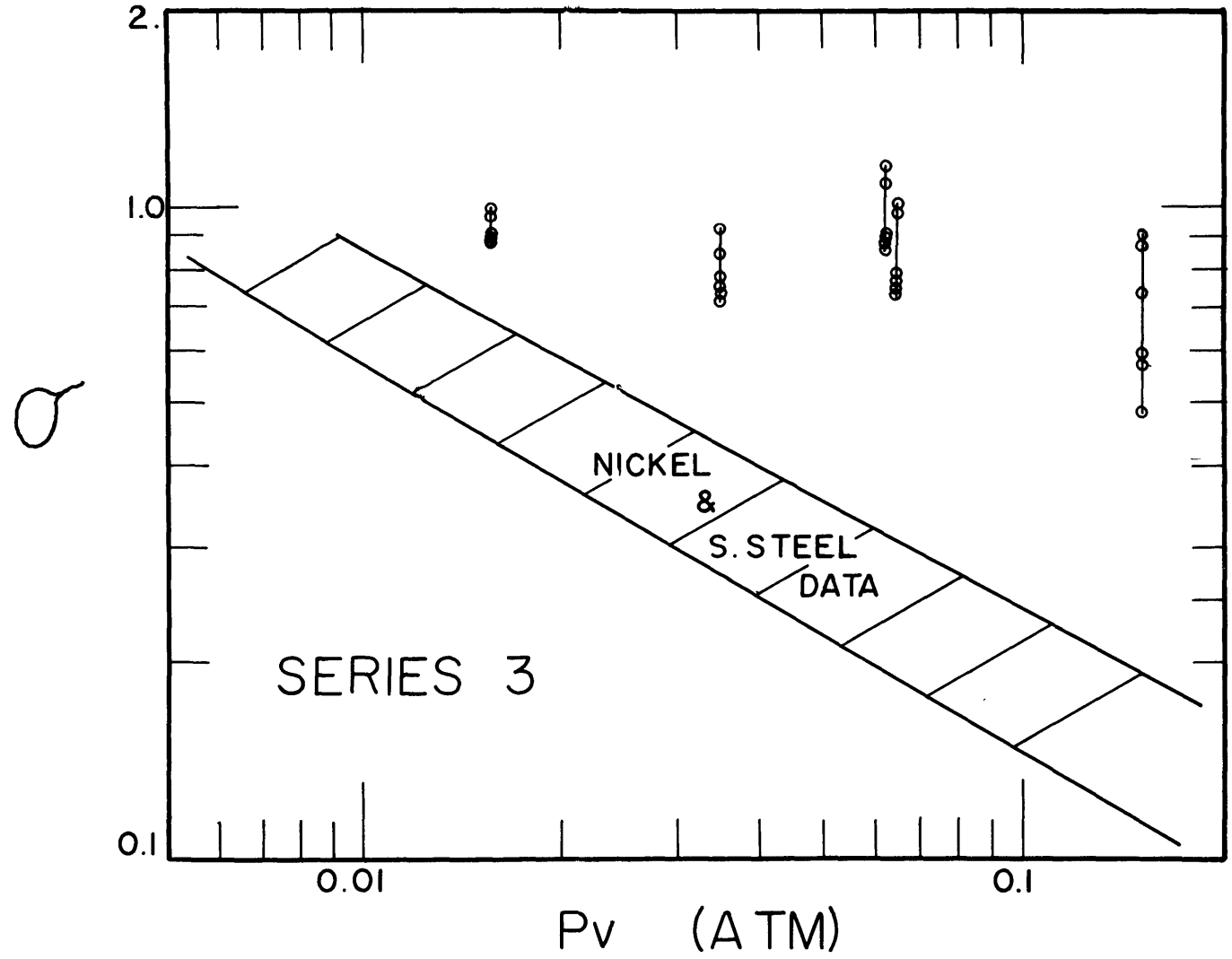

FIG. E-3 EFFECT OF Tv DATA - SERIES 3

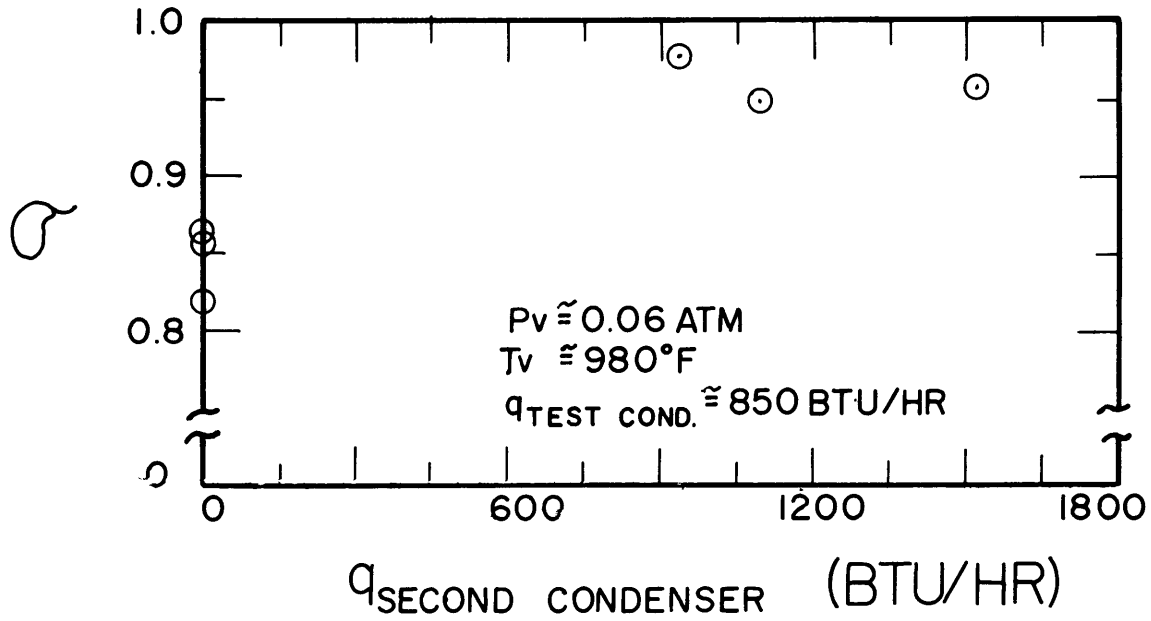

FIG. F-1 EFFECT OF SECOND CONDENSER AT 0.06 ATM